UNIVERSITÀ DEGLI STUDI DI PADOVA

DIPARTIMENTO DI INGEGNERIA INDUSTRIALE

CORSO DI LAUREA IN INGEGNERIA CHIMICA E DEI PROCESSI INDUSTRIALI

Tesi di Laurea Magistrale in Ingegneria Chimica e dei Processi Industriali

Fused Deposition Modeling of 3D porous structures and their characterisation.

Relatore: Dr. Andrea Claudio Santomaso

Correlatore: Dr. Marco Ramaioli

Laureando: MARCO MEGGIORIN

ANNO ACCADEMICO 2017-2018

I’d like to dedicate this dissertation to myself and to my tenacity
able to overcome every hard barrier/obstacle

Abstract

This work of thesis focuses on the application of Fused Deposition Modeling (FDM) for additive manufacturing of food. The aim is to assess the feasibility of this printing process for creating 3D food porous structures. Such technique uses thermoplastic filaments, extruded from a nozzle head, for layer-by-layer fabrication of objects. Among the several 3D printing techniques reviewed, FDM is chosen because it has not found application in the food field yet. In this study, maltodextrin has been selected as main ingredient since it is commonly used in food industry and available as powder. Initially, maltodextrin was characterized, and degradation behaviour and glass transition were evaluated. This information was useful for further processing the material, which was extruded to obtain filaments according to different process conditions. Despite the process complexity, maltodextrin filaments were successfully extruded and were optically and mechanically characterized to predict their suitability for the 3D printing processes. The characterization results were compared with the properties of acrylonitrile butadiene styrene (ABS) filaments, which is commonly used material for 3D printing. Lastly, 3D printing was used to produce three-dimensional porous structures, made of polyvinyl alcohol (PVA), and a dissolution method was developed to assess the quality of the printed objects.

Finally, a tool to control the sequence of operation during 3D printing of simple shapes is developed. It has been used with the Choc-edge 3D printer employed for chocolate 3D printing.

Abstract esteso

La stampa 3D è una tecnologia in forte crescita utilizzata per la produzione di oggetti di alta qualità, con varie strutture e geometrie specifiche. Questa tecnologia è ampiamente utilizzata in diversi comparti industriali (automobilistico, aerospaziale, medico ed anche alimentare) in cui, grazie all'elevata versatilità e rapidità operativa, ha consentito di ridurre i costi di produzione. Più recentemente, questa tecnica è stata adottata nell'industria alimentare per produrre beni su misura e con differenti proprietà nutrizionali. Nonostante l'elevata potenzialità, le applicazioni della stampa 3D in questo campo sono ancora limitate.

Questo lavoro di tesi si concentra sull'applicazione del Fused Deposition Modeling (FDM) per la produzione additiva di beni alimentari. L'obiettivo è valutare la fattibilità di questo processo di stampa 3D per la creazione di strutture porose alimentari. Tale tecnica utilizza filamenti polimerici fusi ed estrusi attraverso un ugello ed opera depositando il materiale strato su strato per la fabbricazione di oggetti di forma desiderata.

In seguito ad una dettagliata analisi di letteratura riguardante la stampa 3D, è stata scelta la tecnica FDM in quanto sono emerse delle lacune circa la sua applicazione nel settore alimentare. In questo studio, è stata selezionata la maltodestrina come ingrediente principale visto il suo largo utilizzo nell'industria alimentare e la sua struttura. Infatti, la maltodestrina è composta da molecole di glucosio legate a formare catene polimeriche più o meno lunghe.

Inizialmente, questo composto è stato caratterizzato e sono state valutate alcune sue proprietà quali degradazione e temperatura di transizione vetrosa. Queste informazioni sono state utili per poter processare successivamente la maltodestrina, che è stata estrusa a diverse condizioni di temperatura e con diverse percentuali d'acqua. In seguito, i filamenti ottenuti sono stati caratterizzati otticamente per verificarne l'omogeneità e meccanicamente per prevedere la fattibilità del loro utilizzo nel processo di stampa 3D. I risultati di caratterizzazione sono stati confrontati con le proprietà dei filamenti ABS, materiale polimerico comunemente usato per la stampa 3D. Infine, la stampa 3D è stata utilizzata per produrre strutture porose tridimensionali e sono stati svolti dei test di dissoluzione per verificare la qualità del prodotto ottenuto.

Inoltre, uno studio sui G-code è stato effettuato per sviluppare uno strumento in grado di controllare i movimenti della stampante 3D durante la stampa di geometrie semplici. Questo *tool* è stato sviluppato per la stampante Choc-edge utilizzata per stampare cioccolato.

Contents

List of symbols

General symbols

Abbreviation	Meaning
a	Total length of the cube
b	Width of material between 2 holes
c	Holes width
c(0)	Conductivity at time 0
c(t)	Conductivity at time t
c(∞)	Conductivity at time infinite
d	Holes height
d_{10}	Diameter of the particle that 10% of a sample's mass is smaller
d_{50}	Diameter of the particle that 50% of a sample's mass is smaller
d_{90}	Diameter of the particle that 90% of a sample's mass is smaller
e	Number of holes per face
ε	Porosity
$\bar{M}n_{theo}$	Mean molecular weight of maltodextrin
N(t)	Normalized conductivity at time t
V_m	Volume of printed material
V_p	Pores volume
V_t	Total volume of the cube
t10	Time to reach the 10% of the final dissolution value
t90	Dissolution characteristic time. Time to reach the 90% of the final dissolution value

Acronyms:

Abbreviation	Definition
ABS	Acrylonitrile-Butadiene-Styrene
AM	Additive manufacturing
DE	Dextrose equivalent
DP	Degree of polymerization
DSC	Differential scanning calorimetry
DVS	Dynamic vapour sorption
FDM	Fused deposition modeling
GRPP	Glass fiber polypropylene
HME	Hot melt extrusion
HPC	Hydroxypropyl cellulose
IM	Injection moulding
MD	Maltodextrin
ME	Material extrusion
PP	Polypropylene
PSD	Particle size distribution
PVA	Polyvinyl alcohol
RH	Relative humidity
T_g	Glass transition temperature
TGA	Thermogravimetric Analysis

Introduction

The use of 3D printing in industry has rapidly grown in the last 30 years, mainly in the electronics, automotive and aerospace fields. In particular, additive manufacturing (AM) can be found useful in the production of prototype and customized objects, as it provides the benefit of reduced time and reduced waste of raw materials compared to injection moulding or subtractive manufacturing. For example, for small and complex shapes AM can be the best option even if it is not convenient for use in high volumes. [27]

Thanks to its flexibility and versatility, 3D printing is becoming an interesting technique also in other fields, including medical and **food**. Over the last 10 years, food industries focused their research in the AM in order to make customized food with different nutritional properties, shapes and colour for different customers. [24]

The International Organization for Standardization (ISO) defines additive manufacturing as "the process of joining materials to make parts from 3D model data, usually layer upon layers as opposed to subtractive manufacturing and formative manufacturing methodologies." [21]. In particular AM processes can be classified into seven categories (Figure 1):

1. binder jetting
2. directed energy deposition
3. material extrusion
4. material jetting
5. powder bed fusion
6. sheet lamination
7. vat photopolymerization

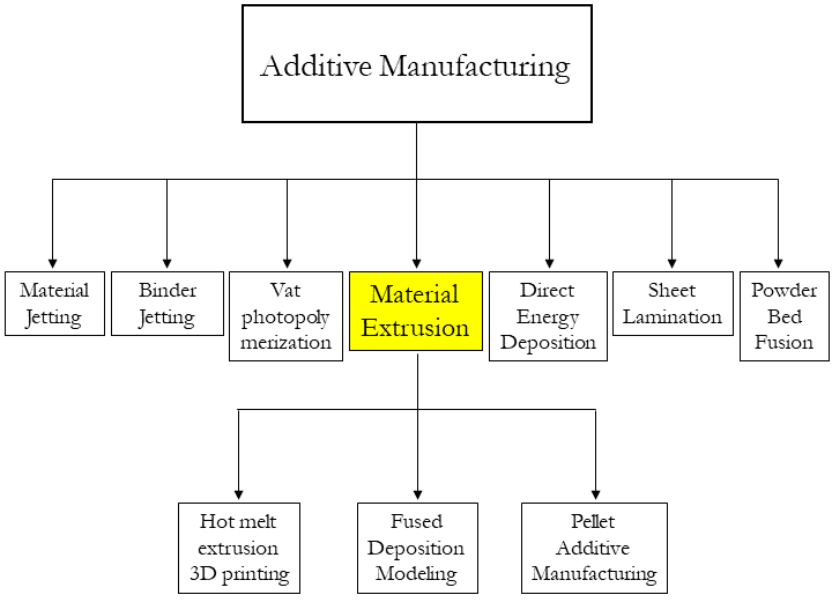

Figure 1: Classification of AM processes

In this paper, only **material extrusion** is deeply investigated. Inside the material extrusion category are included many techniques, such as fused deposition modeling (FDM), hot-melt extrusion 3D printing and pellet additive manufacturing.
FDM is the most widely used 3D technology applied on polymers nowadays.

The aim of this research is to enlarge the use of the Fused Deposition Modeling technique and to investigate its feasibility and effectiveness for food production.

Maltodextrin has been chosen as printing material because it is a common ingredient and it is a polymeric chains made of d-glucose units connected by (1-4) glucosidic linkage. FDM has been chosen because, despite its potential, it has not been used with food formulations.

In order to study the feasibility of the FDM technique the research work has been carried out in 4 steps:

1. Characterization of Maltodextrin powder: The knowledge of raw materials is necessary to predict operating conditions and rheological properties during extrusion. In particular, water content influences important properties, such as glass transition temperature (Tg), flowability and dissolution. Furthermore, analysis of particle size distribution, water activity and degradation are performed in order to compare the results with the relevant data reported in the literature.

2. Extrusion of Maltodextrin powder: Maltodextrin powders is not commonly extruded. Issues and complexity of extrusion are reported in the literature review (§1.2). Hence, investigation of MD powder extrusion is imperative. Filament production can be considered the challenging but necessary step to answer to the open research question: Is maltodextrin suitable for FDM 3D printing?

3. 3D printing with FDM technique**:** Once filaments are obtained, it is necessary to study their mechanical properties to verify the feasibility for 3D printing. Afterwards, the aim is to print 3D porous structures and assess how process parameters and "ink" properties of the material affect the quality of the printed object.

4. Dissolution tests: Dissolution tests is an established technique to verify the quality of drugs and excipients (§2.6). In this project, they are developed to verify the quality of the 3D printed objects.

Moreover, due to the needs of the research group, a second objective related to food 3D printing arises. This was the **development of a tool to control the sequence of operations that a 3D printer is performing when printing simple shapes.**

Printing operations are determined by G-codes (§2.2.13). G-codes contains all the information concerning the printing and are usually produced by the printer software. The aim of this study is to use Matlab to generate G-codes, with well-defined movements in order to reduce printing time and increase printing quality for simple geometries. The obtained G-codes are compatible with the Choc Edge 3D printer employed for the chocolate printing.

Chapter 1

Literature review

In this chapter, a critical analysis of the literature is performed. Initially, the available information on maltodextrin, which is the main compound studied, are reported. Afterwards, a review of extrusion techniques combined with 3D printing is proposed, especially focusing on food 3D printing. Lastly, literature on dissolution tests is reported.

1.1. Maltodextrin

Maltodextrins (MD) are obtain by acid and/or enzymatic hydrolysis of starch. They are composed of d-glucose units connected by (1-4) glucosidic linkage to give d-glucose polymers of variable length, therefore different molecular weight. [4] Furthermore, maltodextrins are considered low converted starch product and they are usually used as food additive. They are easily digestible, moderately sweet, commonly used as sweeteners instead of sugar in soft drinks and candy. They are also used in other applications in food industry, such as confectionery, meat products, alcohol-free beers, sauces, dry soup and sport beverages. [7] Moreover, maltodextrins are water-soluble.

Maltodextrins are classified by dextrose equivalent value (DE). This value is very important because is the only information from which most of the properties of the powder can be estimated. [1]

Dextrose equivalent value is a measure of the amount of reducing sugars present in a sugar product, relative to dextrose (a.k.a. glucose), expressed as a percentage on a dry basis. For example, a maltodextrin with a DE of 10 would have 10% of the reducing power of dextrose (which has a DE of 100). [8] DE gives an indication of the average degree of polymerisation (DP), in particular, the "Theoretical" degree of polymerization and the molecular weight can be determined by the following equations [8]:

$$DP_{theo} = \frac{111.11}{DE} \tag{1.1}$$

$$\bar{M}n_{theo} = 162DP + 18 \tag{1.2}$$

It means that DP and DE are inversely proportional quantities. This value is important because it influences also other properties, such as glass transition temperature Tg and viscosity η.

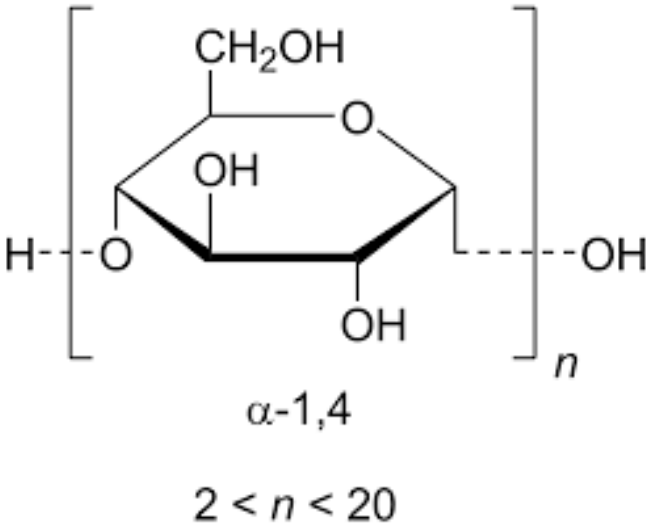

Figure 1.1: Maltodextrin structure. (From Wikipedia)

Furthermore, glass transition temperature Tg and viscosity η are influenced also from other factors, such as the moisture content.

Many authors studied the glass transition behaviour of different maltodextrins [1], [7], [29]. Glass transition temperature usually decreases while DE value increases (e.g. shorter chains has lower Tg) and it usually decreases while moisture content rises. Descamps et al. [7] evaluated glass transition temperature of MD21 for different moisture contents. The experimental data are fitted with the Gordon-Taylor model:

$$T_g = \frac{w_1 \cdot T_{g1} + K \cdot w_2 \cdot T_{g2}}{w_1 + K \cdot w_2} \tag{1.3}$$

Where w_1 and w_2 are respectively the mass fractions of water and maltodextrin, T_{g1} is the glass transition temperature of pure water (-135°C), T_{g2} is the glass transition temperature of dry maltodextrin and K is a fitting parameter. Furthermore, in the paper glass transition temperature measurement method is explained. In order to obtain a better result the powder was placed in an hermetic sealed pan in order to avoid water loss. Thanks to this, it was possible to evaluate Tg at the second upscan. All measurements were carried out in duplicated with a heating rate of 5°C/min from 30°C below T_g onset up to 30°C above T_g endset.

Glass transition temperature of Maltodextrin is also studied by Avaltroni et al. [1]. The authors used a phase transition analyser in order to evaluate it. The test was performed on maltodextrin 19 with a temperature between 10-140°C. T_g was determined as the temperature at which the first derivative of the piston displacement leaves the region of linearity. Despite the different technique used, the results obtained can be used as comparison.

Castro et al. [4] studied the degradation and the hygroscopic behaviour of maltodextrin with different DE. They performed a TGA analysis heating the maltodextrin until 600°C. After an initial loss of weight, between 25°C and 150°C, due to the water evaporation, maltodextrin looks stable until 250°C. The test was performed in an inert atmosphere (N_2) at room pressure.

Hence, particular attention has to be taken while extruding at high temperature and high pressure is performed to avoid degradation.

1.2. Material extrusion

Material extrusion (ME) is one of the most widely used technique in AM processes. It is commonly exploited for polymers 3D printing but it is being also applied with other materials, such as pharmaceutical excipients and food. This technique can be visualized similar to HME, with the difference that it is used to produce a 3D object built layer-by-layer.

The material is melted and forced through a nozzle when pressure is applied. The material exits in form of filament with a small diameter, determined by the nozzle size.

The nozzle is usually able to move on the X-Y axes, building the 2D shape, while the build plate usually moves in the Z axis.

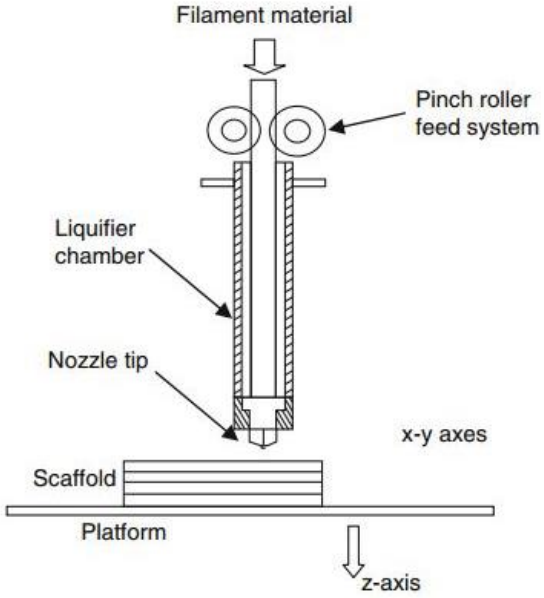

Fig.1.2: Schematic of extrusion-based system [11].

Figure 1.2 illustrates the general scheme of a material extrusion 3D printer. The material state is controlled by the temperature. The material inside the liquefier chamber is completely melted so it can flow out through the nozzle. Temperature has to be set to have a semi-solid material coming out from the nozzle. The material has to fully solidify in order to maintain the designed shape and to bond to the material previously extruded.

There are different kinds of material extrusion, based on the different material loading. Material can be load in form of:

- Filaments
- Pellets or powders

When the material is load in form of filaments the technique is called fused deposition modeling. When the material is load in form of pellets or powders it is usually pre-melted in a

reservoir and pumped in the chamber. The pressure to extrude the material is usually given by a plunger or a screw. This technique is commonly used in the food industry and it is called hot melt extrusion 3D printing.

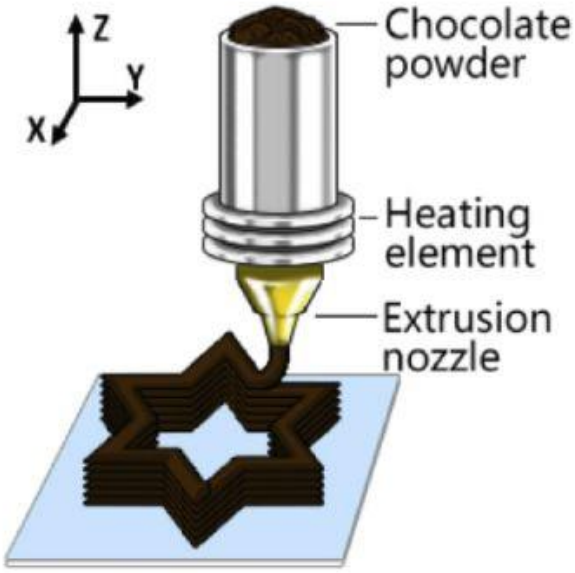

Fig.1.3: Schematic diagram of hot melt extrusion 3D printing [35].

Material extrusion, and in general AM, starts with a 3D object designed using a Computer-Aided Design (CAD) software. The CAD file is converted in stereolithography file (STL) and it is imported inside the printer software. The printer software is used to define process parameters, such as printing temperature, printing speed and many others. Hence, a G-code file is generated, which contains all the information related to the printing conditions. Afterwards, the G-code is uploaded inside the 3D printer and the building process can start. The object is printed layer-by-layer, pushing a filament through a hot nozzle, in which it melts. Once the print is ended, the designed object can be removed and, if required, some post-process treatments can be done. The overall process is summarized in the picture 1.4:

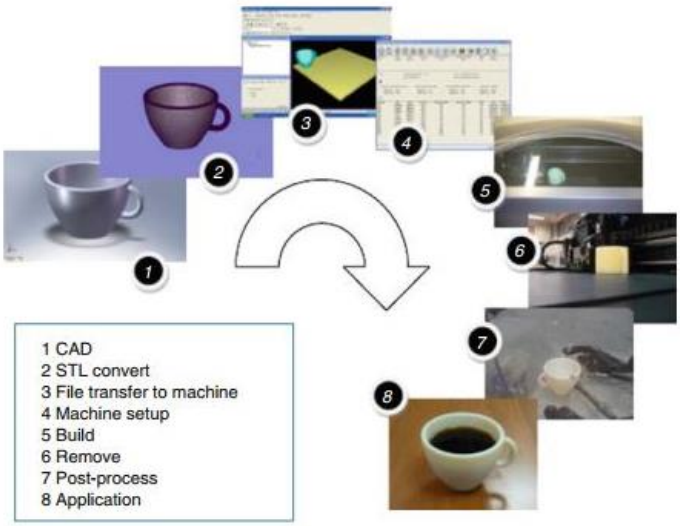

Figure 1.4: Generic Additive Manufacturing process [11]

Material extrusion, is currently of significant interest for numerous food application. In particular, 3D food manufacturing could completely change the food industry. It could allow obtaining personalized nutrition, tailored shapes and customized taste [6]. The most popular method in food printing is the hot melt extrusion 3D printing, also known as extrusion-based food printing. Sun et al. [35] speculate on the future of this technique and analyse the published works. The most important material extrusion techniques applied in the food industry are reported in Figure 1.5.

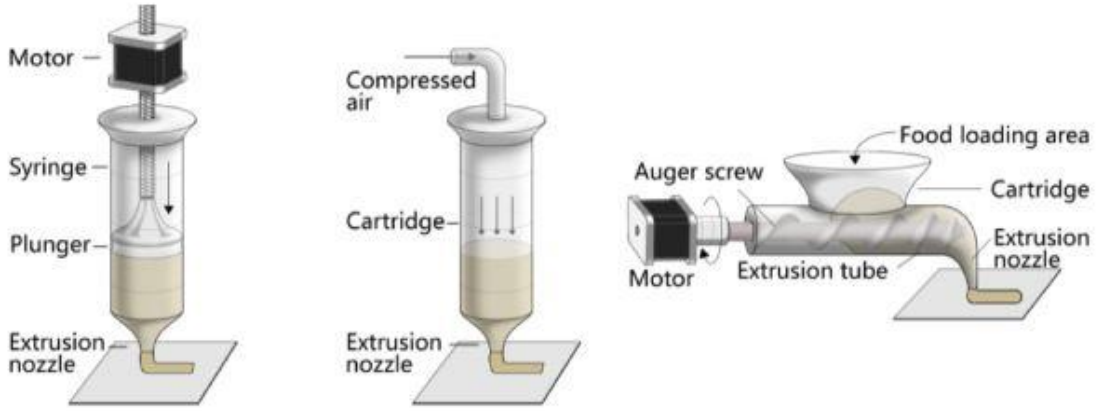

Figure 1.5: (a) Syringe-Based Extrusion, (b) Air Pressure Driven Extrusion (c) Screw-Based Extrusion. [35]

Syringe-Based extrusion is usually used in chocolate 3D printing. For instance, the Choc Edge 3D printer, described below (§2.2.12), is designed based on this technique. As in standard 3D printing objects are produced by material deposition layer-by-layer.

Sun et al. [35] also speculated on the future of this technique, predicting a complete personalized service.

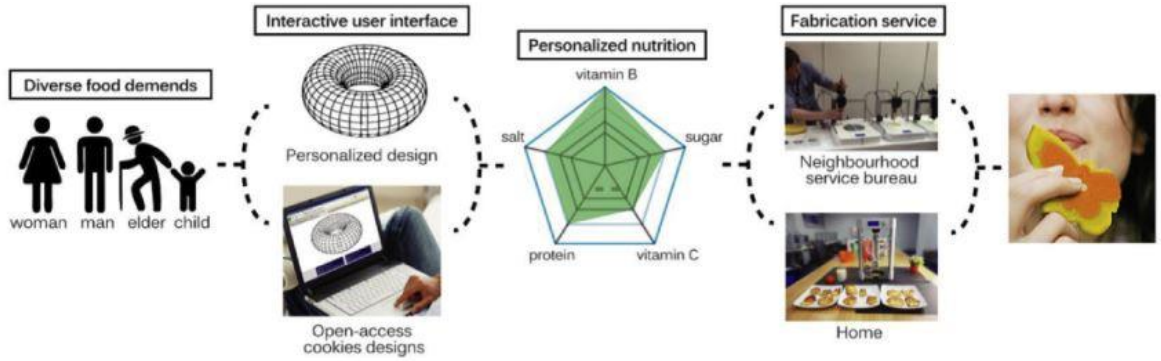

Figure 1.6: Schematic diagram of food design and fabrication service [35]

Despite the speculation, food 3D printing involves several operations and can be very complicated to describe. Quality and precision are fundamental in the appealing of the final product. Hence, many authors focused their study on product quality assessment and on process parameters. Liu et al. [22] suggested that the key parameters that have to be considered in order to obtain good final-product precision are:

1. 3D printing mechanism

2. Material properties: rheological properties, gelling/melting, glass transition temperature, surface tension and extensional properties.
3. Processing factors: extrusion speed, extrusion temperature and nozzle diameter.
4. Post-processing treatments.

Many authors [19], [17], [24], focused their study on rheological properties, considering low melting temperature materials printed with the ME technique (e.g. Chocolate).

It must be remembered that the ME category is usually divided in FDM and hot melt extrusion 3D printing. In food industry hot melt extrusion 3D printing is usually employed.

1.2.1. Hot melt extrusion 3D printing

Hot melt extrusion 3D printing is a ME technique based on the printing of a melted material through a heated nozzle. It can be seen as a modification of the standard HME process described in the next paragraph (§1.3). Hot melt extrusion 3D printing of different food formulations is widely performed. The equipment employed are reported in Figures 1.3 and 1.5. A syringe-based extrusion is usually used as 3D printing technique.

Hao et al. [17] and Mantihal et at. [24] used this technique to study how process parameters, such as extrusion flowrate, extrusion temperature, nozzle diameter and many others, are critical for successful chocolate 3D printing. Chocolate has been selected for its physical properties such as its melting point of 25°C. Moreover, chocolate properties can be easily modified changing the fat amount.

Also Lanaro et al. [19] focused their work on 3D printing of complex chocolate objects. For consistency purposes, the thermal properties and rheology of the chocolate were determined prior to printing and then the printing parameters like movement speed and extrusion rate were altered during the testing phase. Test temperature was set between 30 and 40 °C. Afterwards, printing parameters were optimized for that chocolate composition. Hence, the link between rheology and ingredients composition was not investigated.

Rheological properties of other food materials are studied. Liu et al. [23] investigated the rheological properties of mixtures made of mashed potatoes and Potato starch (PS). PS concentration was changed in order to study its effect on rheology and on final product quality.

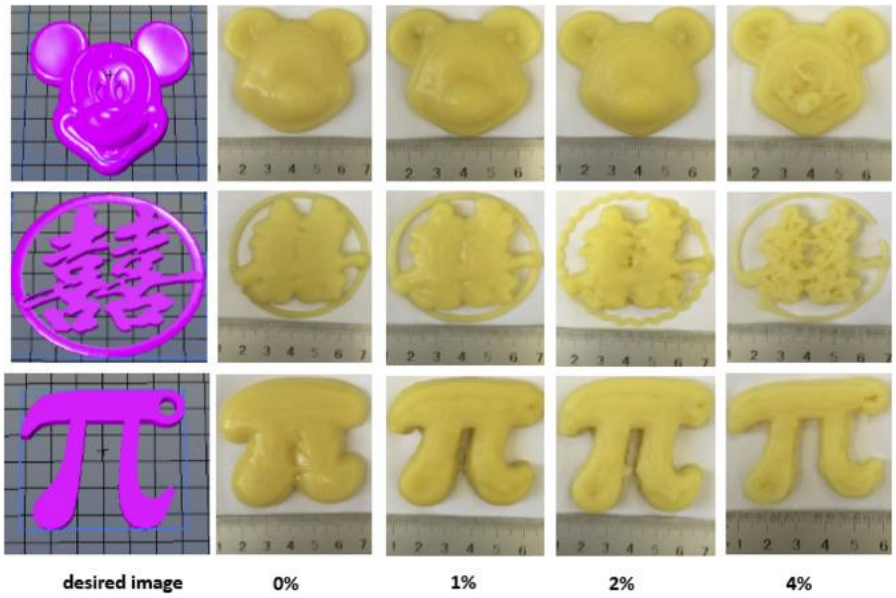

Figure1.7: Shapes printed with different composition of mashed potatoes and potato starch. [23]

They found that the optimal "extrudability" and "printability" can be obtain using a mixture made of 2% of PS. It is necessary to specify that the analysis of the printed shapes was carried out visually, with little to no quantification.

Wang et al. [38] studied the effect of nozzle diameter, nozzle distance from the plate, printing speed and extrusion rate of a viscous food gel system, called surimi. The food composition was changed adding NaCl in different concentration. It affects material, viscoelastic and rheological properties. Rotational rheometer was used to measure the material viscosity. Also in this case, the optimal process conditions were found using a visual analysis.

Moreover, this technique is used for other low melting temperature materials. For instance, Derossi et al. [6] tried to use this technique in order to obtain fruit-based snacks with high nutritional properties. Also in this article, rheological properties were evaluated and final product quality was assess.

Le Tohic et al. [20] investigated the structural and textural alteration of processed cheese during 3D printing. The differences between un-treated and manufactured cheeses were analysed using not only standard rheological investigation, but also studying different material properties, such as hardness, ashesiveness, springiness, cohesiveness, resilience and the microstructure of fat.

All these papers analysed, in different ways, properties of low melting food formulation and the results shows how many physical properties influences the final product quality, and how often it is difficult to determine or predict them. Furthermore, despite many authors [12], [24], refers to "printability", characterization is usually only qualitative. The challenge is to relate "ink" materials properties to process parameters and product quality.

In the end, it is interesting to describe the article of Schutyser et al. [32]. The article, as many others, study the rheology of a food composition, in this case sodium caseinate dispersion.

Moreover, they investigated the gelatination and the dispersing behaviour. The interesting thing is that the authors refers to FDM as 3D printing technique, despite the machine was equipped with a customized dispenser based on pressure driven extrusion and temperature was set below 90°C. Hence, a melted formulation was printed instead of a solid filament. For these reason it has been decided to review this article as hot melt extrusion 3D printing. It is therefore necessary to highlight the weak border between the 2 techniques.

1.2.2. Fused deposition modeling

Fused deposition modeling, is among one of the most popular AM processes. It creates physical objects directly from CAD 3D models via extrusion of a polymeric filament in a layer-by-layer deposition process. The filament is fed from a rotating rollers pulling system through a heated nozzle and the object is built layer-by-layer on a building-plate as shown in the Figure 1.8.

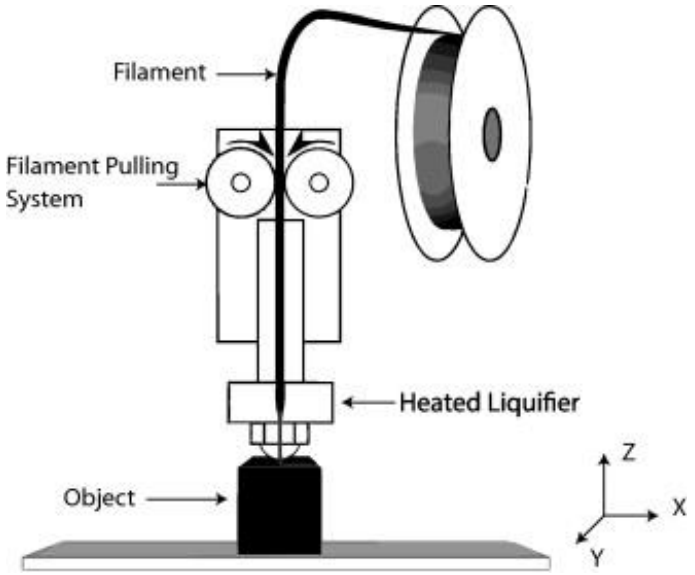

Figure 1.8: Scheme of FDM 3D Printer [3].

The polymer is melted in the Heated Liquifier and pushed through the nozzle die by the solid upstream solid filament. The fused polymer link with the previous layer in order to build up the desired object. The nozzle usually moves in the X-Y direction, creating a 2D object, while the plate moves in the Z direction, to provide the third dimension, namely the height.

The most common materials used in FDM are amorphous thermoplastics, Turner et al. [27] performed a critical review of the literature related to process design and mathematical modeling. Particularly, they focused their attention on filaments mechanical properties and on buckling phenomena. In fact, one of the key requirements of the feedstock filament is the capability to pass through the pinch roller mechanism without crushing and to push the melted filament without buckling. Buckling phenomena is explained in Figure 1.12.

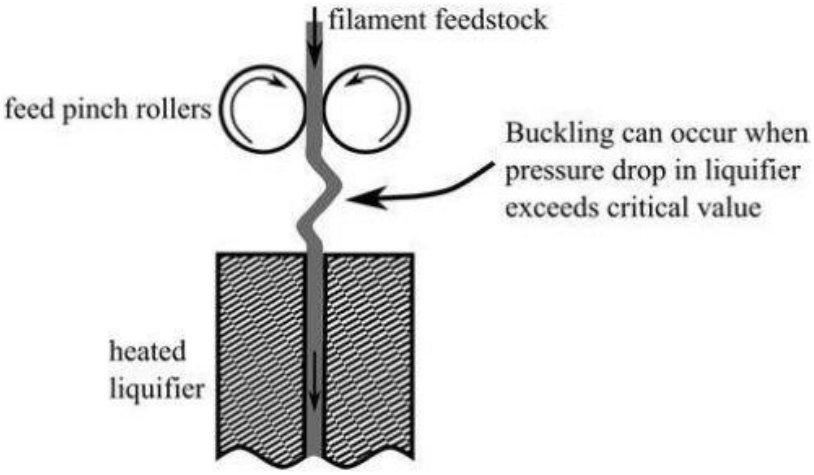

Figure 1.9: buckling of a filament due to excess compression. [27]

An approximation of the critical Load (P_{cr}) can be obtain from an Euler buckling analysis.

$$P_{cr} = \frac{\pi^2 \cdot E \cdot d_f^2}{16 L_f^2} \tag{1.2}$$

Where d_f is the diameter filament and L_f is the distance between the rollers and the entrance of the liquefier and E is the young's modulus.

Filaments mechanical properties are also studied by Nasereddin et al. [28]. The authors focused their study on the possible rupture that can happen during the printing and on the critical process parameters. Particularly, it is necessary to consider machine-specific, operation-specific and material specific parameters. Machine parameters are related to the specific pulling system, as shown below (§2.2.9). Material parameters are the mechanical properties and can be evaluated using a texture analyser. The authors speculated on the possible breakings and performed a compression test in order to assess filaments feedability.

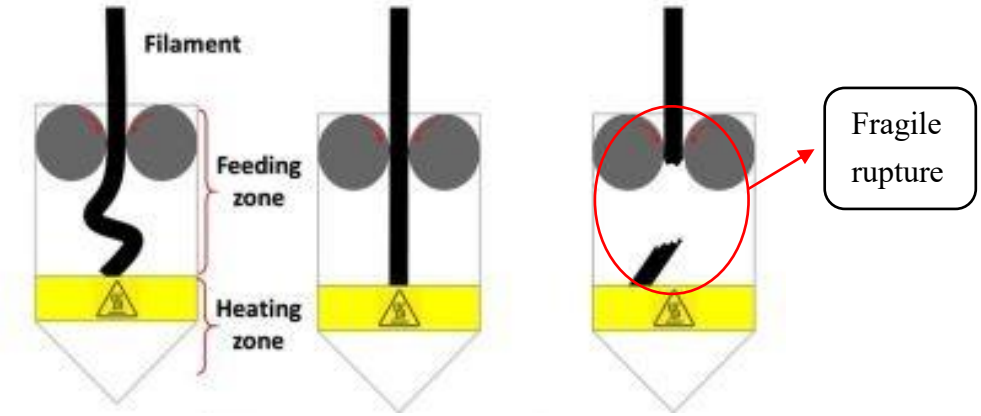

Figure 1.10: Rupture due to buckling (left picture) or fragile rupture (right picture). [28]

Therefore, Nasereddin et al. [28] have developed a customized method, based on machine-specific parameters, to assess mechanical properties of extruded filaments and to compare them with ABS and other commercial filaments.

Despite the huge potentiality, fused deposition modeling has not found practical uses yet in the nutritional field, while it has been studied in the pharmaceutical field in order to improve therapy personalization (e.g. drug customization).

For instance, Goyanes et al. [13], [14], studied the feasibility of using FDM to product tablets with different shapes and drug loads. Firstly, [13] they loaded the PVA filaments with fluorescein, placing the PVA filaments inside an ethanolic solution of fluorescein (2%w/v) for 24 hours. Afterwards, dried filaments were used to produce tablets with different infill. Finally, the dissolution behaviour was studied. Tablets with higher infill showed slower drug release. Furthermore, they discovered that drug loading could not be the optimal technique of loading. In fact, due to the low diffusion coefficient of fluorescein the maximum drug-loading obtainable was 0.29±0.01% w/w.

Moreover, Goyanes et al. tried to combine hot melt extrusion with the FDM technique. [14] Hence, they mixed and extruded PVA pellets and paracetamol (5%drug w/w) in order to study the feasibility of filaments production with customize drug-loading functional for FDM. The obtained filaments were fed into a MakerBot 3D printed and tablets with different geometries were obtained. As in the previous article, dissolution tests were performed in order to evaluate how geometrical parameters influence the drug release.

Also Melocchi et al. [26], [27], and Maroni et al. [25], investigated the feasibility of FDM as production technique for customized drugs. Firstly, they developed capsular devices for oral pulsatile release, using hydroxypropyl cellulose (HPC) [26]. HPC filaments were produced with a twin-screw extruder (Haake MiniLab II). Afterwards, the capsular devices with a controlled shape were produced by FDM. Finally, the breakage behaviour of 3D printed capsules was studied and compared with capsules obtained by injection moulding (IM). The test, performed in a baker filled with 900 mL of DI water at 37±0.5°C, showed a similar behaviour. It proves the feasibility of FDM as alternative way of capsular devices production.

Furthermore, Melocchi et al. [27] pointed their attention on the production of different filaments composed of pharmaceutical grade materials and on the possibility of employing them in the 3D printer. Filaments of various materials with insoluble, promptly soluble, enteric soluble and swellable/erodible characteristics were successfully produced and used for 3D printing by FDM. These filaments can be potentially suitable, once loaded with the proper excipient, for 3D printing of capsules with modified release based on their dissolution behaviour.

Afterwards, Maroni and Melocchi used the previous studies in order to design multi-compartment capsular devices for two-pulse oral drug delivery [25]. The capsular device, designed with different thickness or produced with different polymers, allows controlling the drug release. Moreover, this technique allows combining different excipients inside the same capsule, thus improving the customization of drugs. It can be used to study the design of new drug-release devices and to product small-size batched. On the contrary, they found it is

currently less convenient than IM for large production. A summary of the previous articles is reported in Table 1.1:

Table 1.1: Summary of articles related to FDM.

Study	Goyanes et al. (2014) [13]	Goyanes et al. (2015) [14]	Melocchi et al. (2015) [26]	Melocchi et al. (2016) [27]	Maroni et al. (2017) [25]
Materials	PVA	PVA	hydroxypropyl cellulose (HPC)	Various materials common in the pharmaceutical field.	Same as [27]
Drug-load	0.29% w/w Fluorescein	5% Paracetamol	Not loaded,	Not loaded	Not loaded
Drug-load method	Passive diffusion	Hot melt extrusion	-	-	-
Extrusion temperature	-	180°C	150-165°C	70-190°C	As [27]
Screw speed	-	35 RPM	50-60 RPM	70-100 RPM Torque: 40-120 $[N \cdot cm]$	As [27]
3D Printing temperature	220°C	180°C	210°C	160-225°C	As [27]
Filaments preparation	Commercially available	Hot melt extrusion	Hot melt extrusion	Hot melt extrusion	Hot melt extrusion
Printed geometries	Tablets with different infill	Tablets with complex shapes	Capsular devices filled with a tracer	Disks	Capsular devices filled with a tracer
Aim	Production of customised drug	Production of customised drug	Investigate FDM as alternative technique for capsule production	Investigate feasibility of various materials for FDM	Improve the previous study [26], obtaining versatile release profiles
Results	Tablets were successfully printed.	Tablets were successfully printed.	FDM was found feasible and capsular properties comparable with the one obtained with IM	FDM was found feasible, despite mechanical properties of some filaments were not optimal.	FDM was found feasible and versatile release profile obtained.

1.3. Hot melt extrusion

Hot melt extrusion is a well-known technique. Indeed, more than 60% of the world production of plastic products is made by extrusion [5]. This technique is used to make end-products and to mix different additives and pigments with polymers to form compounds.

Extruders are machines that force a molten polymer through a nozzle to provide a well-define 2D form, such as pipes, tubes, films, sheets and other profiles.

Extruders can be single or double screw, depending on the needs. Double screw extruders have a higher productivity and a higher mixing efficiency compared with single screw extruders; however, they are more complex and more expensive. In order to obtain plastic filaments a single screw extruder is usually used. A general single screw extruder is shown in the Figure 1.11.

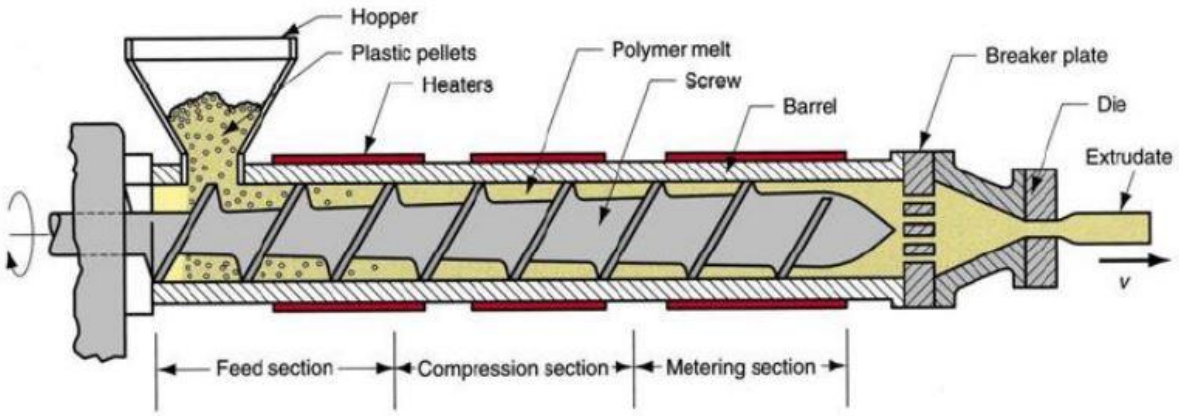

Figure 1.11: Schematic of conventional extruder [31]

As it can be seen from the picture, the extruder consists of screw, barrel, hopper, die and heaters. Moreover, it is usually divided in 3 zones.

The first one is the feed section. In this section, the material is fed through the hopper, conveyed by the screw, compressed and pre-heated. In order to be feed properly the material has to be in pellets or free flowing powders form. Moreover, the temperature of this zone has to be properly controlled to obtain a partially melted material.

The second zone is the compression section. In this section, the material is completely melted. The energy required to melt the material is provided by the motor and the heaters. In particular, most of the mechanical energy of the motor is converted into heat by shearing and viscous dissipation between the screw, the barrel and the melted material. Furthermore, in this section the material is mixed, compressed and pushed to the metering zone, which is the last section.

In the metering section, the molten material is homogenised, by an increase of shear rate, and it is extruded from the die. In order to pump the material through the nozzle the screw is designed to provide enough pressure.

Moreover, each section has different geometrical properties, designed to reach the aim required. Particularly, the geometry of the screw is very important to provide the necessary energy to pump and mix the material. The effective pumping is influenced by many parameters, such as material viscosity, process temperature, shaft speed, screw geometry and die geometry. For these reasons, hundreds of screws are designed and used for different working conditions and materials.

A general scheme is report below:

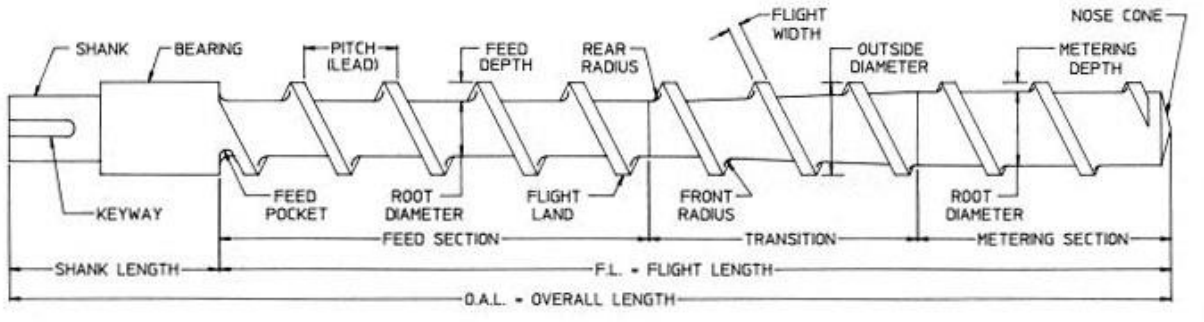

Figure 1.12: Schematic of conventional extruder screw [31]

The Figure shows how many parameters are involved in the design of a screw. Generally speaking the screw can be considered as a cylinder with an internal diameter, named root diameter, with flights. The root diameter increases along the length of the screw in order to increase the pressure. However, sometimes the root diameter is kept constant and the compression results by changing the pitch. In conclusion, the screw is the most important part of the extruder and it has to be designed properly for each application.

The application of extrusion, combined also with 3D printing, in order to product customized plastic objects is well-established. On the other hand, the application of these techniques in order to produce customized food is not completely studied yet.

In the last decade, HME has been applied to produce filaments suitable for FDM.

For instance, Carneiro et al. [3] extruded polypropylene (PP) and polypropylene reinforced with a glass fiber (GRPP) in order to use them in the 3D printer and study mechanical properties of the printed objects. The prototype extrusion line used is shown in the picture 2.4.

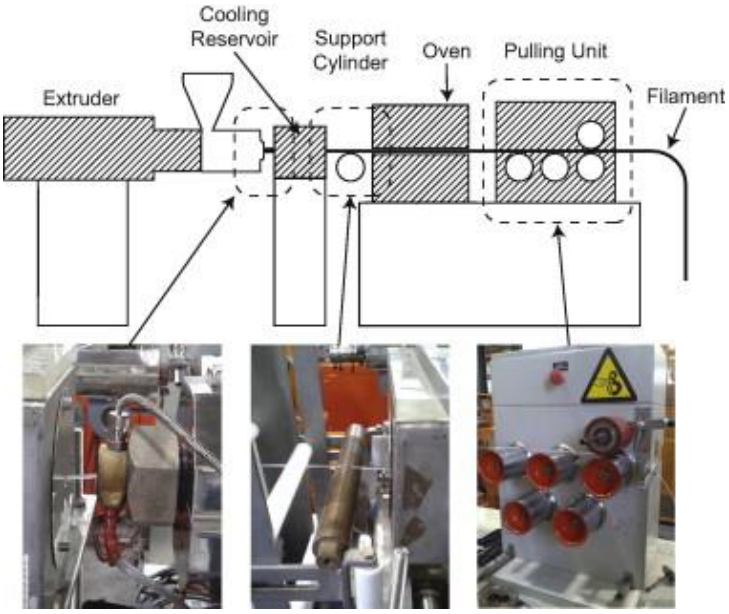

Figure 1.13: General view of the prototype extrusion line used in the production of the filaments. [3]

The system is composed by a double screw extruder, a cooling reservoir, an oven to homogenise the filament and a pulling unit. The main process parameters are:

- Extruder/ die temperature (°C)
- Extruder screw speed (rpm)
- Pulling rolls speed (m/min)
- Oven temperature (°C)
- Distance die-cooling reservoir (cm)

Figure 1.13 and the previous bullet points show the complexity of the extrusion system and the parameters that it is necessary to set in order to obtain filaments with the required diameter. Also other authors [40], use similar devices in order to obtain reinforced filaments suitable for FDM 3D printing.

Hot melt extrusion is also applied in the medical field in order to obtain drug-loaded filaments [13] and to obtain filaments made by polymers of common use in pharmaceutical formulation [27].

Melocchi et al. [27] extruded different materials using a twin-screw extruder with a wide range of process condition. They reported that some filaments had low mechanical properties. This caused rupture or wrapping while the filaments were used in the 3D printer. Hence, plasticizer amount in the initial composition was changed with a trial and error procedure to override these issues. In conclusion, the authors drew attention to the importance of the mechanical properties of the extruded filaments in order to make them feasible for the FDM technique.

Yeung & Rein [40] studied HME as alternative method to produce starch pellets. Starch powders mixed with sucrose and water (plasticizers) are extruded using a co-rotating twin-screw extruded designed with 12 different heating zone. The screw was customized to induce

high-energy impact. Extrusion temperature was set between 30 and 50 °C above the T_g and adjusted using a trial and error procedure. This work describes the complexity of starch extrusion. It must be remembered that maltodextrin is a low converted starch product (§1.1).

In conclusion, the previous articles shows the importance of the extrusion process to obtain filaments, made by non conventional materials, feasible for FDM. Moreover, issues related to extrusion are reported, suggesting that a huge effort was required to find the optimal process conditions.

1.4. Dissolution test

Dissolution tests are widely used to evaluate reconstitution and dissolution properties of a various range of materials. For instance, they are used in the pharmaceutical field to simulate drug release [26], [27], [25], [14]. They are also used in the food industry to evaluate reconstruction of dehydrated beverages. [9] Dupas et al. [9] studied maltodextrin dissolution kinetics. In order to analyse how different parameters, such as powder diameter, moisture content and temperature, affects the dissolution. Dissolution test of dense cuboids with different DE, moisture content and temperature were performed. The measurement procedure is similar to the one used in this paper, explained in chapter 2 (§2.2.11). The time to reach 90% of the final value (t_{90}) was used.

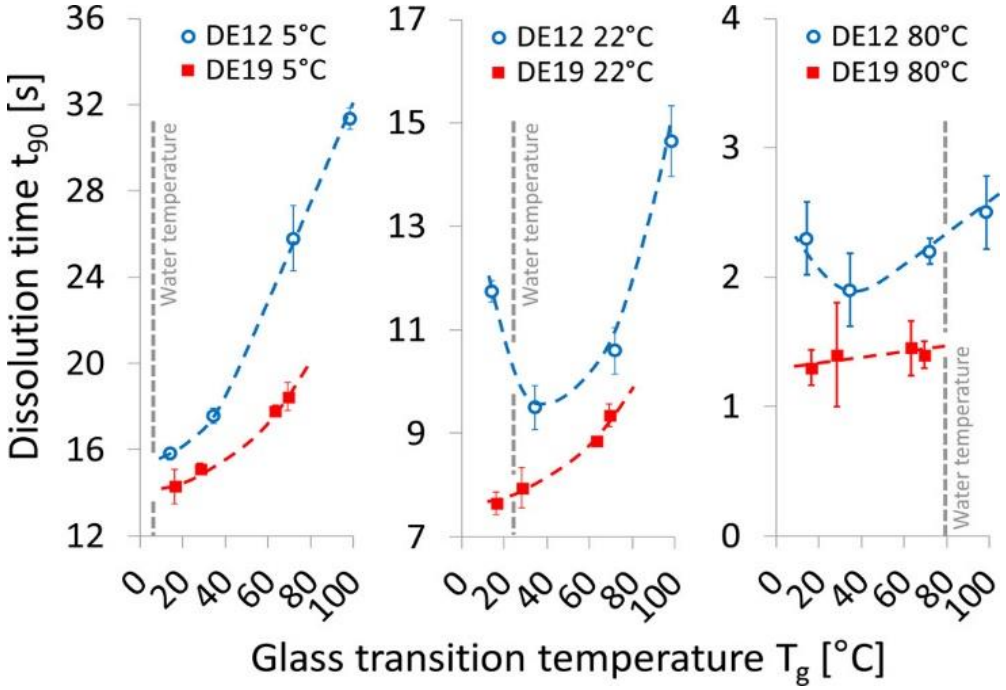

Figure 1.14. Dissolution time t90 of MD versus glass-transition temperature for three different water temperatures (5, 22, and 80 °C from left to right)

Maltodextrin characteristic dissolution time has been found lower than 30 seconds for all the experiments performed.

Maroni et al. [25] evaluated the dissolution of PVA capsular devices. The aim of their experiment is to assess the feasibility of the capsular device in order to have a two-pulse release.

The results obtained show how the drug release is related to the PVA dissolution and in particular to the thickness of the compartment. 600 μm device dissolved in about 15 minutes, while the 1200 μm device dissolved in about 45 minutes under stirred conditions.

Goyanes et al. [14] simulated gastrointestinal behaviour of different mesalamine tablets. The authors were able to developed a method in which pH was controlled in order to simulate the path of the drug through the stomach and the intestine.

The same authors [13] performed dissolution tests on PVA + paracetamol 3D printed objects. Tablets with different geometries and geometrical properties, such as surface area, ratio area/volume and weight, were designed and dissolution behaviour was studied. It has been found that the area/volume ratio is the key parameter in the dissolution behaviour.

Chapter 2

Materials and methods

In this chapter of the thesis, materials and instruments used during the research will be described. Furthermore, the methods developed to perform the experiments will be illustrated.

2.1. Materials

Maltodextrins (GLUCIDEX® 19-GLUCIDEX® 21) were supplied by Roquette (Lestrem, France). They are obtained by undisclosed degradation of native corn-starch. Maltodextrins are hydrated in desiccators using saturated salt solutions. The salts used are reported in the Table below:

Table 2.1: Salts and related relative humidity.

Salt	RH[%]
$LiCl$	11.30 ± 0.27
CH_3CO_2K	22.51 ± 0.32
K_2CO_3	43.16 ± 0.39
$Mg(NO_3)_2$	52.89 ± 0.22
$Na(NO_3)_2$	64.78 ± 0.22

Saturated salts solutions are prepared in 100mL of D.I. water. The salt is dissolved, while mixing is performed, until saturation is reached. Salt was added considering the saturation conditions studied by Greenspan [16].

Polyvinyl alcohol (PVA) filaments, D=2.85mm, used to print 3D porous structures, were supplied by Ultimaker. Acrylonitrile butadiene styrene (ABS) filaments, D=1.75mm, were supplied by Verbatim.

Chocolate (recipe BC-811) was supplied by Barry Callebaut. It is a dark chocolate of 54.5% cocoa solids and it is in the form of callets. Unaltered, it contains approximately 37.8% fat. The cocoa butter used to alter the formulation is also Barry Callebaut brand and is as 100% cocoa butter callets.

2.2. Method

2.2.1. Particle Size Distribution

As naturally occurring powders are generally of non-uniform size and shape distribution, engineers have developed a range of measures to adequately compare them. These include parameters such as the equivalent project area diameter, Feret diameter and stokes diameter.

A particle can be defined as single unit of material having discrete physical boundaries that define its size. The particle-size distribution (PSD) of a powder is a list of values, or a

mathematical function that define the distribution of particles inside the powder. It can be define by mass, volume or number [33]. It is an important parameter because it can determine some bulk properties of the solid powder, such as density, surface area, flowability, dissolution and dispersion. Many methods and instruments for measuring particle size have been developed for different purposes.

The instrument used in this paper is the QicPic (Sympatec Inc., Clausthal-Zellerfeld, Germany). It uses a dynamic image analysis, which consists in a pulsed light source, with illumination time of less than 1 nanosecond, coupled with a high speed camera. The scheme is reported below:

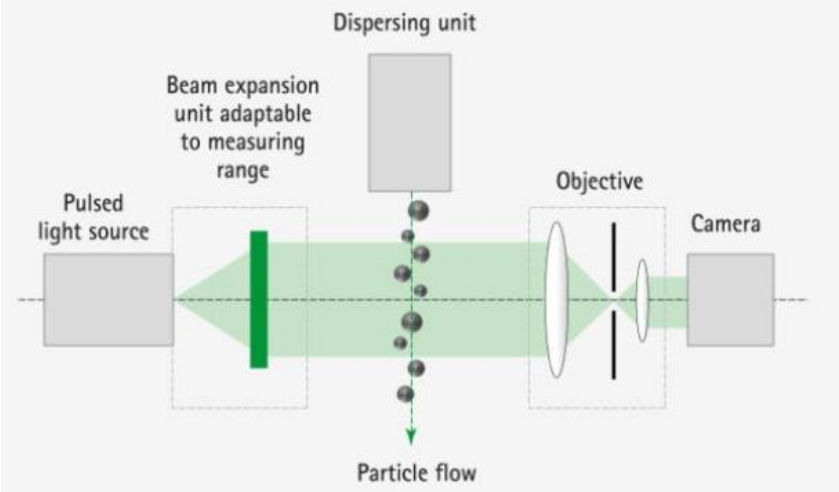

Figure 2.1: Scheme of a dynamic image analysis instrument (From QicPic manual).

The powders are fed into the sample dispenser where they are accelerated and dispersed. The light source and the camera are designed in order to capture particle from 1µm to 34000 µm.

In order to improve the performance of the QicPic it is coupled with RODOS disperser (Sympatec Inc., Clausthal-Zellerfeld, Germany) as shown in the picture below.

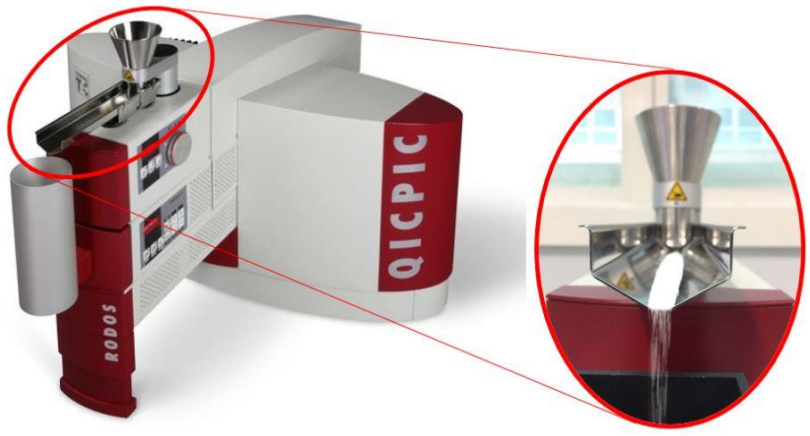

Figure 2.2: QICPIC instrument with the detail of the RODOS dispenser. (Adapted from the Manual)

The instrument provides different information on the particles analysed, such as aspect ratio, sphericity and particle size distribution.

2.2.2. Thermogravimetric Analysis

Thermogravimetric analyses (TGA) are performed with TGA500 (TA instruments, Hertfordshire, UK) in order to evaluate the thermal stability of the maltodextrin. It is based on the principle of measuring the change in weight of a sample as the temperature is varied. Furthermore, also the atmosphere can be controlled, e.g. amount of O_2 and N_2, in order to change the nature of the thermal degradation occurring. The temperature is set between 25°C and 400 °C with a ramp of 5°C/min in air and in N_2. TGA and DSC tests were kindly performed by a specialised technician.

2.2.3. Differential scanning calorimetry

Differential scanning calorimetry (DSC) is a thermoanalytical technique in which the difference of heat ΔE, required to maintain the temperature difference at 0 ($\Delta T = 0$) between the sample and the reference, is measured as function of temperature. [34], [10]. Thus by monitoring the differences in power supplied it is possible to evaluate the differences in enthalpy, ΔH. It can be used not only to follow the thermal behaviour but also to evaluate some important properties, such as glass transition temperature (T_g), crystallization temperature or melting temperature of the material.

The equipment used is a Q2000 (TA instruments, Hertfordshire, UK), it is shown in Figure 2.3.

Figure 2.3: Q2000 TA instrument (From TA instruments website).

This equipment consists of a measurement chamber in which two different materials are heated. The sample and the reference are heated in 2 different furnaces. Each furnace has its independent heater and thermocouple to control the energy supply and the temperature. The results are plotted as $T\ vs\ \Delta H$. The protocol used is a change of temperature from 20ºC to 140ºC with a ramp of 20ºC/min.

Typically, the glass transition temperature is identified as a gradual change in the Temperature vs heat flow curve. Particularly, glass transition phenomena does not occur instantaneously but

in a range of temperature. The glass transition temperature can be identify from the tangents of the heat flow curve, as explained in the picture 2.4:

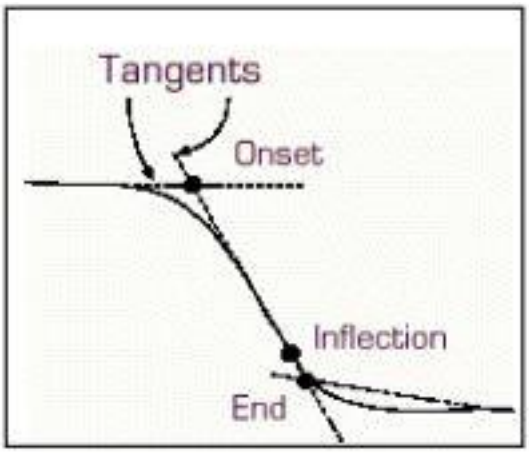

Figure 2.4: Glass transition temperature determination (From Q2000 TA Manual).

Glass transition temperature is usually determined as Onset T_g or inflection T_g. Onset T_g is the intersection of the first and second tangents, while inflection T_g is the portion of the curve between the first and third tangents with the steepest slope.

2.2.4. Dynamic Vapor Sorption

Dynamic Vapor Sorption (DVS) is a gravimetric technique that measures how quickly and how much of a solvent is absorbed by a sample, such as water absorption by a dry powder. The instrument does it by varying the vapour concentration surrounding the sample and measuring the change in mass that occurs due to this change. Water vapour is most commonly used, but it is also possible to use a wide range of organic solvents.

A scheme of a DVS system is shown in the picture 2.5:

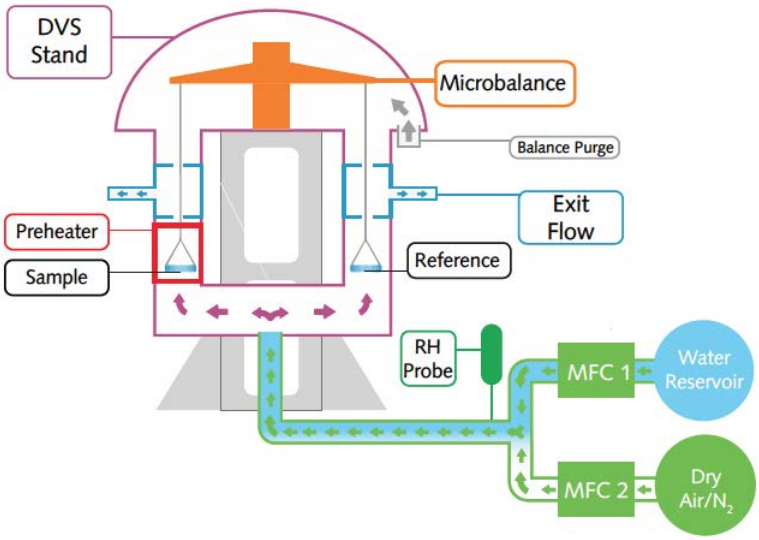

Figure 2.5: Scheme of a dynamic vapor sorption instrument. (From Surface Measurement Systems website).

The equipment used in this paper is the DVS Adventure (Surface Measurement Systems, London, UK).

It is equipped with a sample hung from a microbalance, a reference holder is place on the other side. An empty pan is used as reference. The microbalance is able to measure changes in the sample mass as low as 0.1 µg. The humidity of the carrier gas is changed by 2 mass flow controllers as set, while the weight of the sample is measured. From these data the instrument automatically evaluate the adsorption or desorption isotherm. The test is performed as follow:

- Initial drying of 1080 minutes to completely dry the sample
- 6 steps with a 15% humidity increase every 720 minutes

Relative humidity is evaluated as defined in equation 2.1.

$$\%RH = \frac{P_{water\ vapour}}{P_{saturated\ vapour}}\ x100 \tag{2.1}$$

From these data it is also possible to evaluate the moisture content of Maltodextrin as:

$$m.c = \frac{w_T - w_{dry}}{w_T} \tag{2.2}$$

Where w_T is the total weight measured when the equilibrium is reached after each humidity step and w_{dry} is the weight of the sample after the initial drying.

2.2.5. Moisture content evaluation

In order to compare the results obtained with the DVS the moisture content of maltodextrin is evaluated with the Ohaus MB35 moisture analyser (OHAUS CORPORATION, Parsippany, USA). The Moisture analyser consist of a heater device that heats a sample placed on an aluminium pan while it measure the loss of weight. A picture of the equipment is shown below:

Figure 2.6: Ohaus MB35 moisture analyser (From Ohaus corporation website).

The samples analysed were of 1.5±0.5 grams. The samples were heated until 105°C with a ramp of 20°C/min. The instrument automatically stops the test when the sample weight does not change for at least 1 minute. The samples were prepared in desiccators with different saturated solutions. Maltodextrin was placed on plastic pan with a thickness of 1mm and left

with a well-defined RH for 3 weeks. The desiccators were placed in a controlled environment at 20°C and were sealed up with silicon grease. The salt solutions used are reported above in Table 4.1. Furthermore, also the humidity chamber climacell (MMM group), is used in order to humidify the powders at different relative humidity.

2.2.6. Maltodextrin extrusion

Extrusion of Maltodextrin powders is performed with two different single screw extruders designed for 3D printing filaments production. The first extruder used was a single screw extruder model Noztek Pro Pellet & Powder Filament Extruder for 3D Printing (Noztek, Shoreham-by-Sea, BN43 6QB, United Kindom). The second extruder was the FilaFab PRO 350 EX (FilaFab, Bristol, United Kindom). Pictures of the two equipment are reported below:

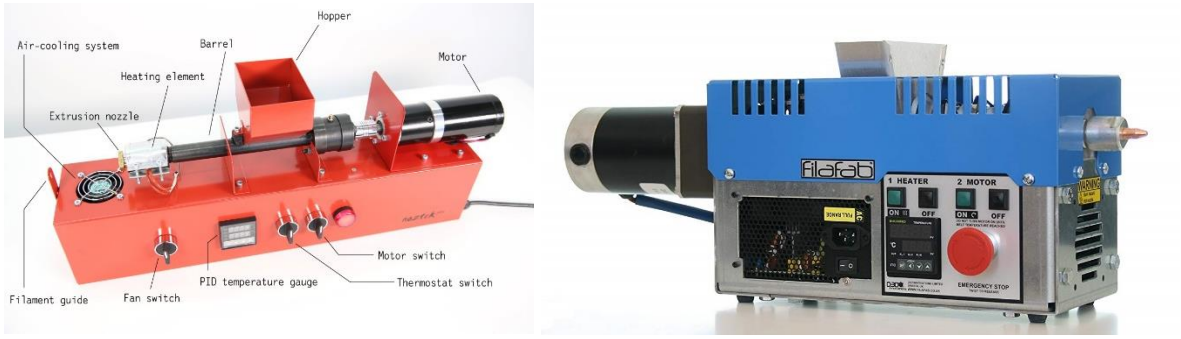

Figure 2.7: Noztek extruder on the right, FilaFab extruder on the left (Adapted from equipment websites).

The two extruders consist in the same main features, but, as explained in chapter 1 (§1.3), the design of the screw and the power of the Motor can influence the quality of the products. The main characteristics are provided in Table 2.2:

Table 2.2: Extruder characteristics.

Properties	**Noztek**	**Filafab**
Motor	24W	200W
Torque max	17Nm	45Nm
Screw Speed (Range)	15 RPM	5-30 RPM
Screw	Standard	Hardened cylinder and 3 stage screw,
Screw compression ratio	n.a	4.5/1
Nozzle diameter	1.75 mm	1.8 mm
Filament fan cooler	YES	YES

Maltodextrin 19 and 21 with different moisture content are extruded in a wide range of temperature and screw speed. Tests are performed in a range of temperature between 185°C and 140°C whereas the screw speed is set between 5 and 15 RPM.

2.2.7. Filaments post production treatment

Filaments are stored in a room with controlled temperature and humidity set at 22°C and 40% RH. In order to modify mechanical properties, post production humidification is performed. The filaments are stored for 24 hours at 70% RH inside a desiccator.

2.2.8. Filaments Characterization

Optical, dimensional and mechanical characterization on the filaments is necessary to establish their feasibility for FDM. As discussed above (§2.3), the 3D printer required filaments with a controlled diameter and good mechanical properties. For this reason, filament diameter is evaluated every 5 cm, using a digital caliper, in order to verify if expansion occurred.

The mechanical properties are estimated using a texture analyser TA.XTPlus, (Texture Technologies Corp. UK). The texture analyser was equipped with a load cell of 1Kg and a flat probe used to apply a compression load to the filament. The instrument is able to measure load, distance and time. Furthermore, the temperature was controlled using an oven and was set as 25°C in order to reproduce standard storing conditions of the 3D printer.

Filaments resistance and flexibility are investigated performing a pseudo 3 points bending test. The filament path inside the pulling system requires a deflection of 1.5mm. Hence, this method is selected because it is possible to deflect the filament, applying a stress, and verify its behaviour. The filament is fixed by 2 clamps and a concentrated load is applied at its centre. This method allows to compare the mechanical properties of ABS and maltodextrin filaments. It is performed to predict MD filaments behaviour inside the filament feeder.

The method is developed as follow: The clamps span is of 12cm, therefore filaments of 18cm are used. The target distance that the probe reaches is set as 6mm; the load applied to reach this distance is dependent of the filament flexibility. Furthermore, the Trigger force is set as 0.05N and the probe velocity is 2mm/s. The setup is showed in picture 2.8.

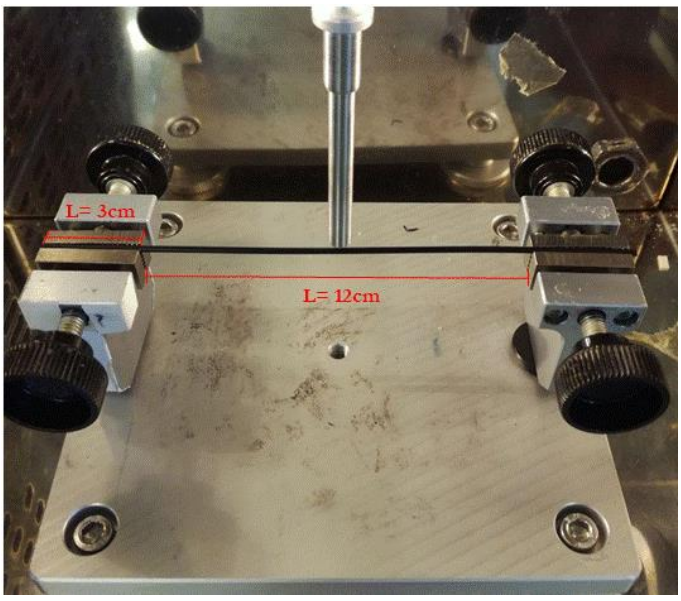

Figure 2.8: Pseudo 3 point bending test set up.

The test is performed both on MD extruded filaments and on ABS commercial filaments. Filaments are cut in order to get the defined length and, for each filament, three samples are tested. Mean and standard deviation are evaluated to verify properties homogeneity. Moreover, MD filaments properties are compared with ABS one to evaluate the suitability for FDM.

In order to assess the microstructural homogeneity of the filaments also an optical analysis is performed. An optical microscope (Olympus BX53M) is used in transmission mode. The filament is cut in pieces of approximately 1mm length and pictures of cross and side section are taken.

2.2.9. 3D printing by FDM technique

As mentioned above (§1.3.2), FDM is a 3D printing technique, in which a filament is melted and pushed through the nozzle to build up 3D structures layer by layer. This technique is wide used in AM and different printers are available in the market. For this project two printers are used. The first one is the Ultimaker 3 (Ultimaker B.V, Netherlands). It is suitable for complex structures printing with PVA support. Hence, this printer was used to produce soluble porous structures of PVA. These structures were used to performed dissolution tests as mentioned below (§2.2.11).

The printer set-up is shown in the picture 2.9.

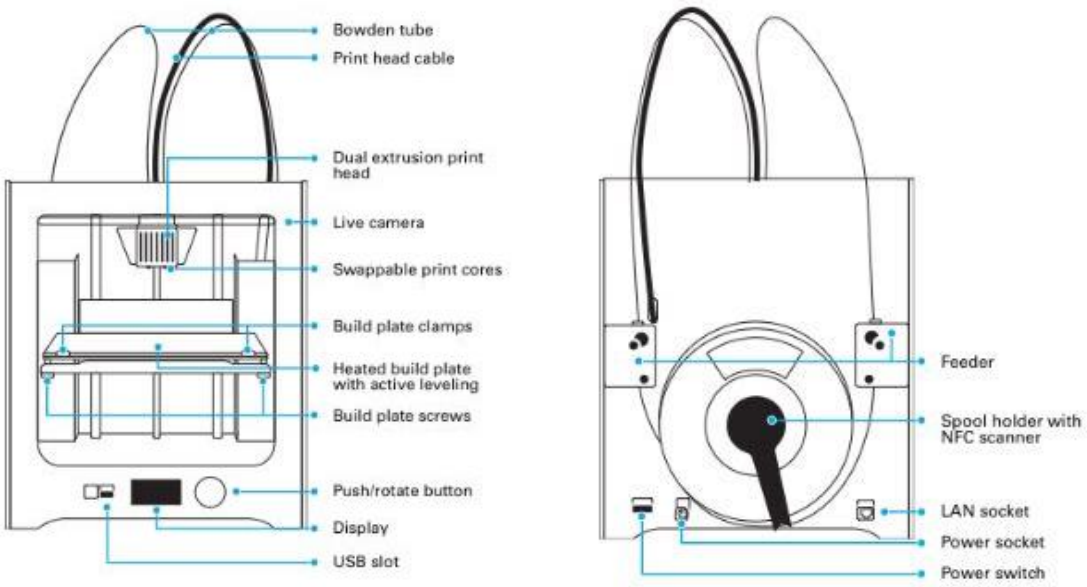

Figure 2.9: Scheme of the Ultimaker 3 3D printer (adapted from the 3D printer manual).

Figure 2.9 shows that the pulling system is placed in the back of the printer and the filament is driven to the print head by Bowden tubes. It means that the distance between the rollers and the entrance of the liquefier is high. Hence, this pulling system is not optimal for 3D printing of MD extruded filaments, which mechanical properties may be low.

Thus, a second printer, Raise N2 Plus (iMakr, UK) is also used. It is able to print porous structure from customized filaments thanks to its configuration showed in Figure 2.10.

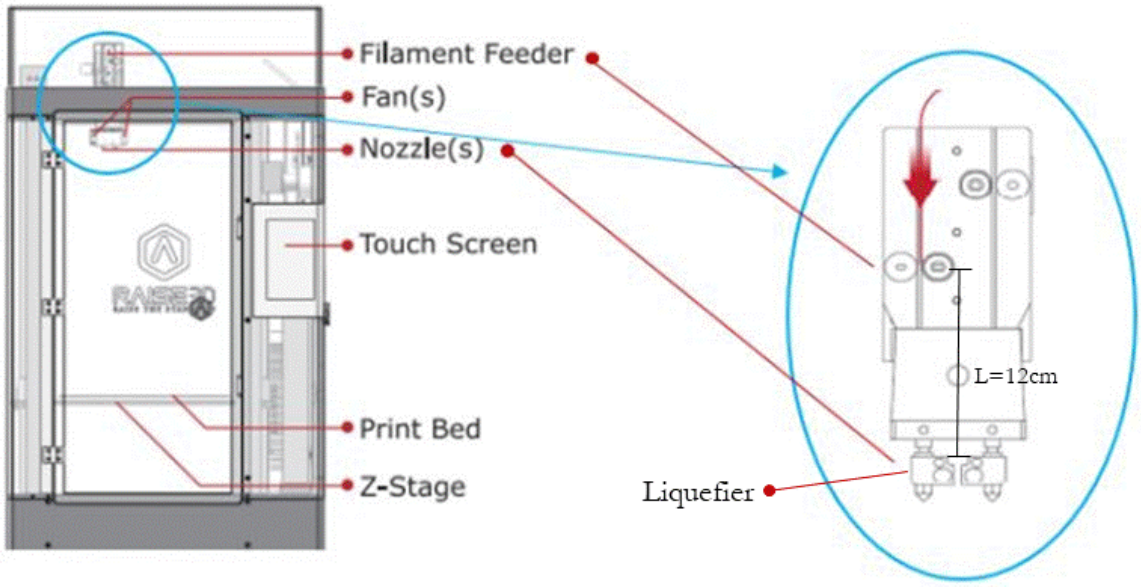

Figure 2.10: Scheme of the Raise N2 plus 3D printer (adapted from the 3D printer manual).

Figure 2.10 illustrates the different pulling system developed in the Raise N2. In particular, the distance between the rollers and the entrance of the liquefier is lower compared with the Ultimaker 3D printer. In this case the distance is of 12 cm, so the critical load is reduced, considering all the other parameters constant. Despite that, the pulling system shows an off-set between the rollers and the filament path in X direction as showed in Figure 2.11.

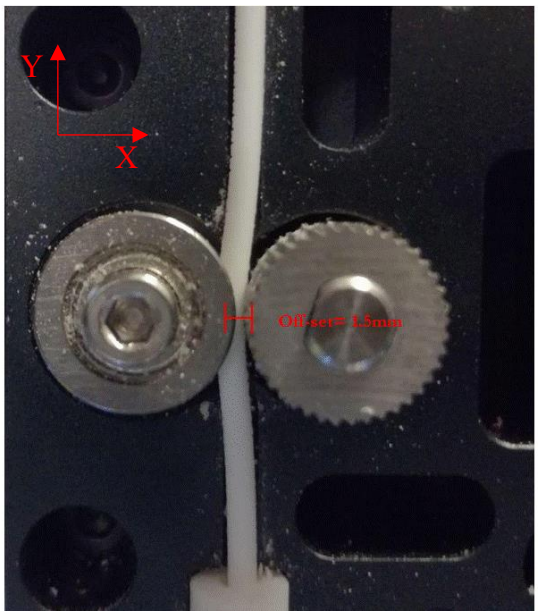

Figure 2.11: Detailed of the counter-rotating rollers.

The off-set is evaluated using a digital caliper and it is 1.5mm. So, as it can be seen, the filament has to be flexible in order to pass through the pulling system.

The most important specs of the two printers are reported in Table 2.3.

Table 2.3: 3D printers characteristics.

Properties	Raise N2 Plus	Ultimaker 3
Filament diameter	1.75 mm	2.85 mm
Nozzle Temperature	170-300 °C	180-280 °C
Plate Temperature	20-110 °C	20-100 °C
Nozzle Diameter	0.4 mm	0.4 mm
Layer Thickness	0.01 mm	0.02 mm
Printing Velocity	10-150 mm/s	30-300 mm/s
Traveling Velocity	150-300 mm/s	30-300 mm/s

2.2.10. 3D porous structures design

The design of 3D object is the first step in AM process. It is performed with a CAD software. In this project, the structures have been designed using FreeCAD, an open source software. The goal is to study the dissolution behaviour of the printed material and to analyse how it is affected by geometrical parameters. Cubes with holes of controlled dimensions were designed considering resolution limitations and research questions. An example is reported in figure 2.12:

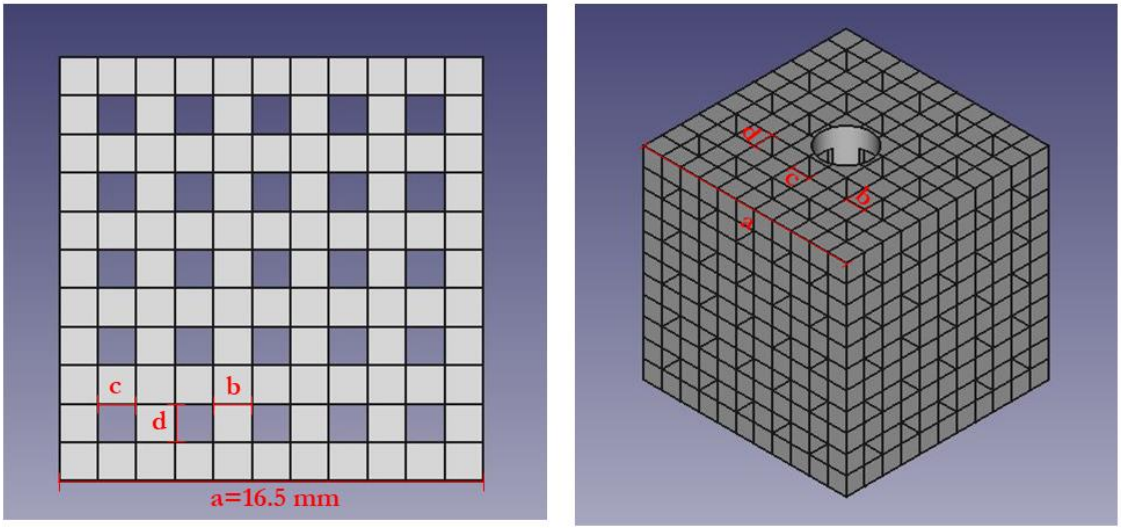

(a) Front view. (b) Side view.

Figure 2.12: CAD design of a porous structure (Geometry: ”Square 25”)

The picture 2.12 illustrate a cube designed. The distance between 2 holes is 1.5mm and the holes dimension is 1.5mm. Furthermore, a bigger central hole is present in the Z direction. It is necessary to fix the porous structures inside the dissolution vessel. The most relevant dimensions are:

- Total length of the cube, named *a*
- Width of material between 2 holes, named *b*
- Holes width, named *c*

- Holes height (same as c for square holes), called *d*
- Number of holes per face, named *e*

The most important geometries are divided in three categories:

A. Same holes dimensions, different number of holes (e.g. different mass and volume)
B. Same mass and volume, different holes dimensions
C. Same holes dimensions, different width of material between 2 holes

Physical parameters of the different categories are reported in Table 2.4.

Firstly, geometries related to the category A were designed and analysed to verify if the total length of the cube influences the dissolution behaviour. Geometries of category A are reported in figure 2.13.

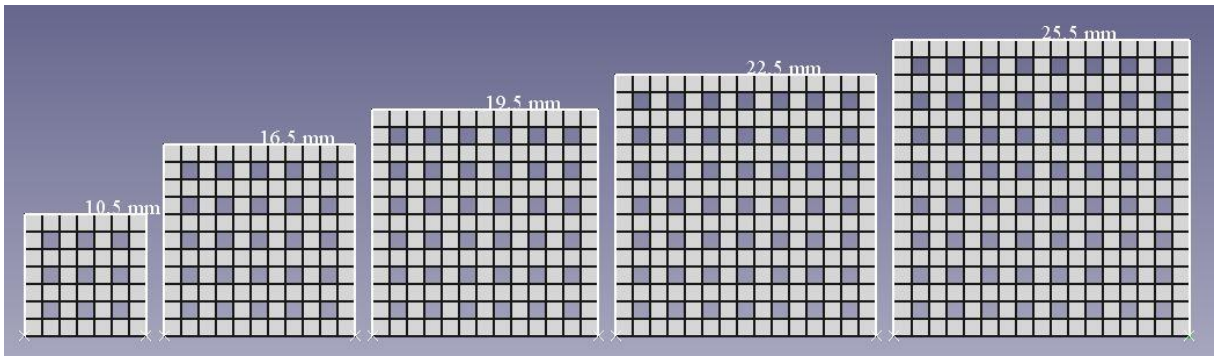

Figure 2.13: CAD design of porous structures, category A. From left to right: square9, square25, square36, square49, square64

Furthermore, in order to understand how dissolution is affected by mass distribution inside the volume (e.g. how dissolution is affected by interfacial area) other geometries were designed. An example is reported below:

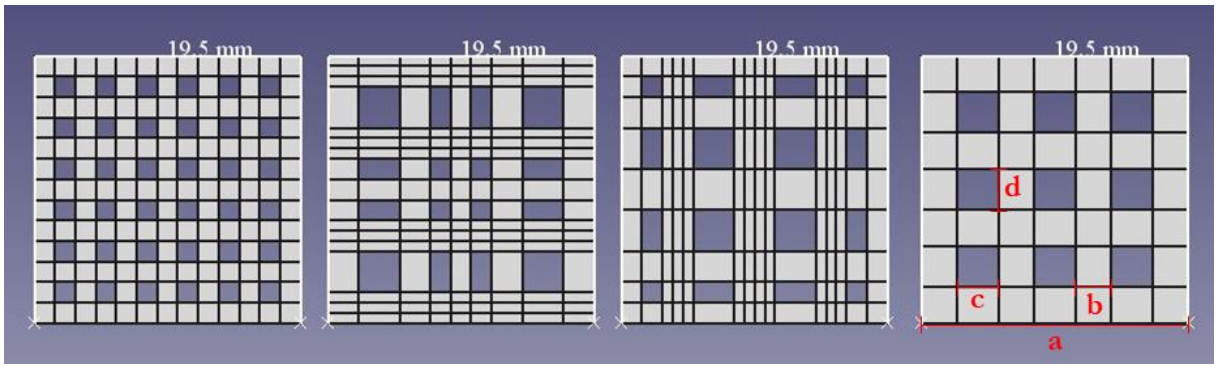

Figure 2.14: CAD design of porous structures, category B. From left to right: square36, G1, G2, G3.

The picture shows geometries G3 and G2. The overall volume is kept constant (a=19.5mm), while number and dimensions of the holes is changed. Moreover, also geometry G1 is designed. Considering geometries G1 and G2 dimensions b and c are equal but the mass is distribute differently inside the volume and the holes geometry are different.

Finally, 2 new geometries were designed to better understand the effect of the width between 2 holes in the dissolution behaviour. The CAD file screenshot is reported in Figure 2.15:

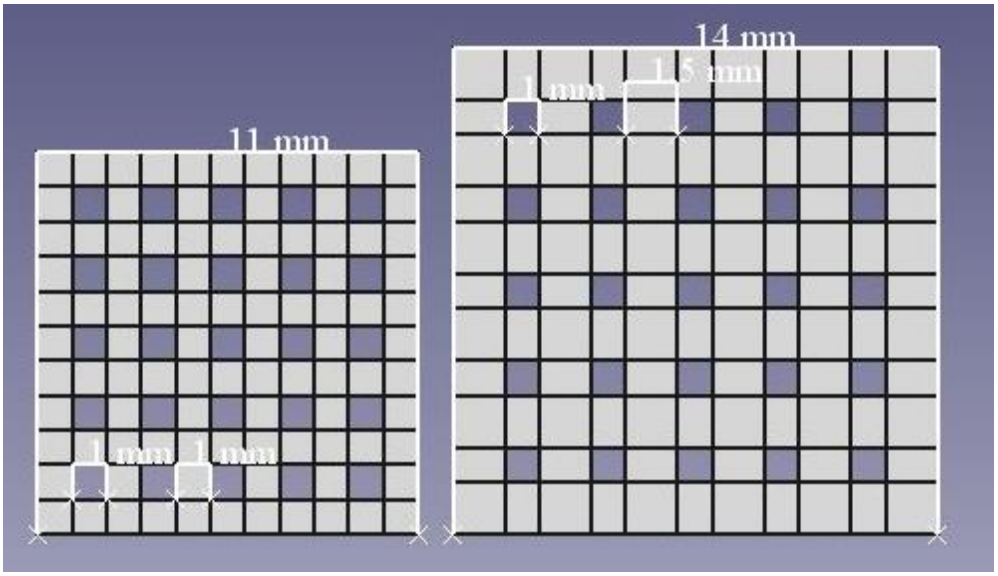

(a) Geometry G4 (b) Geometry G5

Figure 2.15: CAD design of porous structures, category C.

All the geometries and the main dimensions are summarized in Table 2.4:

Table 2.4: Physical parameters of designed structures.

Geometry name	Category	*a* [mm]	*b* [mm]	*c* [mm]	*d* [mm]	*e* [-]	Weight [g]
Square9	A	10.5	1.5	1.5	As c	9	0.77±0.05
Square25	A	16.5	1.5	1.5	As c	25	2.5±0.1
Square36	A-B	19.5	1.5	1.5	As c	36	4.4±0.2
Square49	A	22.5	1.5	1.5	As c	49	5.5
Square64	A	25.5	1.5	1.5	As c	64	10.3
G1	B	19.5	1.5-2.25-3	1.5-3	1.5-3	16	5.1±0.2
G2	B	19.5	1.5-2.25-3	1.5-3	1.5-3	16	4.8±0.1
G3	B	19.5	2.62	3	As c	9	4.8±0.2
G4	C	11.5	1	1	As c	25	0.81±0.05
G5	C	14	1.5	1	As c	25	2.2±0.05

Moreover, also the porosity of the different structures was evaluated. The definition of porosity is:

$$\varepsilon = \frac{V_p}{V_t} \tag{2.3}$$

Where V_p is the volume occupied by the pores, while V_t is the total volume. The total volume can be defined as:

$$V_t = V_p + V_m \tag{2.4}$$

Where V_m is the volume occupied by the printed mass. Substituting 2.4 in 2.3 and rearranging is possible to obtain:

$$\varepsilon = 1 - \frac{V_m}{V_t} \tag{2.5}$$

The total volume can be easily evaluated as:

$$V_t = a^3 \ [cm^3] \tag{2.6}$$

Where a is the total length of the cube as defined above. Concerning V_m it can be evaluated from the knowledge of the mass and of the density of the printed material as:

$$V_m = \frac{M_m}{\rho} \ [cm^3] \tag{2.7}$$

The density of PVA filaments was provided by the supplier, and checked by weighting pieces of filaments with a known length and diameter. The weight was measured using a Sartorius micro balance.

2.2.11. Ultimaker Cura software

Ultimaker Cura is an open source 3D printing software compatible with some 3D printers designed for FDM. It has been used to manage and optimize the printing process of 3D porous structures designed in the previous section (§2.2.10). As input, it requires an STL file with the 3D geometry of the object. As output, it gives the G-code that allows the production of the object.

The loaded geometry can be modified in terms of dimensions and orientation. Particularly, the model can be rotated in the three directions to modify the vertical grown and to improve the adhesion on the build plate. Moreover, the 3D object can be rescaled in one or more directions. The software also offers three different graphic visualization of the object:

- Solid view: The geometry of the object is shown
- X-ray view: The internal parts of the objects are shown and the different parts can be selected and visualized
- Layer view: all the layers are shown, it allows to simulate the printing movements, to control them and to verify how settings influence movements' selection.

Standard settings for printing can be used (e.g. high quality, normal quality, fast printing) but Cura also allows to control a wide range of parameters and to customize the printing process. All the parameters are categorize in eight sections that are reported below:

1. **Quality:** It regards the resolution of the object. The main parameter of this section is the layer height. It represents the vertical size of each layer. It affects resolution, printing movements and printing time. A higher layer height leads to a shorter printing time but it leads also to a lower resolution, vice versa a lower layer height produce a most precise object but an increase of the printing time.

2. **Shell:** It deals with parameters related to the external layers of the object. For instance, some parameters are the horizontal thickness of the external layers that are bottom, top and wall layers.
3. **Infill:** It involves the infill properties. Hence, it regards the section of the object between the external layers. The main parameters are the infill density and the infill pattern. The infill density is expressed as percentage of the maximum theoretical value. A higher infill density leads to higher mechanical properties and also higher printing time and costs.

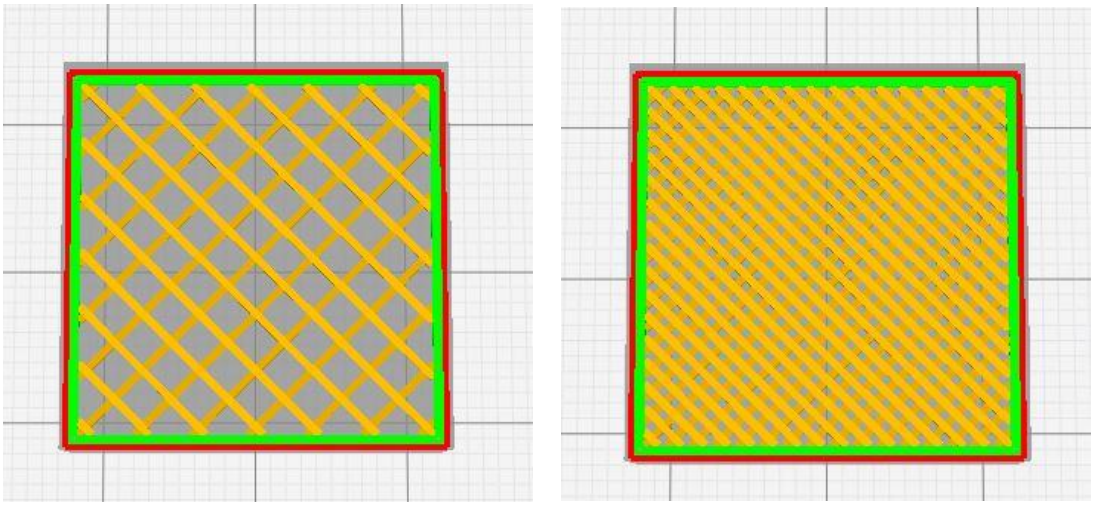

a b

Figure 2.16: Cube with different infill. (a=20%, b=50%)

4. **Material:** it controls the extrusion temperature and flowrates based on materials properties. Printing temperature is the most important parameter to guarantee a good melting inside the nozzle and an optimal deposition on the previous layer. It is related to the material type and for commercially available filaments it is usually suggested by the supplier.
5. **Speed:** it deals with printing speed of the different parts of the object. Hence, there are multiple speed that can be adjusted. It is advisable to set similar speeds to do not affect the structural and aesthetical quality in a negative way. It is usually sufficient to set the printing speed, then the software automatically sets outer/inner wall speed, top/bottom speed.
6. **Cooling:** it involves the fan and the cooling system. The ultimaker 3 printer is equipped with 2 fans placed near the nozzle. Cooling can be enabled to improve the deposition of the melted material.
7. **Support:** it is related to the design of the support, when it is necessary. The support material is usually a water soluble polymer (e.g. PVA).
8. **Build Plate Adhesion:** it controls the adhesion of the object to the build plate. Cura offers three different types of plate adhesion: Raft, Brim, Skirt.

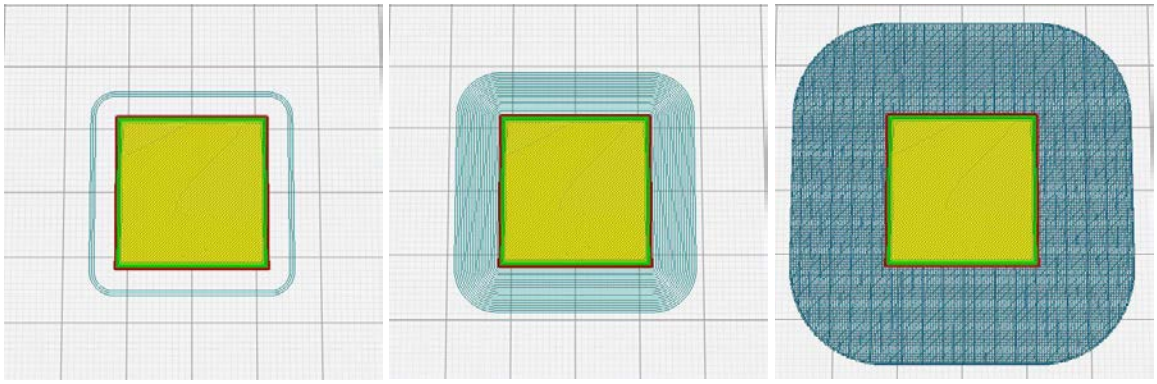

Figure 2.17: Build plate adhesion, from left to right: Skirt, Brim, Raft.

Skirt is simply a line printed around the model. Brim adds a single layer flat area around the base of the model. It helps to prevent wrapping. Raft adds a thick grid with a roof below the model.

A higher number of parameters can be modified through Cura, but they are usually related to the main one reported above and are automatically set by the software.

2.2.12. Dissolution test

Dissolution tests are very important and are commonly applied in the pharmaceutical field and in the food industry. They are used to simulate release of drugs, simulate food behaviour inside the mouth, assess the reconstitution of dehydrated beverages and control the quality of soluble materials.

The aim of these tests is to develop a simplified approach to provide some information on the behaviour of food 3D printed porous structure inside the mouth and to check material degradation. For instance, degradation or presence of impurities in the printed maltodextrin can be evaluated comparing powder dissolution with 3D printed object dissolution. As discussed before (§1.1), maltodextrin is a soluble material, so if there are huge differences in dissolution time or presence of residuals, it means degradation/contamination occurred during extrusion. PVA is used to develop the method.

The method is developed using a customized jacketed vessel, inside which refractive index (FISO, FTI-10, fiber optic conditioner) and conductivity probe (METTLER TOLEDO, FiveEasy Plus) are installed. The customized jacketed vessel was designed by Xin Yin Ong and used for powders dissolution test. In this project, it has been modified to use it for 3D porous structures dissolution. The dissolution set-up is shown in Figure 2.18:

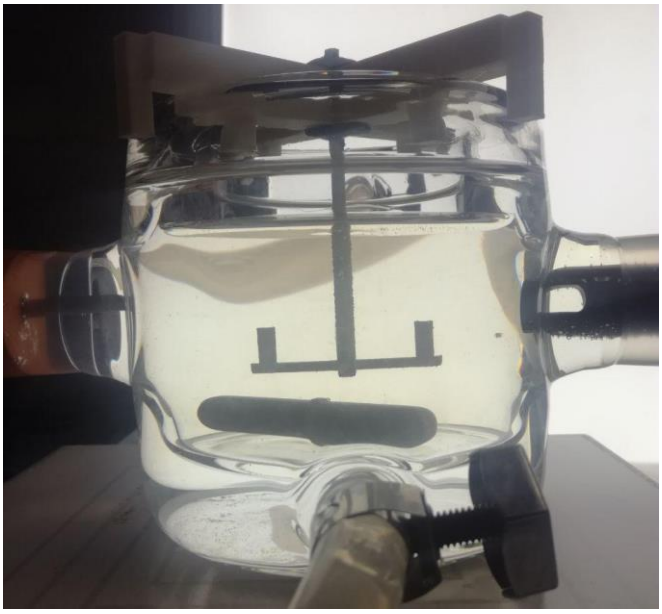

Figure 2.18: Dissolution test set-up.

The Figure shows the customized jacketed vessel and the support for the porous cubes. The probes were assembled on a 250mL jacketed vessel connected to a water bath in order to control the temperature at 37.5±0.5°. Magnetic stirring was performed using a pseudo cylindrical bar ($45 \times 8mm$) rotating a 450 rpm. The experiments were performed immersing the cube into 180mL of demineralized water. The cube was immersed slowly (around 20 seconds) to reduce air presence inside the pores. The acquisition frequency of the probes was set as $1s^{-1}$. Furthermore, the test was recorded, using a speed camera, with a recording time of 45 minutes. The conductivity data was used to follow the dissolution and compare the different geometries. Data are normalized to compare tests performed on cubes with different weight. Normalization is done using the equation 2.8.

$$N(t) = \frac{c(t)-c(0)}{c(\infty)-c(0)} \tag{2.8}$$

Where $N(t)$ is the normalized value at time t, $c(t)$ is the measured conductivity at time t, $c(0)$ is the measured conductivity at time 0 and $c(\infty)$ is the measured conductivity at infinite time.

2.2.13. Chocolate printing

The chocolate is prepared for 3D printing by first tempering it in a ChocRevolation2B Temperer, (Vantage House, UK) which consists of an air heated, rotating bowl and a dividing baffle. The chocolate is printed using the hot melt extrusion 3D printing technique with a Choc Edge 2.0 3D Chocolate Printer (iMakr, UK).

The printer operates by using a corkscrew to push on a 30 mL syringe plunger by a fixed displacement and allowing chocolate to pass through the 0.8 mm nozzle, which is wrapped in a heated jacket; the temperature can vary from 20 to 50 °C. Melted chocolate is deposited on a building plate forming layers which then solidify. Each 2D layer is built by repeated deposition of extruded material, called roads, along paths defined by the algorithm.

The printing head is able to move on the X axis extruding while translating or translating without extruding, and on the Z axis pulling up and moving down the nozzle without extruding. On the other hand, the building plate can move on the Y axis.

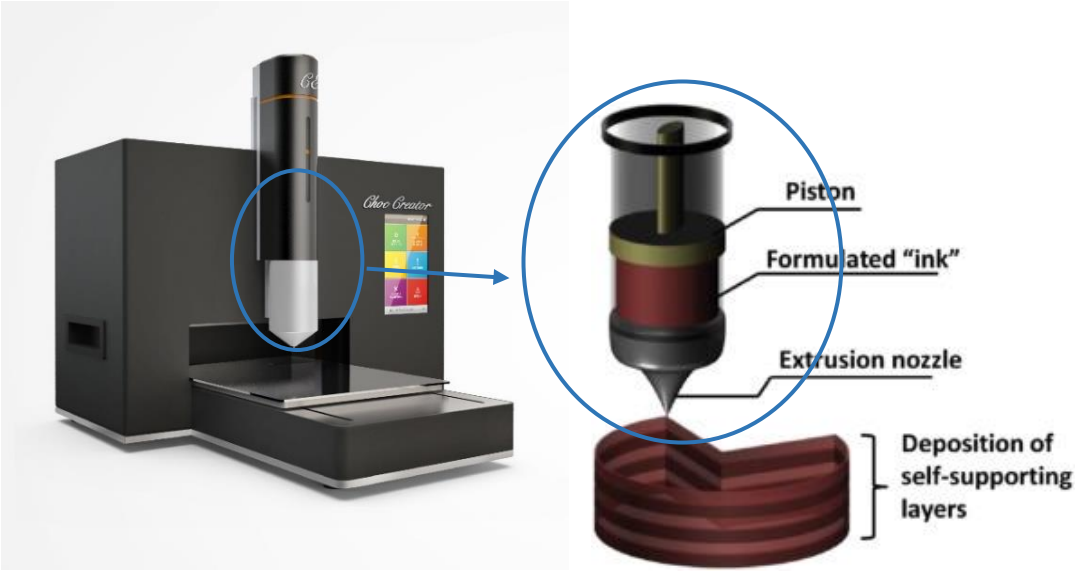

Figure 2.19: ChocEdge 2.0 3D Chocolate Printer (Rearranged from printer website and [11]).

As discussed in the introduction only G-codes of the chocolate printer are analysed in order to cooperate with the master students.

2.2.14. G-code

G-code is the language of 3D printers. It is a numerically controlled programming language made of a series of command. Each printer has its own G-code even if all G-codes are similar.

As explained above (§1.3), FDM technique starts with a CAD file, which is usually converted in stereolithography file (.stl). This file is opened with the printer software, in which all parameters can be set, and a G-code file is generated. The software is also called Slicer because it "slices" the CAD file in different layers and splits the realization of a designed object in a series of simple, single operations.

G-code contains all the information on how the object is printed:

- Printing velocity
- Travel velocity
- Layer thickness
- Feed rate
- Nozzle temperature

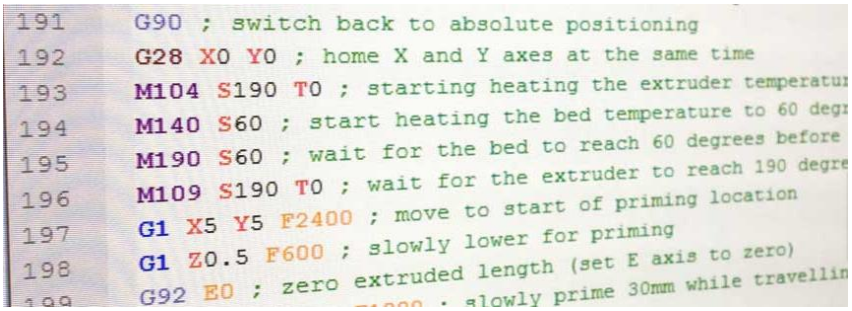

Figure 2.20: G-code example.

All the parameters described above influence the quality of the printed object, therefore, it is necessary to control and select them properly. Optimization of the settings is not assessed in this project, where settings suggested by master students were used.

The G-codes were generated using Choc-Edge software from the CAD files. Next, the G-codes were modified using Notepad in order to improve them. Finally, new G-codes were generated from 2D (X-Y) coordinates using Matlab in order to develop more efficient G-codes able to reduce printing time and to increase printing quality.

The geometries tested were selected and designed such that the printer would be tested at simple as well as complex geometries. These geometries included:

- Straight Line (100mm in Length), used to study printing velocity and the extrusion of a single layer.
- Dashed Line (110mm total Length, made of individual dashes 10mm in Length) used to verify the ability of the 3D printer to finish extruding without dripping.
- Cylinder (20mm Diameter, 30mm Height) to study the capability of the bottom layer to support a high weight.
- Star (33mm Length [point to point, left to right], 10mm Height) to verify the accuracy of the printer on the realization of sharp angles.
- Leaning Tower (20x20mm Base, 10x10mm Tower, 20mm Height, 70° from floor) to study the capability of the bottom deposited layer to support an higher weight of layers which is slightly translated.
- Bridge (Two 10x10mm Vertical Towers of 20mm Height, 20mm apart, connected by a Single Strand of 30mm Length) to verify the ability of printing a suspended layer under the gravity effect.

Low printing quality and non-streamlined movements were reported for the geometries “star” and “dashed line”. The development of the Matlab tool in order to generate G-codes was developed on these geometries and then applied to generic simple geometries. The CAD file of the star geometry is reported in picture 2.21.

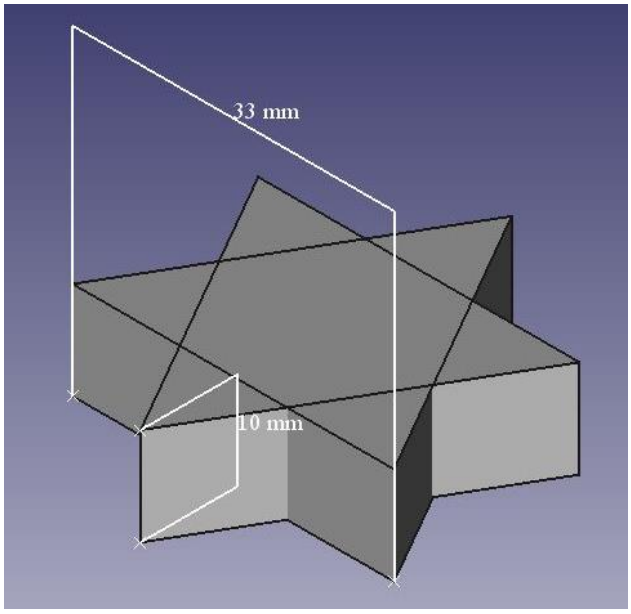

Figure 2.21: Star geometry CAD file.

Figure 2.18 shows the CAD file of the star designed to generate G-codes using the choc-edge software. Moreover, from the geometrical dimensions reported in the file, 2D coordinates used in the Matlab script are extracted.

Chapter 3

Maltodextrin characterization and extrusion

In this chapter, the results obtained from the experiments are illustrated. Firstly, results related maltodextrin characterization will be described. Secondly, details of powder extrusion and related issues will be explicated. Finally, filament characterization and 3D printing will be described.

3.1. Particle Size Analysis

Particle size distribution analysis is performed as described in chapter 2 (§2.2.1) on Maltodextrin 19, the results are reported in the picture 3.1.

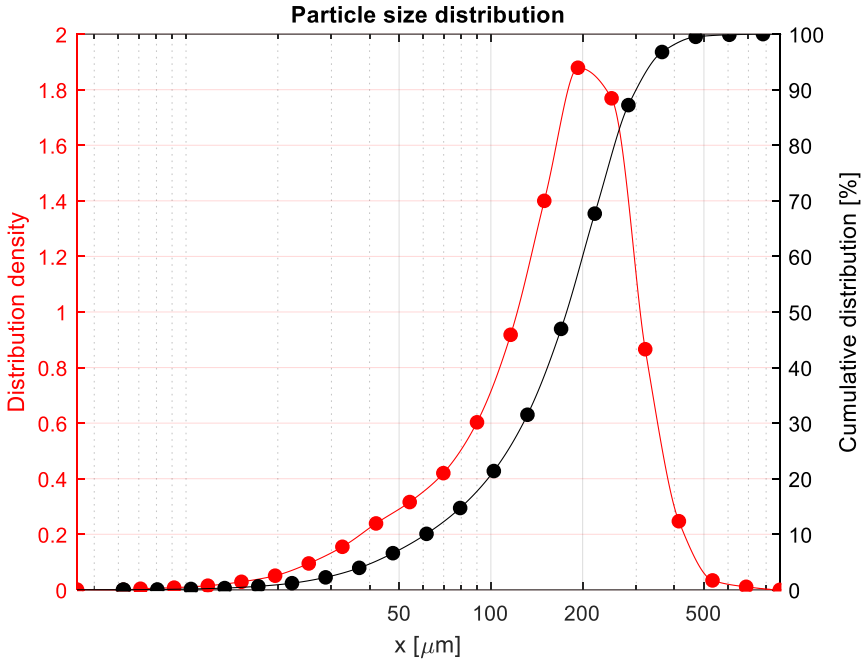

Figure 3.1: Particle size distribution of MD19,

The Figure illustrates the particle size distribution both as probability and cumulative distribution function. The probability, reported in the yleft-axis is evaluated in terms of volume q_3. It means that the image analysis software evaluates the equivalent diameter defined as the diameter of a sphere having the same value of the particle project area captured by the speed camera. Afterwards, the volume is evaluated from the equivalent diameter. The two distributions allow to characterized quantitative the particle size. The probability density function shows the unimodal distribution of the powder with a peak around 200 μm, while the cumulative distribution allows to evaluate percentage value, such as d_{10}, d_{50} *and* d_{90}. For example d_{90} represents the particle diameter at which 90% of the sample's mass is contained.

Furthermore, from the cumulative distribution also the span can be evaluated. It is used in order to evaluate the width of the particle size distribution and it is defined as follow.

$$Span = \frac{d_{90} - d_{10}}{d_{50}} \tag{3.1}$$

The main percentages and the span are reported in the Table below.

Table 3.1: Percentage values of PSD.

d_{10} [µm]	d_{50} [µm]	d_{90} [µm]	Span [-]
61.18	177.21	306.41	1.384

3.2. Dynamic Vapor Sorption

As mentioned before (§2.2.4), the Dynamic Vapor Sorption is a very precise technique used to evaluate the sorption isotherm of materials. It is an important information because it allows to understand the powder behaviour in different humidity conditions. As already discussed in the previous chapters, moisture content influences maltodextrins physical properties, such as glass transition temperature. Therefore, the knowledge of the sorption behaviour allows to correlate the moisture content of MD powders with the RH of the environment. The result of the test performed on a sample of 9.3085 mg is shown in Figure 3.2.

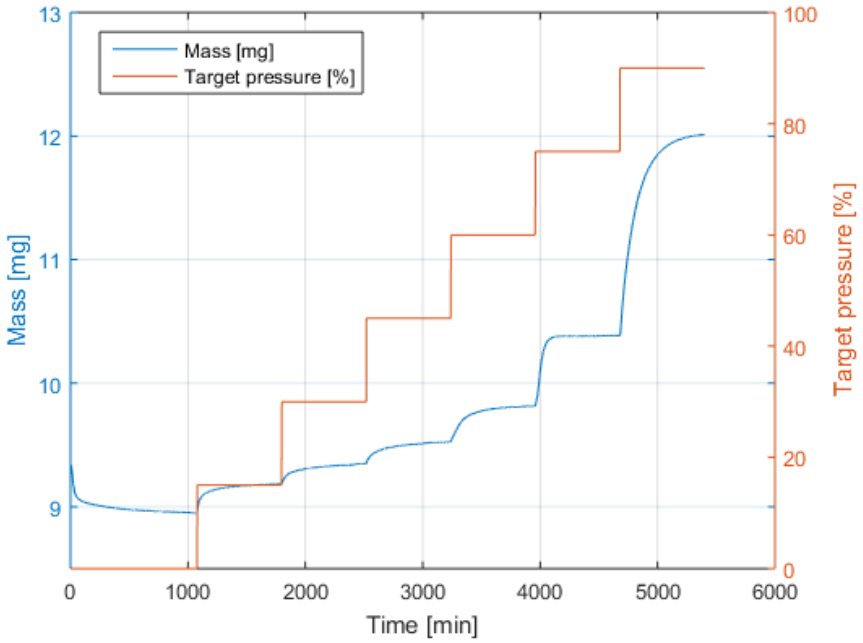

Figure 3.2: Kinetic data for moisture sorption of MD19 on the DVS instrument.

Figure 3.2 illustrates the behaviour of MD19. The sample used was pre-dried in an oven at 70°C for 3 days. Despite it, 1100 hours at 0% RH were set in order to have a completely dry powder. Afterwards, the relative humidity was increased as describe in chapter 2 (§2.2.4). In the first 4 steps there is an increase of mass, as expected, and equilibrium is reached. In the

75% RH step and in the 90% RH step the increase of the mass is higher related to the previous steps, meaning that a higher vapour sorption occurs.

The moisture content is evaluated at each step, after the equilibrium is reached, using Eq. 2.1. The results obtained are plotted in Figure 3.3 and compared with the data obtained by Castro et al. [4]

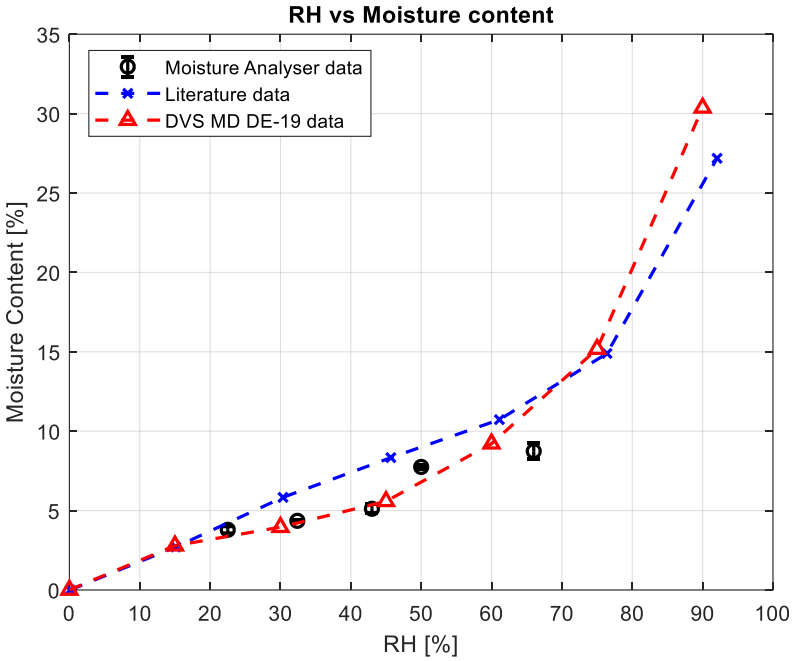

Figure 3.3: Comparison of RH vs moisture content data obtained with different techniques.

The Figure compared the data obtained by Castro et al. [4] with the one obtained from the DVS and the moisture analyser. It can be seen that the moisture content obtained with the moisture analyser are similar to the one obtained with the DVS. A significant difference is present in the data obtained at 65% RH. Furthermore, the measured moisture content at 65% RH has the highest standard deviation.

Concerning the comparison with the literature, the 2 curves have a similar shape, but significant differences are present at 30 and 45% RH. One of the reasons explaining such differences is the botanical origin of maltodextrin and the type of hydrolysis. In fact, even if the supplier is the same, significant differences in the results can be found as mentioned by Castro et al. [4].

3.3. Moisture content evaluation

As mention in chapter 1 (§1.1), the moisture content is one of the key parameters in order to characterized Maltodextrin properties. The capability to predict and to control the moisture content is very important, for this reason also moisture content analyses are performed. Samples of maltodextrin were humidify, both using the humidity chamber and the desiccators prepared with the salt solutions reported in chapter 2 (§2.2). The samples were tested 3 times, mean and standard deviation were evaluated and compared with the one obtained from the

TGA as reported in Table 3.2. Moreover, the results were compared with the DVS and the literature one [4] as reported in Figure 3.3.

Table 3.2: Moisture content at equilibrium extrapolated from DVS result.

RH[%]	Moisture content [%] (Moisture analyser)	Moisture content [%] (TGA)
22	3.79 ± 0.19	4.12
32	4.36 ± 0.04	4.77
43	5.11 ± 0.29	-
50	7.75 ± 0.13	-
65	8.74 ± 0.50	9.10

Table 3.2 compares the data obtained with the moisture analyser and the TGA. The moisture content evaluated with the TGA is slightly higher for all the RH analysed. The differences between the three techniques used to evaluate the moisture content can be also related to the fact that a perfect homogeneity in the water distribution inside the powder is difficult to reach.

3.4. Thermogravimetric Analysis

Thermogravimetric analysis (TGA) is a technique performed to evaluate the temperature at which degradation occurs under heating and how the atmosphere influences it. The results are reported in the plot below.

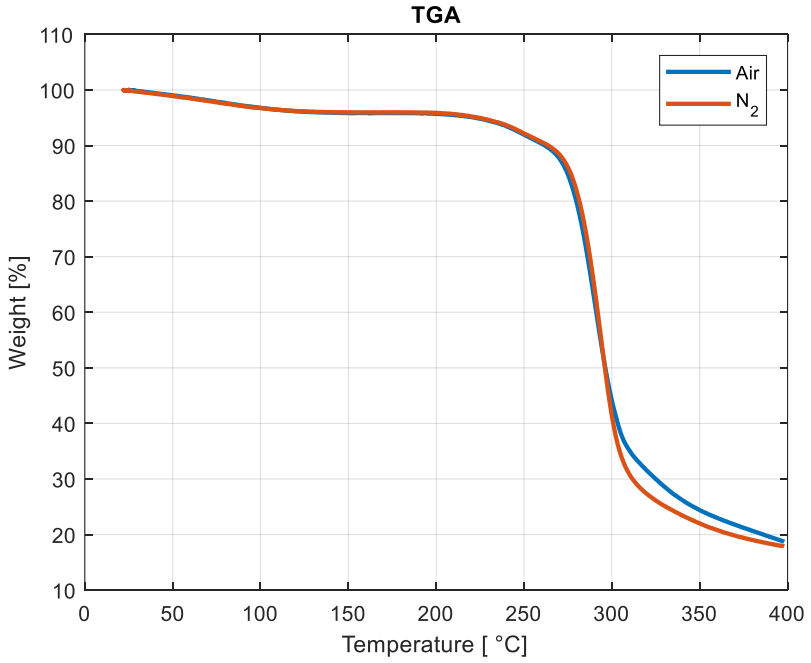

Figure3.4: MD 19 degradation in Air and N_2 atmosphere.

The Figure shows an initial loss of weight due to evaporation of water between 50 and 150°C. Maltodextrin degradation occurs from 250 to 400°C and in this region the major weight loss is measured. Furthermore, the behaviour is very similar in Air and N_2 environment. Hence, the

presence of oxygen does not enhance the decomposition, which in fact occurs due to thermal decomposition of long molecular chains. The total degradation of maltodextrin to the ash content was not completed since the maximum temperature reached was 400°C.

Using the same protocol, described in chapter 2 (§2.2.3), TGA was used to evaluate the moisture content of the powders stored at different controlled RH environments. In order to highlight the loss of weight due to water evaporation only the behaviour between 20 and 180°C is plotted.

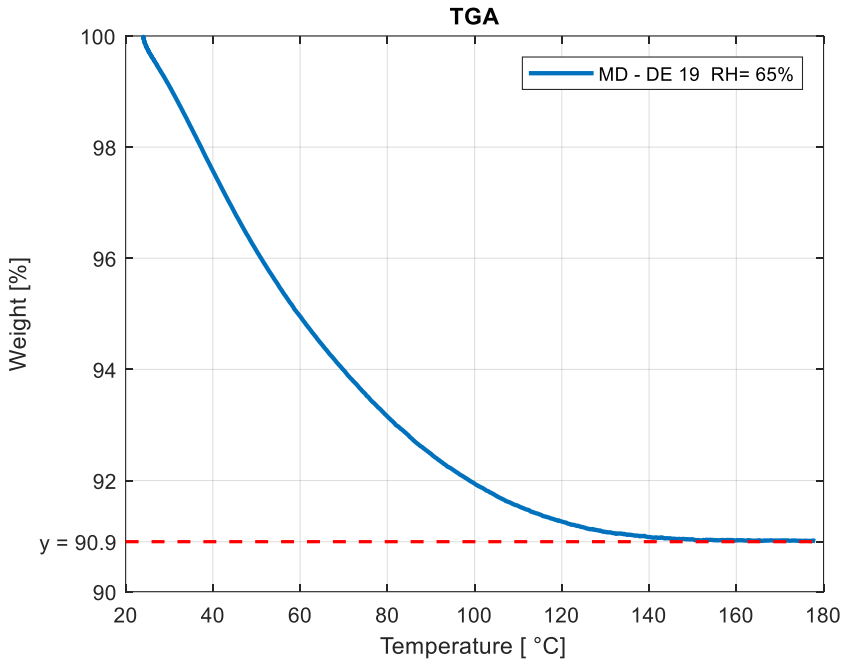

Figure 3.5: MD 19 stored at 65% RH TGA in Air.

The Figure illustrates the data of the TGA performed on a sample of MD19 stored in a desiccator at 65% RH for 2 weeks. The lost in weight in the range of temperature reported in the plot is equal to 9.1% and it is due to the water evaporation.

Data obtained from samples stored at different RH are reported in Table 3.2 and compared with the data obtained with the moisture analyser.

3.5. Differential Scanning Calorimetry

Differential scanning calorimetry is performed on MD19 with different moisture content. Two repetition are performed at each moisture content. Data are analysed with the TA instrument software and glass transition temperature is evaluated as explained in chapter 2 (§2.2.3).

The knowledge of the glass transition temperature is fundamental to evaluate the powder behaviour. In particular, the moisture content influences the glass transition temperature and consequentially the state of the powder. Once the T_g is lower than the material temperature, due to an increase of the moisture content or an increase of the material temperature, the transition between the glassy state and the rubbery state occurs. In the rubbery state molecules

are able to flow and move into the gap between neighbouring particles [7]. Moreover, in this state the powders can start to act like a viscous fluid.

Results obtained at 22% RH are reported below.

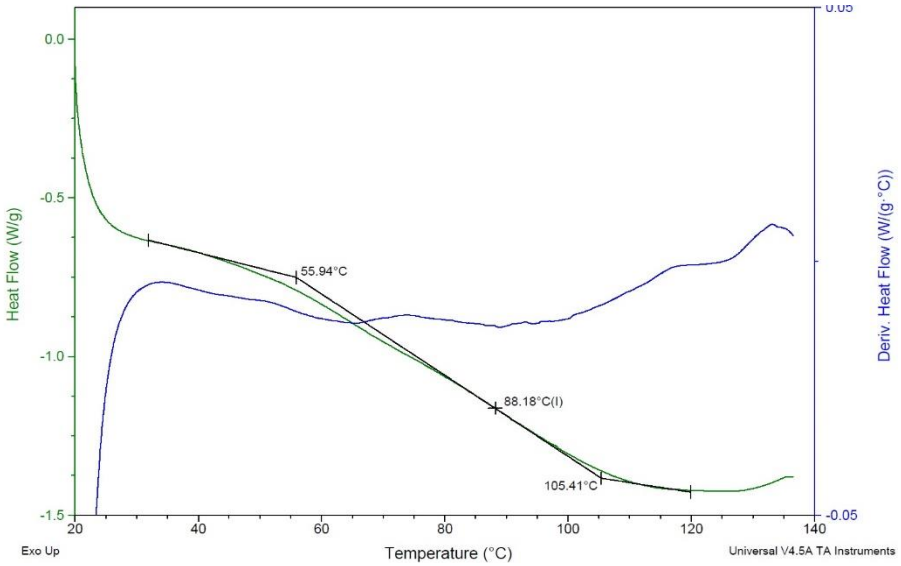

Figure 3.6: DSC analysis of humidified maltodextrin at 22% RH and T = 21°C. Sample 1

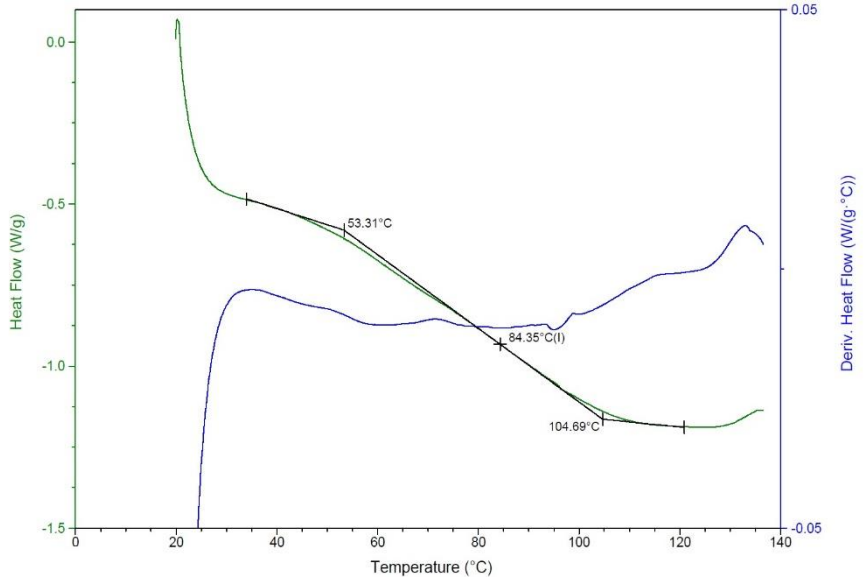

Figure 3.7: DSC analysis of humidified maltodextrin at 22% RH and T = 21°C. Sample 2

Figures illustrate both heat flow and derivative heat flow signals. Three tangents have been found between the two peaks of the derivative signal. Glass transition temperature is evaluated as describe in chapter 2 (§2.2.3) as onset T_g and inflection T_g. Samples at 22, 32, 43, 50, 65% RH are analysed. The graphical results of all the tests are reported in appendix A, while the related moisture content is calculated with the moisture analyser and it is reported in Table 3.2. Onset and Inflection T_g are reported in Figure 3.8. Moreover, the obtained data are fitted using the Gordon-Taylor equation (Eq. 1.3).

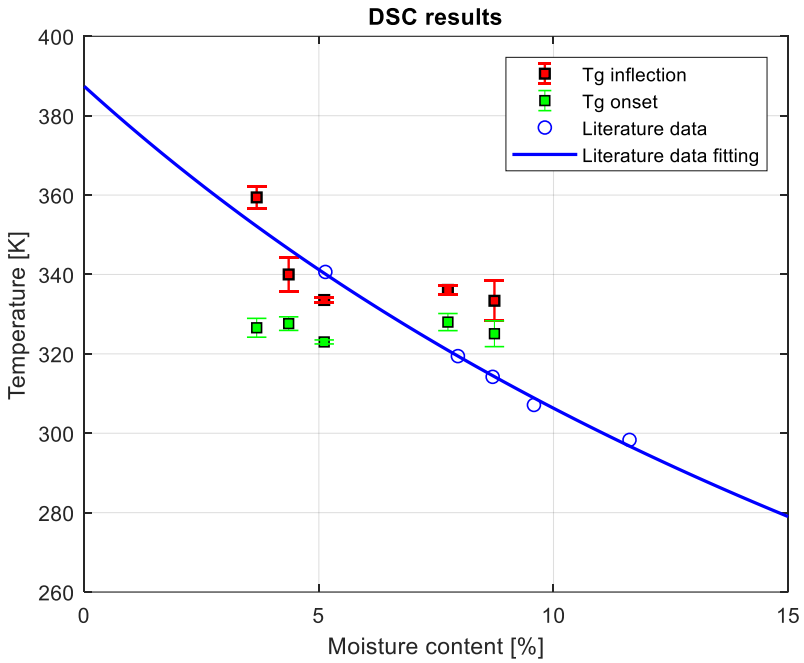

Figure 3.8: Comparison between obtained results and literature data [1].

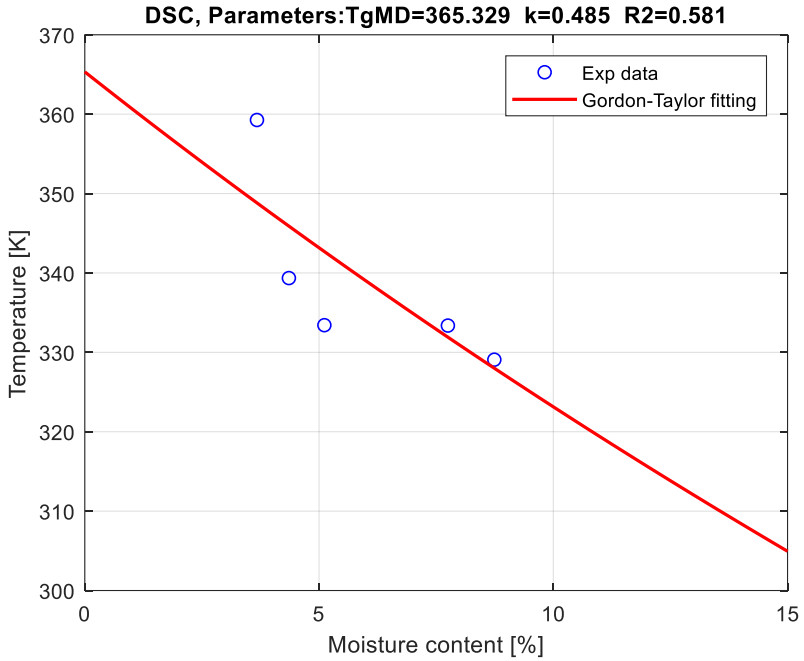

Figure 3.9: Fitting of the Inflection Tg using Gordon-Taylor equation (Eq.1.3) .

Figure 3.9 and illustrate the fitting of the data obtained from the DSC, using the Gordon-Taylor model (Eq. 1.3), while Figure 3.8, illustrates the results obtained and compares them with the one available in the literature [1]. It must be remembered that Avaltroni et al. [1] evaluated the glass transition temperature with a different technique.

Concerning the data obtained from the DSC, it can be seen that onset T_g (green squares) is not influenced by the moisture content, while, regarding inflection T_g (red squares), there is a

significant difference between the data at 3.8 and 4.35% moisture content, but the T_g measured at higher moisture content is almost constant.

Moreover, the data obtained at RH equal to 22%, 32% and 43% (3.8, 4.35, 5.1% moisture content) are comparable with the data obtained by Avaltroni et al. [1], while the data obtained at RH equal to 50% and 65% are different from the literature one.

The fitting shown in Figure 3.7 is not good and the R^2 is 0.581. Moreover, the glass transition temperature of the dry maltodextrin reported by Avaltroni et al. [1] is 112°C. The fitting performed on experimental data lead to a dry MD T_g of 92°C. Hence, a significand difference is present. The low R-square and the difference in the dry T_g can be due to the low reliability of the data obtained at higher moisture content.

Therefore, samples at 65% RH were analysed four time instead of two to exclude measurement errors and in order to further analyse these data the heat flow measured on sample stored at different RH are reported in Figure 3.10.

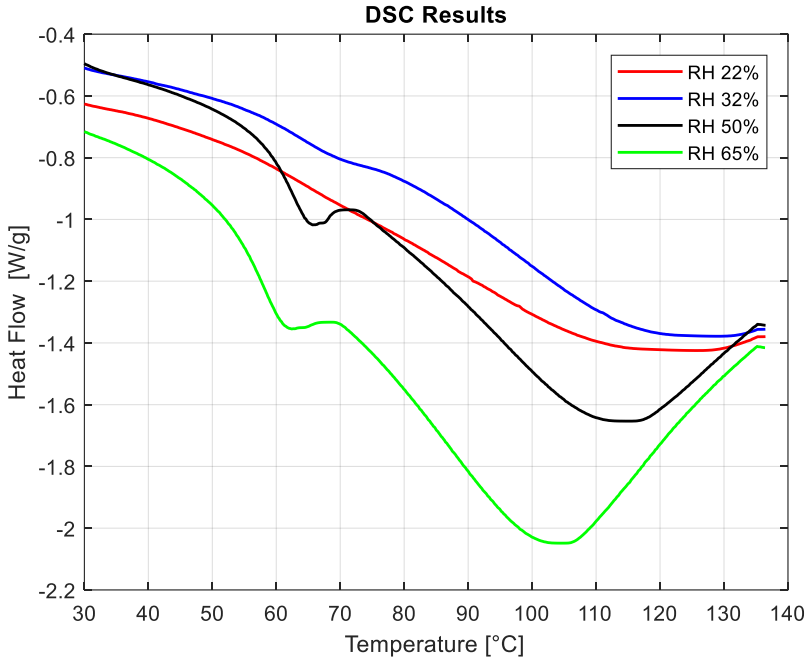

Figure 3.10: Heat flow signal of sample stored at different moisture content.

Figure 3.10 illustrates the heat flow as a function of the temperature. The curves at 50% and 65% RH show an endothermic peak in the heat flow around 60°C related to the enthalpy relaxation phenomena. In the curves at 22% RH and 32% RH the phenomena is less visible. Relaxation phenomena can affect T_g evaluation. Hence, some authors [7], evaluated the glass transition temperature at the second upscan to reduce enthalpy relaxation.

In order to improve the results, the protocol was changed and it was set similar to the one explained by Descamp et al. [7]. Particularly, after the first heating, a cooling between 140°C and 20°C and a second heating with the same ramp were performed. The aim of this protocol

was to try to evaluate the T_g from the second upscan as performed by Descamp. The result for the test performed at 65% RH is reported in the picture 3.11.

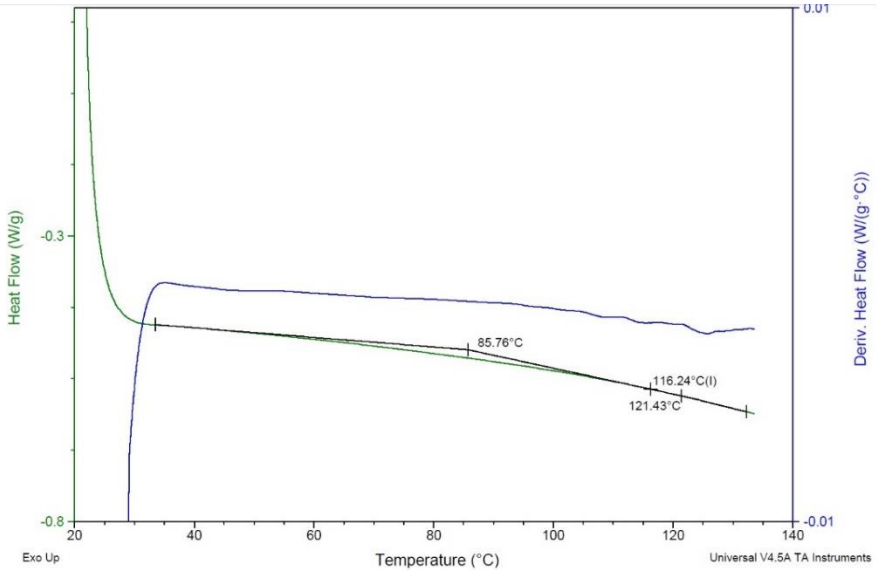

Figure 3.11: DSC analysis of humidified maltodextrin at 65% RH and T = 21°C. Second upscan.

Figure 3.11 shows the signal measured at the second upscan. Glass transition temperature is evaluated as explained before, but it can be seen that there are not two peaks in the derivative signal, therefore the signal is considered low. Moreover, the T_g is higher than the one evaluated during the first upscan and completely different from data obtained in the literature for this moisture content. Hence, this protocol does not allow to improve the quality of the results.

Despite the test were performed on samples stored at different RH, the inflection glass transition temperature evaluated at the second upscan resulted almost constant for all the tests and equal to 111.72 ± 4.82 °C.

The result is comparable with the one obtained in the literature [1], hence that value can be considered as the glass transition temperature of dry maltodextrin. In fact, even if the sealed hermetic pan, the water evaporation affected the results and it was not possible to measure the glass transition temperature of wet maltodextrin from the second upscan. Moreover, a significant difference is present between the T_g evaluated with the DSC and the T_g obtained from the fitting shown in Figure 3.9. This difference confirms the low precision of the T_g evaluated at high moisture content.

3.6. Maltodextrin extrusion

Extrusion can be considered the challenging step of this research work. In order to extrude the maltodextrin two extruders with different characteristics were used. For this reason the results obtained will be discussed separately.

3.6.1. Noztek extruder

The noztek extruder is a lab-scale extruder designed for polymers extrusion. Different polymers can be extruded to obtain filaments suitable for 3D printers.

Maltodextrin extrusion is performed through a trial and error procedure based on the knowledge acquired from literature review and powder characterization. In the literature review, the extrusion temperature is usually 50-90°C higher than the glass transition temperature. Moreover, it has been reported (§1.2) that plasticizers, like water, can help the extrusion process and that a twin-screw extruder designed to induce high-energy impact can be more efficient for starch extrusion. Yeung et al. [40] reported that the melting of starch is obtained with a gelatinization process.

As mentioned in Table 2.2, the extruder is equipped with a 24W motor that can generate a torque of 17Nm. It is equipped with a 1.75mm nozzle. The screw speed cannot be controlled and it is set at 15RPM. On the other hand, two electrical resistant allows to heat the compression section, the metering section and the nozzle and to control properly the temperature. Concerning the feed section it is quite long and it occupies almost half of the total length as shown in the picture below.

Figure 3.12: Details of the barrel and of the screw of the noztek extruder.

Before every test, maltodextrin moisture content was evaluated as described in chapter 2 (§2.2.5). The first trial of extrusion was performed using maltodextrin stored in a hermetic batch provided by the supplier. The moisture content was 4.8 ± 0.2 % . From the knowledge acquired in the previous paragraph (§3.5), the glass transition temperature of the powder can be assessed around 60°C. Despite it, it has been decided to heat up the extruder for 15 minutes at 180°C and then to start the extrusion process at that temperature to reduce viscosity of the maltodextrin and to unload the motor burden. The temperature has always been set lower than

185°C in order to be far from the degradation temperature that has been found around 250°C. The obtained filaments are shown in Figure 3.13.

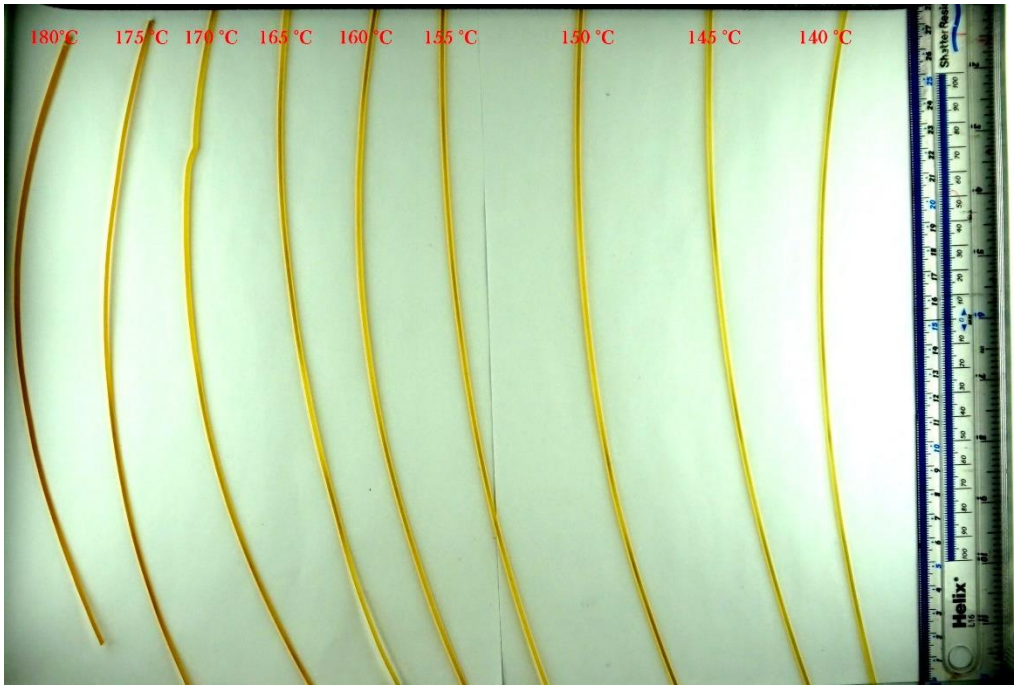

Figure 3.13: MD DE-19 filaments.

The picture illustrates filaments obtained in a range of temperature between 180°C and 140°C. The filament obtained at 180°C has a dark colour. It can be related to degradation of the maltodextrin. Shearing and viscous dissipation can lead to hot spots in which a partial degradation occurs. At lower temperature degradation is less visible.

It was not possible to further decrease the temperature due to the high viscosity of the maltodextrin. In fact, the motor power was not sufficient to keep the rotational speed of the screw constant. It has to be also mentioned that, during the test, the screw stopped to rotate. This increased the resident time inside the extruder enhancing degradation phenomena and does not allow to obtain a consistent number of filaments.

Moreover, to proof the poor quality (degradation) of the filaments a dissolution test was performed on a 5cm length sample. The test was performed at ambient temperature using 180mL of mineralized water (Evian water). The mixing was performed with a magnetic stirrer set at 450RPM.

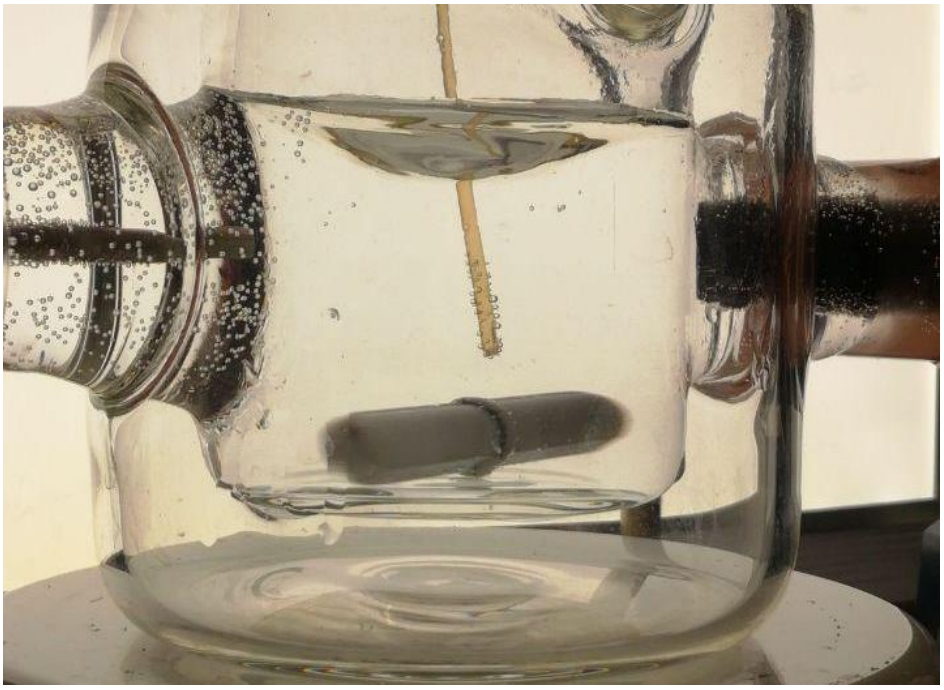

Figure 3.14: Dissolution test of Maltodextrin 19 filaments extruded at 140°C, picture taken after 10 minutes.

Figure 3.14 illustrates the filament after 10 minutes of test. The test does not give a quantitative result because the amount of material used in the test is equal to 0.1g (0.05%w/w concentration). This value is too low to affect the conductivity. Hence, the probe is not able to measure any changes in the conductivity value. Despite that, in 15 minutes the filament does not dissolved. Results reported in the literature [9], regarding MD19 powders, show that powder dissolution occurs in less than one minute. Therefore, significant differences in the dissolution behaviour before and after extrusion are present and they cannot be explained by the lower interfacial area between MD and water.

The low dissolution of the filament can be related to a degradation of the maltodextrin. For this reason the filaments were discarded and new extrusion tests were performed.

The characteristics of the extruder allows to control only one process parameter (extrusion temperature). Thus, powder moisture content has been changed modifying the storage conditions. As described in chapter 1 (§1.1), water acts as plasticizer and affects also the glass transition temperature. Therefore, moisture content can influence the extruded filament properties.

45g of maltodextrin were stored at 65% RH inside the desiccator. The obtained moisture content was $8.5 \pm 0.2\%$. Moreover 45g of maltodextrin were stored inside the chamber at 50% RH for a short period of time. Also in this case moisture content was evaluated. It was $6.5 \pm 0.2\%$.

The moisture content was increased in order to reduce the T_g of the powder and to enhance extrusion. The temperature was set, as before, between 180°C and 140°C.

Firstly, the highest humidified maltodextrin was extruded.

The lower viscosity allows to avoid motor overload issues, but expansion and swelling phenomena occurred. Swelling is a common phenomenon in polymer processing. It occurs when a melted material is forced through a die (nozzle). When the stream passed through the die it is compressed and the flowrate increased. When it exit from the die, it tends to recover its initial shape with an increase of diameter. Moreover, due to the high temperature, water evaporates, forming steam that is confined at high pressure inside the extruder. When it exits from the nozzle it is able to separate from the maltodextrin filament expanding the filament with the formation of a porous structure.

The higher moisture content enhances expansion. The phenomena was present in all the range of temperature. A screw speed control could help to properly control the flowrate and reduce filament expansion. The obtained filaments were porous and brittle, with an increase of diameter of 45%. A picture of a produced filament is reported below.

Figure 3.15: MD19 Filament extruded at 140°C, powder moisture content equal to 8.5%.

The picture 3.15 illustrate a filament obtained from MD19 powder extruded at 140°C. Comparing Figure 3.13 and 3.15 significant differences can be found. Firstly, it can be seen a difference in the colour. The filament shown in picture 3.9 has a white colour similar to the powders one. Moreover, dissolution in non-stirred water was almost instantaneous. It means that degradation was avoided. Unfortunately, the reduced length and the higher diameter, combined with the weakness of the filaments does not allow to use them.

Furthermore, it must be mentioned that also caking in the hopper occurs. As described by Descamps et al. [7], caking is a phenomenon where free-flowing particles aggregates to form a larger lumps of particles. The agglomeration depends on temperature, pressure and relative

humidity conditions. The extruder design enhances an increase of temperature inside the hopper due to heat conduction from the barrel. Moreover, the higher moisture content enhances bonds formation and caking. Caking usually occurs at temperature higher than T_g. As discussed before (§3.3), increasing the moisture content the T_g decreases. In particular, with a 8.5% moisture content the maltodextrin T_g is around 35°C. For these reasons, caking occurred in the hopper with the formation of hard agglomerates that needed to be discharged and complicated the extrusion.

Lastly, powders at 6.5% moisture content were extruded. Also in this case caking and expansion occurred. Hence, the temperature was directly decreased at 140°C. Due to caking phenomena a huge amount of powder agglomerated and therefore it was discharged. Only few filaments were obtained. A filament is shown in Figure 3.16.

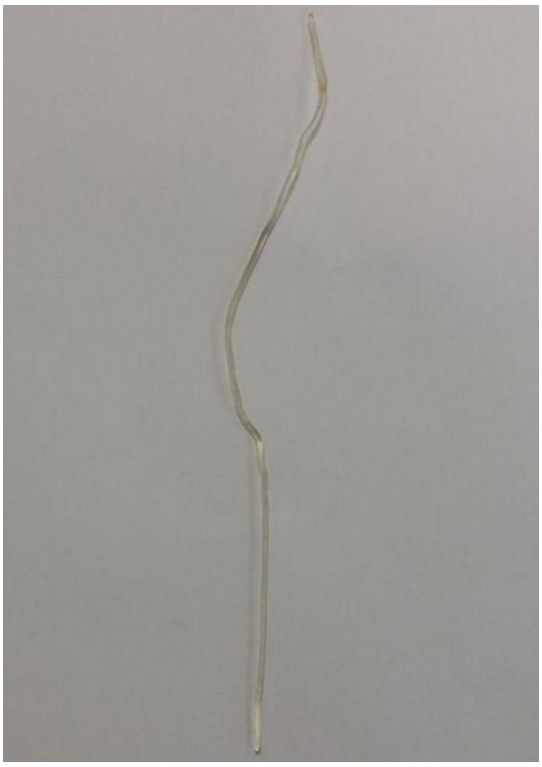

Figure 3.16: MD19 Filament extruded at 140°C, powder moisture content equal to 6.5%.

The Figure shows a filament extruded at 140°C. The filament is almost transparent and dissolution almost instantaneous. Also expansion effects are reduced, the filament diameter is 1.80 ± 0.5mm. On the other hand, the filament is not straight, and filaments longer than 15cm were not obtained. A summary of the three test performed is reported in Table 3.3.

Table 3.3: Extrusion results.

Parameter	Test 1	Test 2	Test 3
Powder	Maltodextrin 19	Maltodextrin 19	Maltodextrin 19
Moisture content	4.8%	8.5%	6.5%
Extrusion temperature	180°C-140°C	180°C-140°C	180°C-140°C
Degradation	Yes	No	No
Expansion	No	Yes	Yes (until 140°C)
Caking	No	Yes	Yes
Number of filaments produced	3 for every temperature	Few	Few
Filament diameter	1.80 ± 0.05	2.50 ± 0.1	1.80 ± 0.1
Filament length	20-50cm	5-10 cm	10-15 cm

Unfortunately, due to continuous mechanical failures, it was not possible to perform more tests with similar conditions. Hence, it has been decided to use a second extruder with a higher power motor and a speed control in order to control two process parameters.

3.6.2. Filafab Extruder

Filafab extruder is similar to the Noztek extruder but it is able to generate a torque 3 times higher. Moreover, the screw speed can be controlled and set between 5 and 30 RPM. Also the screw designed is different. A picture of the screw is reported below.

Figure 3.17: Screw and barrel of the Filafab extruder.

Figure 3.17 illustrates the screw and the barrel installed in the Filafab extruder. The hopper hole is smaller and the feed section is shorter. The number of pitch is equal to 12. On the other hand, only the metering section is directly heated with an electrical resistance. The rest of the barrel and the nozzle are not heated directly. Therefore, temperature can be properly controlled only in the metering section. A second thermocouple was placed on the nozzle to monitor the nozzle temperature.

In the experiments performed with the previous extruder, MD caking was one of the main issues. Thus, a plastic hopper was designed, 3D printed and fixed above the metal one to diminish heat conductivity and to minimize caking.

The first test was performed using MD19 stored in the batch provided by the supplier (e.g. moisture content equal to 4.8%) between 180 and 140°C.

However, expansion phenomena occurred and was not possible to control it. It means that, due to a different design also the extrusion process conditions have to be change.

After that test, it has been decided to use MD21. The properties are similar to the one of MD DE-19 but the molecular chains are slightly shorter. Hence, extrudability should be higher.

Various tests are performed. Filaments, with the proper diameter are obtained with the following conditions:

- Metering zone temperature: between 185°C and 165°C.
- Nozzle temperature: between 175°C and 155°C.
- Moisture content: $1.75 \pm 0.2\%$.
- Screw speed: 5RPM.
- Nozzle diameter: 1.80 mm.

5 filaments of approximately 1 meter length were obtained for each temperature. They are reported in Figure 3.18.

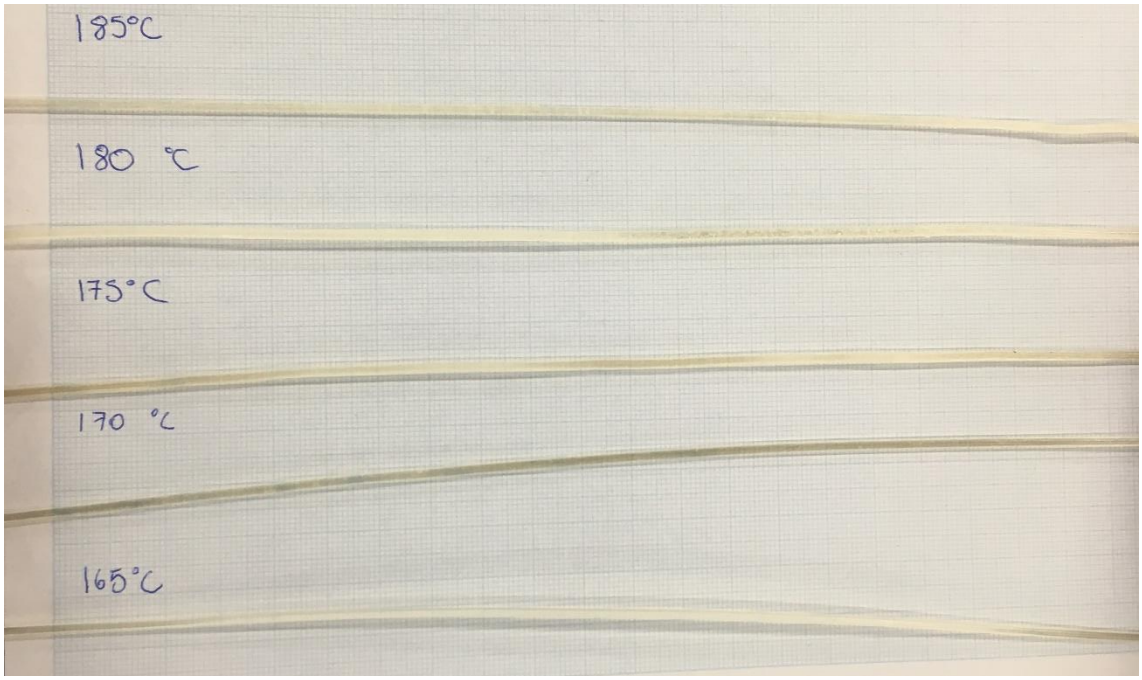

Figure 3.18: MD21 Filaments.

The Figure shows the filaments obtained in the range between 185°C and 165°C. Maltodextrin 21 with a moisture content of $1.75 \pm 0.2\%$ was used. The filaments are straight, transparent and swelling did not occurred. Moreover, a significant number of filaments was produced.

For these reasons, a further analysis was performed to characterize them.

3.7. Filament Characterization

As described in chapter 2 (§2.2.8), filaments are optically and mechanically characterized in order to evaluate the diameter, the homogeneity and the mechanical properties.

Firstly, the diameter was evaluated with a calibrated calipers every 5cm. The diameter was almost constant in all the filaments and the measured value is: $D = 1.82 \pm 0.03\ mm$. So, expansion did not occurred and the diameter is slightly higher than the nozzle one.

Afterwards, a filament was stored for 24 hours at 70% RH to try to modify the mechanical properties. The measured diameter of the filament after the humidification was equal to $1.87 \pm 0.03\ mm$. It means that filament humidification leads to an increase of the diameter.

3.7.1. Optical analysis

The optical analysis is performed on filaments to study the microstructural homogeneity. Filaments obtained at the highest and lowest temperature are analysed. Picture of cross and side section are taken and reported below.

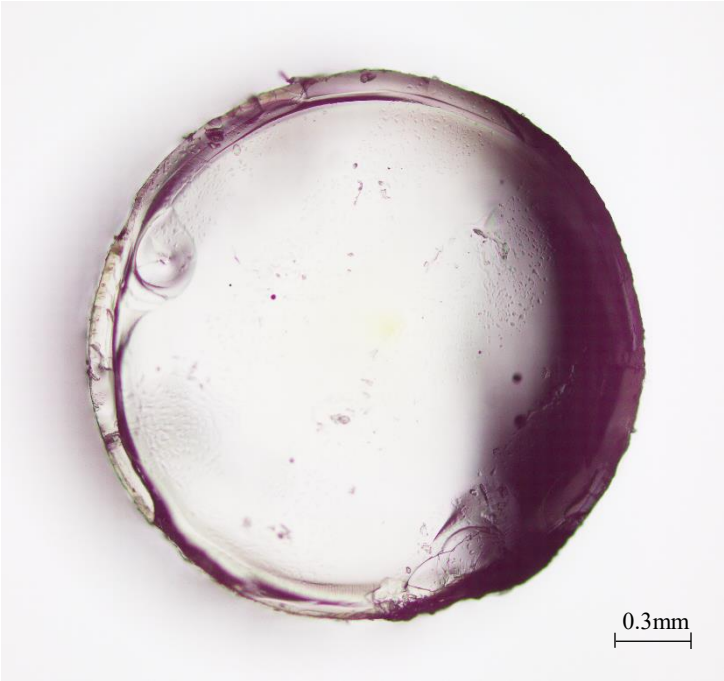

Figure 3.19: MD21 Filaments extruded at 165°C, cross sectional image.

Figure 3.20: MD21 Filaments extruded at 185°C, cross sectional image.

Figures 3.19 and 3.20 illustrate the cross section of filaments obtained at 165°C and 185°C. The filament obtained at 165°C has a homogeneous section, while in the filament obtained at 185°C some bubbles are present.

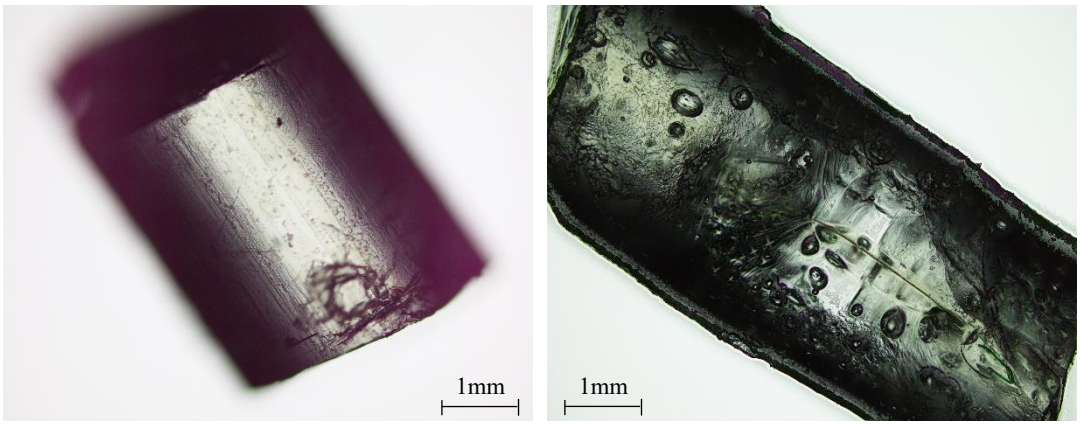

Figure 3.21: MD21 Filaments extruded at 165°C (right) and 185°C (left). Longitudinal section.

Figure 3.21 shows the longitudinal section of the filament extruded at 165 and 185°C. As in the cross sectional view, it can be seen that the filament obtained at 165°C is homogeneous while there are bubbles in the one obtained at 185°C. Hence, reducing the temperature it is possible to increase homogeneity and reduce evaporation and phase separation between water and MD.

Afterwards, optical analysis is performed to a filament extruded at 165°C stored for 24 hours at 70% RH. The results are shown in Figure 3.22.

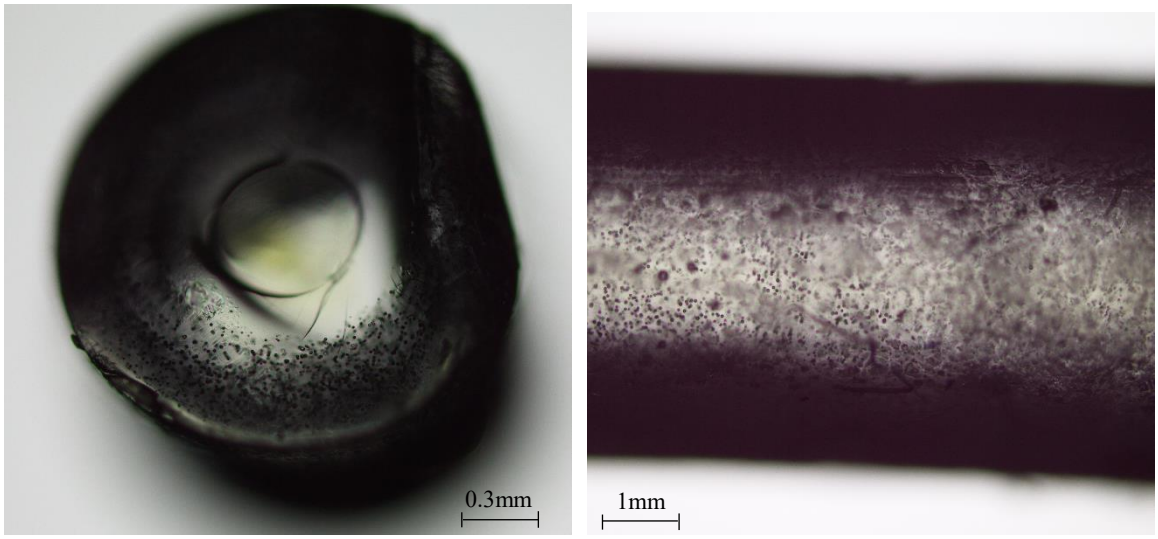

Figure 3.22: MD21 Filaments extruded at 165°C, stored at 70% RH for 24 hours.

Figure 3.22 reported the optical images obtained on the filament stored at 70% RH. The filament is no more homogeneous. In the external layer there is a higher presence of microbubbles, while they are not present in the central section. It can be explain by the diffusion behaviour. In fact, moisture is absorbed from the environment, hence the driving force is higher in the external layers and decreases gradually approaching the centre of the filament. Consequentially, the higher presence of water in the external layers is physically explained and homogeneity is not reached.

3.7.2. Mechanical characterization

Mechanical characterization is essential to predict the behaviour of the filaments inside the 3D printer. First of all, the filament has to be resilient and flexible to pass through the pulling system and do not break inside it. Secondly, it has to be tough to resist to buckling.

The test is performed to filaments obtained at 165°C because they are microstructurally homogeneous. One filament is cut in 4 pieces of 18cm in order to perform 4 tests. Moreover, to compare the results, the same test is performed on ABS filaments suitable for FDM 3D printing. A qualitative and quantitative analysis is performed. Afterwards, the test is performed on the humidified filament.

The tests are recorded with a speed camera with a frequency of $0.05s^{-1}$. It allows to visually analyse the behaviour of the filaments. A montage obtained from one test performed on MD21 filaments is reported in picture 3.23.

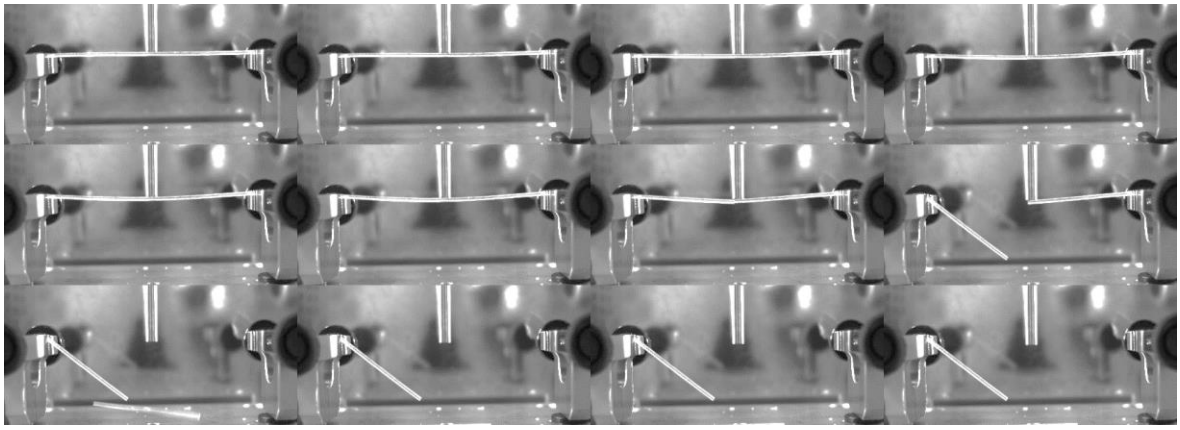

Figure 3.23: Pseudo 3 points bending test on MD21 stored at 40% RH and 25°C. Time between 2 consecutive frames= 0.25 s.

Figure 3.23 shows the behaviour of the filament during the test. The time between 2 consecutive frames is of 0.25 seconds. The filament rupture was almost instantaneously after the test started. It must to be remembered that the test starts only after the triggered force is reached. Hence, the first three frames captured the pre-test movement of the probe. Results of the 4 tests performed are reported in Figures 3.24 and 3.25.

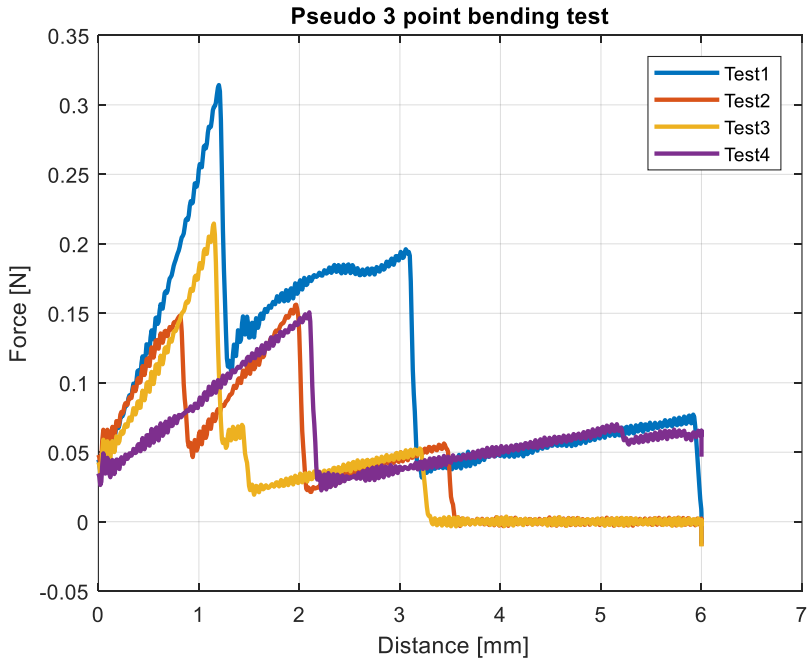

Figure 3.24: Pseudo 3 points bending test on MD21 filaments. Distance vs Force chart.

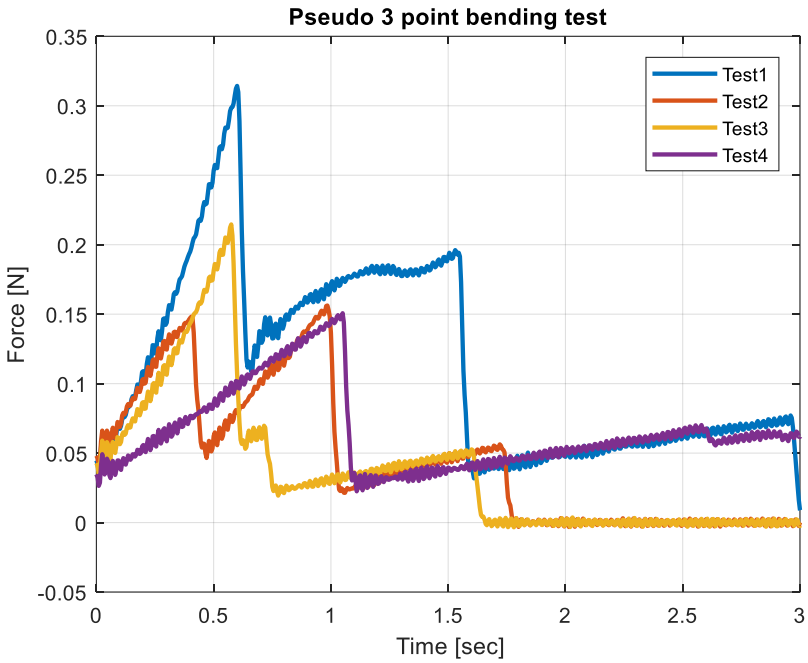

Figure 3.25: Pseudo 3 points bending test on MD21 filaments. Time vs Force chart.

Figures 3.24 and 3.25 report the results of the 4 tests. Figure 3.24 illustrates the force applied as a function of the movement of the probe (distance). Figure 3.25 shows the force applied as a function of the time. When the triggered force is reached the test starts, the probe reaches the maximum distance, 6 mm, in 3 seconds and then it comes back to its initial position in approximately 1 second.

The filament is brittle and a fragile breakage occurs. As describe qualitatively, the filament breakage happens in less than 1 second. Breakage time can be evaluated as the time before the first sudden decrease in the applied force. The consecutive increases in the force can be related to the contact between the probe and the broken filament.

The same analysis is performed on ABS filaments. The recorded test is reported in the Figure 3.26.

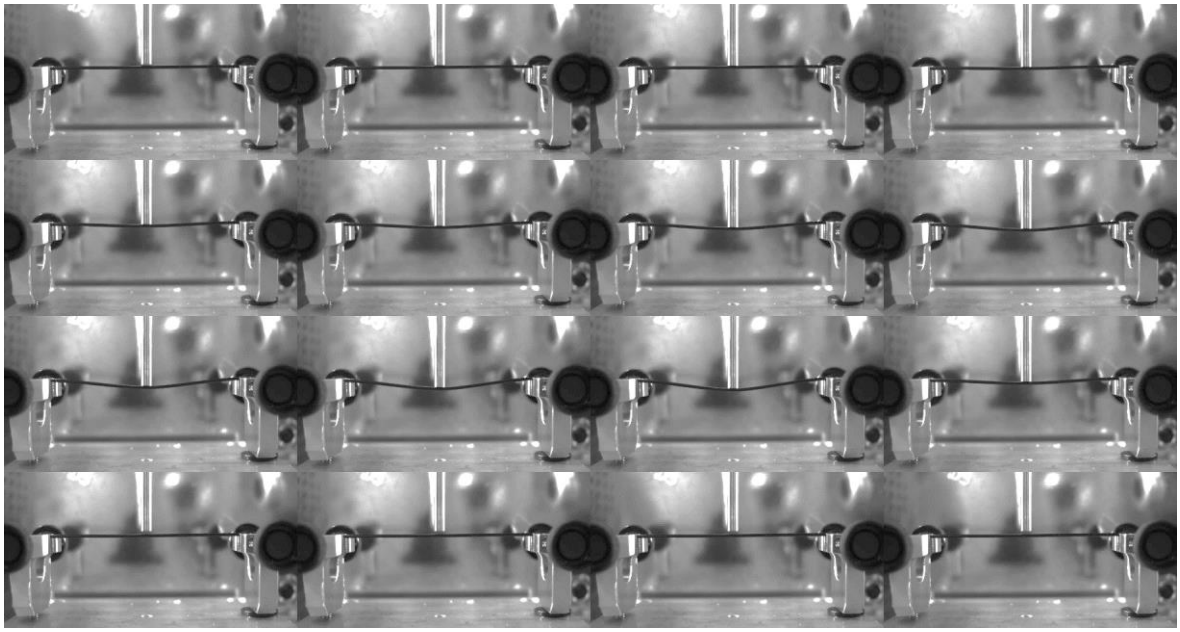

Figure 3.26 Pseudo 3 points bending test on ABS filaments. Time between 2 consecutive frames= 0.35 s.

Figure 3.26 shows the record of the pseudo 3 points bending test performed on commercially available filaments of ABS. The filament has an elastic behaviour and does not break. Once the probe stops to apply a load the filament returns to its initial position. Quantitative results are reported in the chart below.

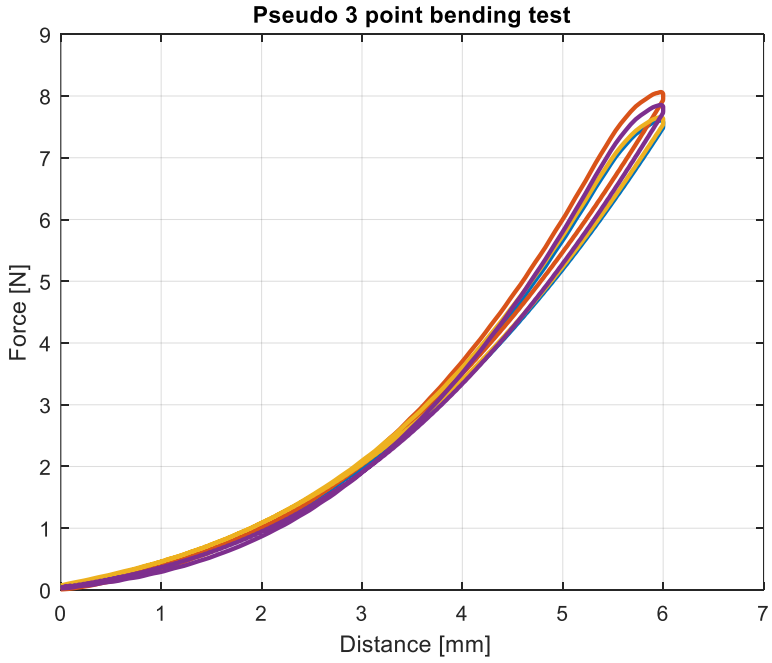

Figure 3.27: Pseudo 3 points bending test on ABS filaments. Distance vs Force chart.

Figure 3.27 shows the measured force as a function of the distance. The curves of the 4 tests are similar, meaning that different filaments of the same material have homogenous mechanical properties. The maximum load reaches is 8 Newton and the filament can deflect of 6mm without being damaged. These results, compared with the one obtained with maltodextrin

filaments, are an indication of the poor mechanical properties of MD filaments. MD filaments breakage occurs with a load 25 times lower than the load sustained from ABS filaments.

Afterwards, the test is performed on filaments stored at 70% RH for 24 hours. As performed with the dry filaments, 4 filaments of 18 cm are prepared and the tests are performed. A montage of the recorded test is done to observe qualitative the behaviour of the humidified filaments.

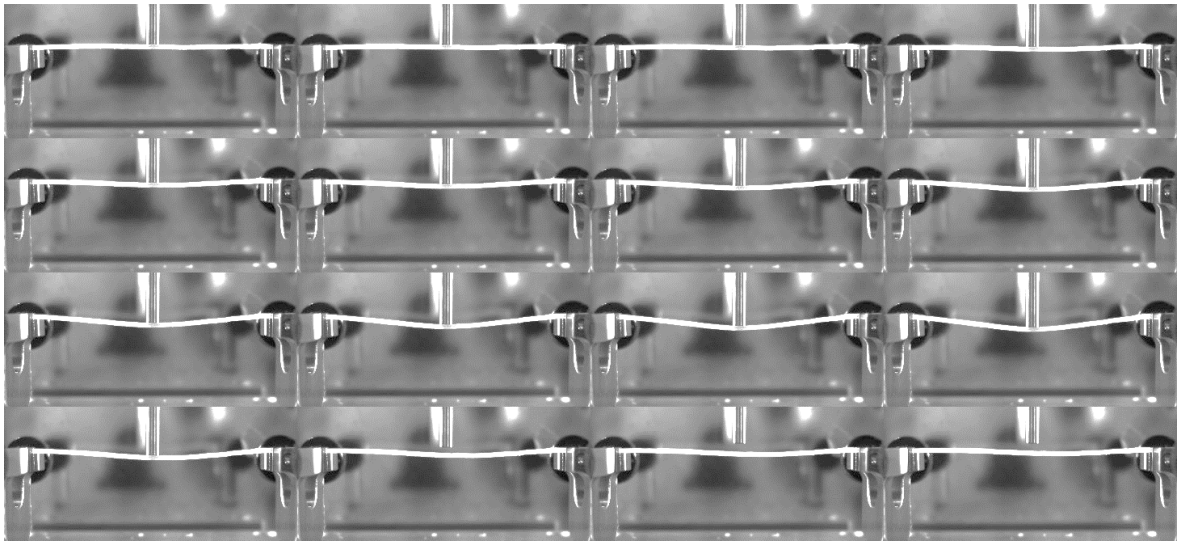

Figure 3.28 Pseudo 3 points bending test on MD21 filaments extruded at 165°C and 70% RH. Time between 2 consecutive frames= 0.35 s.

Figure 3.28 shows the record of the pseudo 3 points bending test performed on humidified filament. The time between 2 frames is of 0.35 seconds. The behaviour is similar to the one shown in Figure 3.26. The filament deforms without breaking and tends to recover its initial position.

In order to gain a more complete understanding of the mechanical properties and predict the behaviour inside the pulling system a quantitative analysis has been performed. The results of the 4 tests are reported in Figure 3.29. It must be remembered that the four filaments were stored in the same desiccator for the same amount of time (24 hours) and that the tests were performed within 30 minutes after the 24 hours.

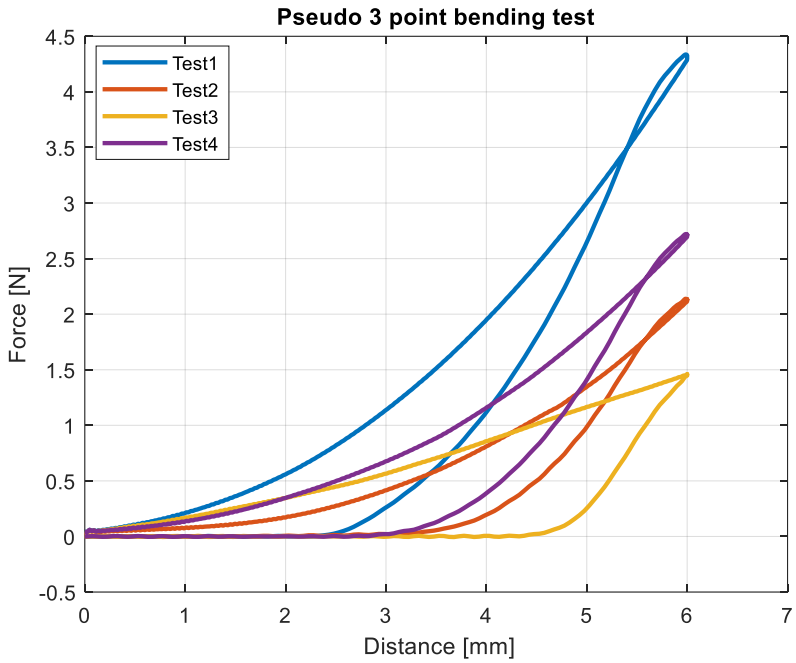

Figure 3.29: Pseudo 3 points bending test on MD21 filaments stored at 70% RH. Distance vs Force chart.

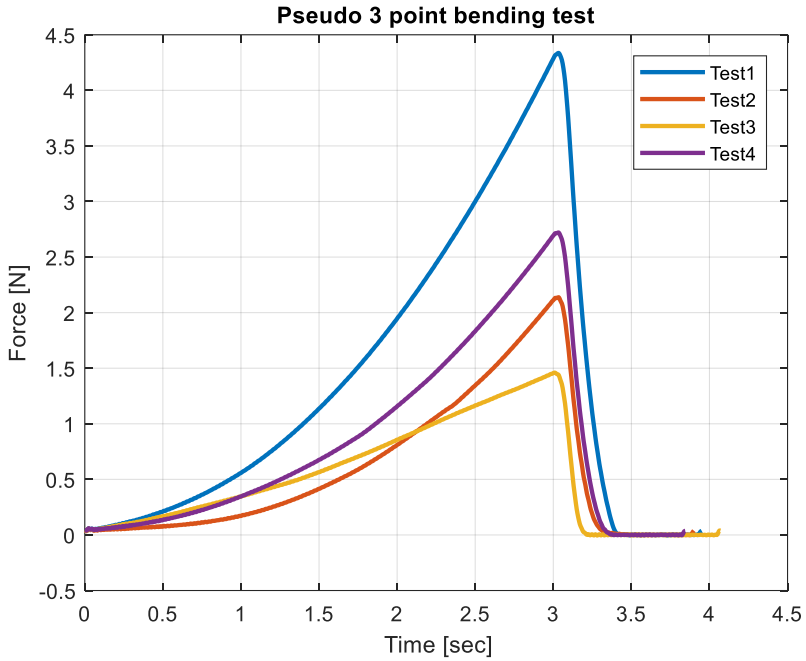

Figure 3.30: Pseudo 3 points bending test on MD21 filaments stored at 70% RH. Time vs Force chart.

The force as a function of distance and of time is reported in Figures 3.29 and 3.30. Filaments does not break and the maximum load applied is between 1.5 and 4 N. The obtained results shows that the mechanical properties are non-homogeneous. It can be due to a non-homogeneous humidification of the different filaments.

The maximum load applied is from 2 to 4 times lower to the one measured on ABS filaments. Hence, filaments are less tough. Figure 3.31 compared the obtained results; mean and standard deviation of the 3 different filaments are evaluated.

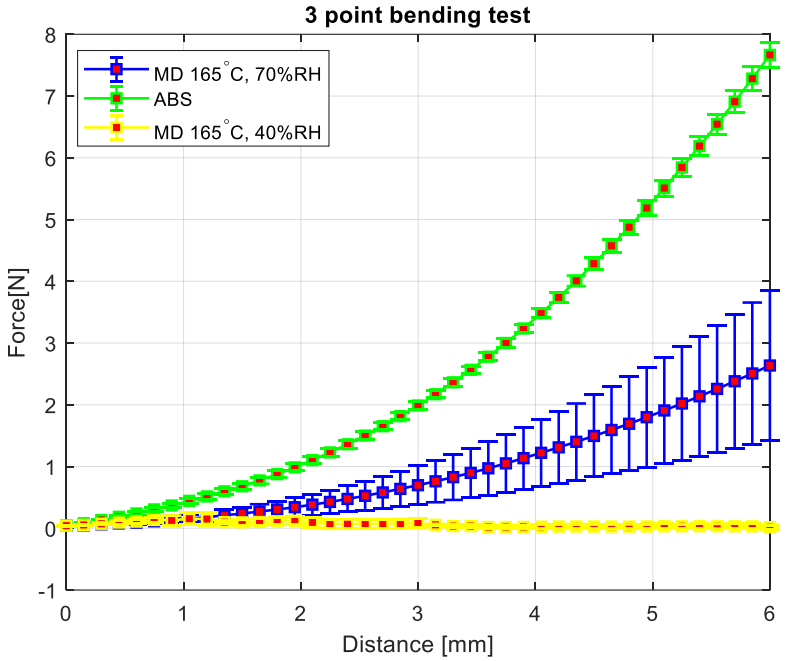

Figure 3.31: Pseudo 3 points bending test. Distance vs Force chart.

ABS filaments are commercially available and feasible for FDM. They have homogeneous mechanical properties. They are flexible and does not break during the test. Moreover, the maximum load reached is 8N, hence they are also tough and in order to flex them a relative high load is required.

MD21 filaments extruded at 165°C and stored at 40% RH are brittle and breaks almost instantaneously. Filaments stored at 70% RH for 24 hours, have higher mechanical properties and are more flexible than filaments stored at 40% RH. This result verifies that water acts like plasticizer.

However, they are microstructurally non-homogeneous as shown in Figure 3.22 and they also have non-homogeneous mechanical properties. Moreover, the mean of the maximum load reached is 2.5N. Therefore, they are less tough than ABS filaments.

Filament characterization allows to predict that MD21 filaments stored at 40% will break inside the pulling system. Concerning MD21 filaments stored at 70%, they have a diameter higher than the one suitable for the Raise 3D printer ($1.75 \pm 0.5mm$) and they are very flexible. Hence, wrapping or obstructing inside the pulling system can occur.

3.8. 3D printing by FDM

Production of food structures through fused deposition modeling is the aim of this research. Maltodextrin has been selected as ingredient, it has been characterized and filaments are extruded using two different extruders (§3.6).

Filament characterization (§3.7) shows the weak mechanical properties of the filaments, but in order to assess the feasibility of the extruded filaments for FDM it is necessary to perform a test on the 3D printer. Raise 3D printer is used for its design and general feasibility with

customized filaments. Details of the printer and of pulling system are shown in Figure 2.11 and Table 2.3. The printer can be fed with filament of 1.75±0.5 mm, hence the filaments diameter evaluated previously (§3.7) could be unfeasible.

Maltodextrin filaments are tested setting the printer in "load" mode. Load mode is used to feed a new filament inside the printer. A file CAD is not necessary, the filament is pushed through the nozzle, and ejected without building any object. Extrusion speed is set at 10 mm/sec and extrusion temperature at 200°C. The test is used to verify if the filaments can pass through the rollers without failures and melt inside the nozzle.

The MD21 filament stored at 40% RH breaks inside the pulling system with a fragile rupture as shown in Figure 3.32.

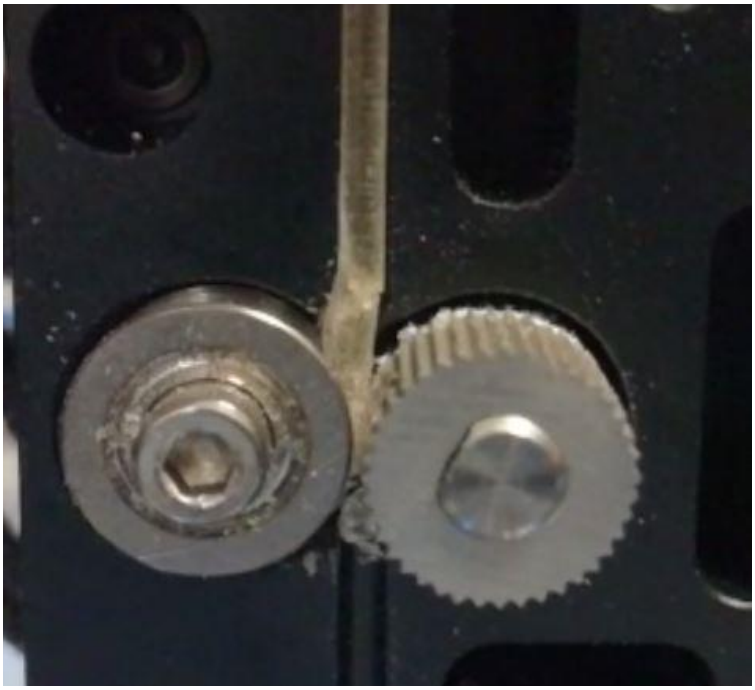

Figure 3.32: Detail of the pulling system of the Raise 3D printer loaded with MD21 filaments stored at 40% RH.

The filament stored at 70% RH for one day has a higher diameter and cannot pass through the pulling system. Hence, no more tests are performed with the available MD filaments. Filaments with a smaller diameter and higher resistance are required.

Chapter 4

3D printing and dissolution tests

In order to study the feasibility of employing the FDM technique in porous structures building, PVA water soluble filaments commercially available were preliminary investigated using the Ultimaker 3 3D printer. PVA was selected because it is commonly used as support material, thanks to its water solubility, but it is usually not employed for object production. Moreover, also maltodextrin is a water soluble material. Hence, dissolution tests were developed with the structures made of PVA with the aim to apply them to maltodextrin 3D printed porous structures when it will be possible.

In this chapter the results of the PVA 3D printing and of the dissolution tests are reported. Afterwards, results of chocolate 3D printing and G-codes are explained.

4.1. PVA filaments 3D printing

Porous structures described in chapter 2 (§2.2.10) are printed with PVA filaments using the Ultimaker 3D printer. The software Cura, described previously, has been used (§2.2.11). The printing parameters has initially been set as suggested by the filaments supplier. After starting trials, the structures are printed using the following parameters:

- Layer height: 0.06mm
- Wall thickness: 1mm
- Infill density: 100%
- Infill pattern: lines
- Printing temperature: 220 °C
- Build plate temperature: 60°C
- Printing speed: 30 mm/s
- Travel speed:200 mm/s
- Infill speed: 30mm/s
- Plate adhesion: skirt

These settings allow to print the designed geometries with the highest resolution possible. The infill density is set equal to 100% to improve the printing. The printing speed is suggested between 30 and 60mm/s. The lower value has been selected because a high precision is preferred to a lower printing time. The skirt adhesion is selected because it is easily removable from the 3D printed object.

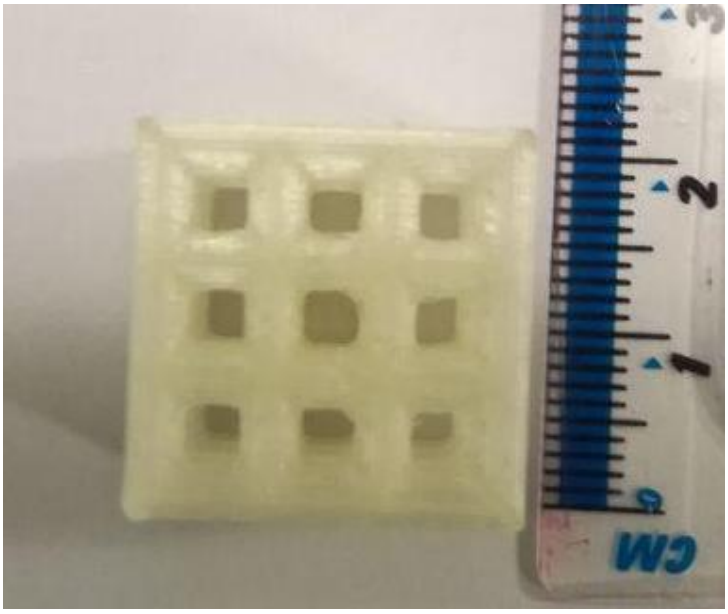

Figure 4.1: Geometry G3 printed with PVA. Top view.

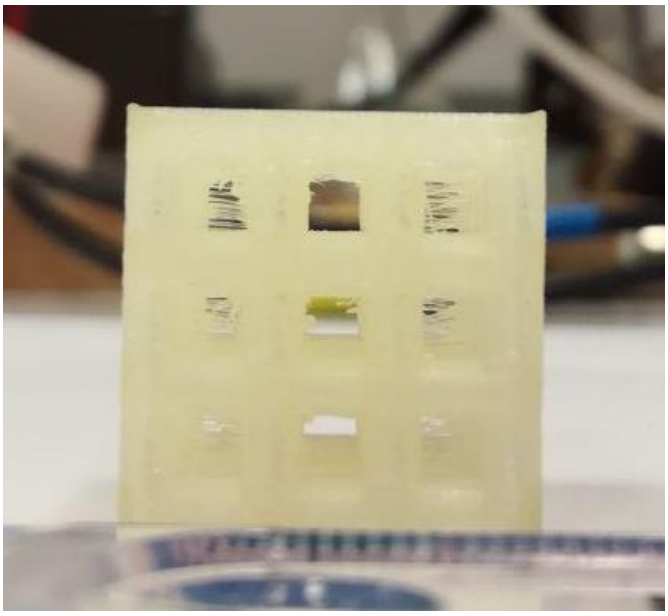

Figure 4.2: Geometry G3 printed with PVA. Frontal view.

Figures 4.1 and 4.2 show the final porous structure obtained. The precision is high, despite the printing of some layer is complicated. In fact, the layers above the holes does not have a support. The printing over a gap can lead to deflection and reduction of the precision. Hence, the real holes sizes is slightly lower than the designed one and they can be partially obstructed. Different quality can be find comparing the different geometries. Particularly, it has been seen that printing of smaller holes leads to a decrease of the printing quality.

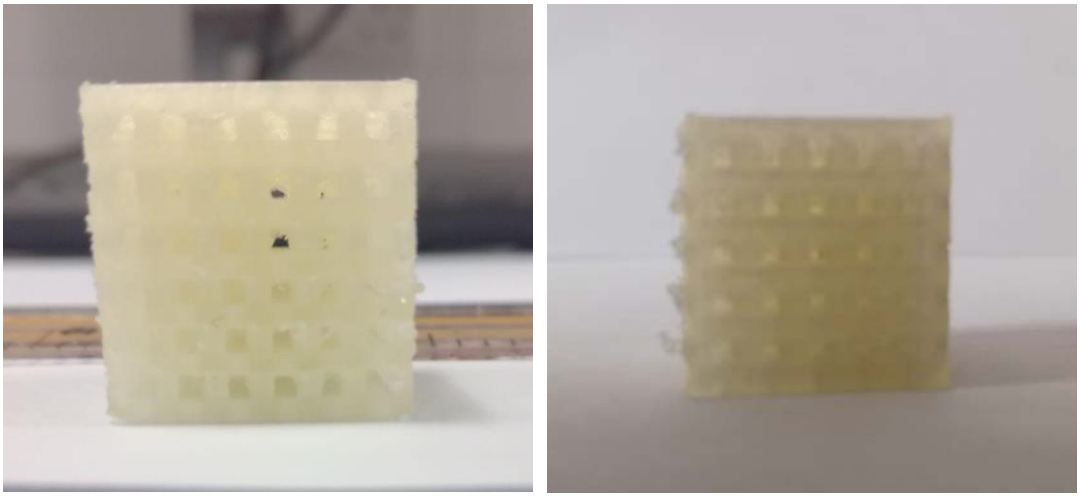

Figure 4.3: From left to right, geometry square36 and geometry G5, frontal view.

Geometry G5 and square36 are reported in Figure 4.3. The pores are partially obstructed by collapsed layers. Despite that, the overall dimensions are equal to the designed one but the resolution is low.

The printing of cubes with smaller width of material between holes (dimension b) is more difficult. It is due to the designed geometry. The printing of layers composed of small and non-connected shapes (e.g. small squares separated each other) can be complicated and leads to a decrease of the printing quality.

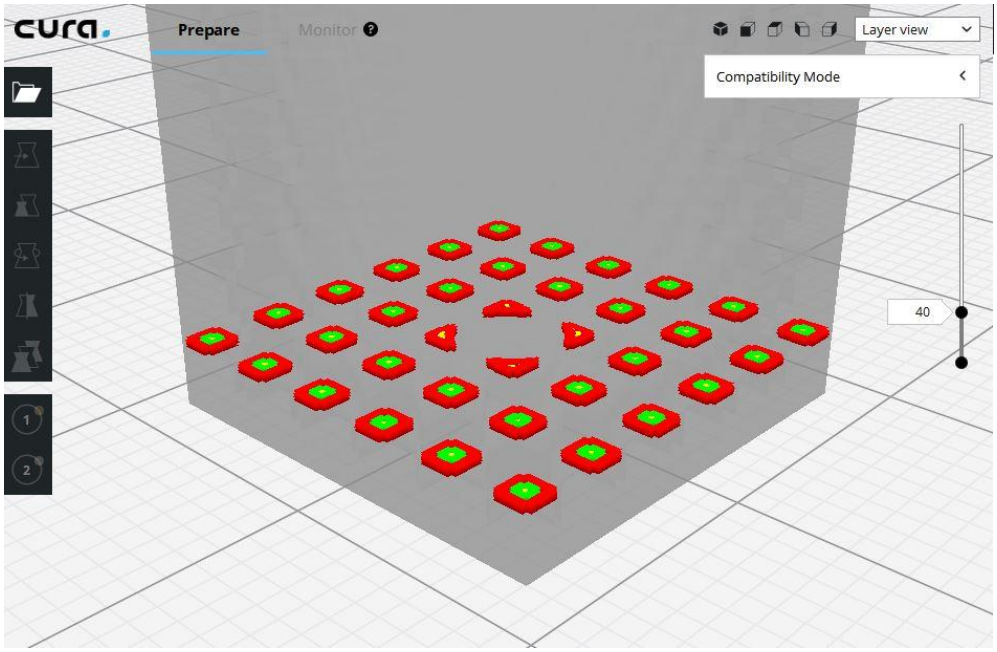

Figure 4.4: Printing detail of the critical layers. Geometry square36.

In order to print the layers show in Figure 4.4 the printer has to start and stop extruding for every small shape. Hence, for geometries with high number of holes and small width between holes the printing process required a continuous start and stop of extrusion that affects printing time and quality.

For these reasons, geometries with holes smaller than 1mm are not designed.

4.2. Dissolution test

Dissolution tests are developed to evaluate the dissolution behaviour of 3D objects printed with maltodextrin. Moreover, from that data it is also possible to verify if degradation/contamination occured.

Due to the difficulties in the maltodextrin 3D printing, reported previously (§3.8), the method is developed using PVA porous structures. PVA dissolution is studied and geometrical characteristics that influences dissolution are discussed. This study is planned to be successively applied to maltodextrin porous structures when it will be possible to print them. Furthermore, this study is interesting to verify the dissolution time of PVA. In fact, as mentioned before (§4.1), PVA is commonly used as support material and needs to be completely dissolved.

4.2.1. Instruments calibration

Before performing the dissolution tests, it is necessary to calibrate the probes in order to verify that a change of the measured value is linearly related to an increase of the dissolved material. Calibration is performed using some trials cubes printed with PVA. The range of final PVA concentration in the water solution used to perform the calibration is between 0 and 6% $^{w}/_{w_{tot}}$. This range has been decided to include all the dissolution tests performed.

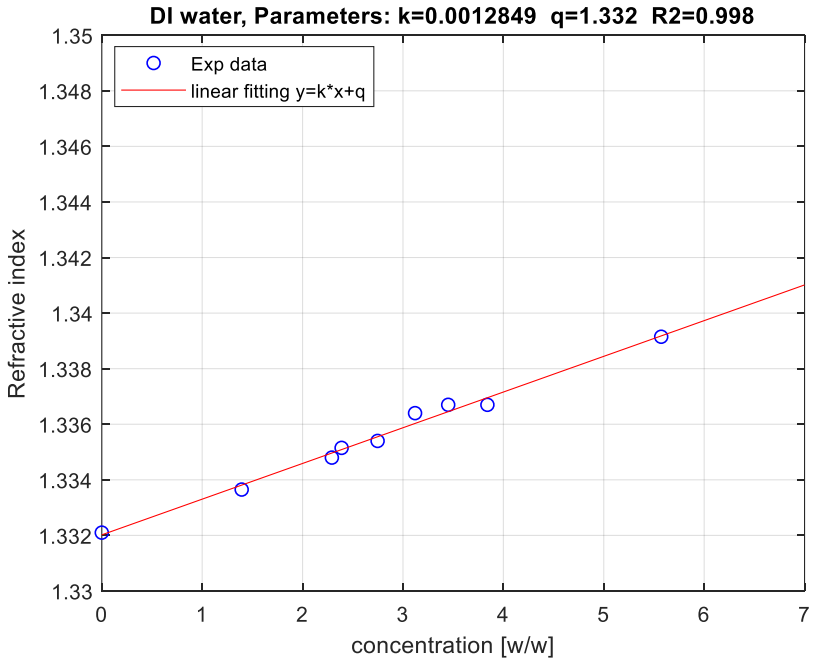

Figure 4.5: Calibration of the refractive index probe.

Calibration of the refractive index probe is reported in Figure 4.5. Experimental data are fitted with the equation of a straight line.

$$y = k \cdot x + q \tag{4.1}$$

y is the measured refractive index, x is the final concentration evaluated as weight of dissolved material divided by the total weight of the solution, k is the gradient of the line and q is the y-intercept. The R-square is 0.991 and it proves the good quality of the fitting. The q value is 1.332±0.0005 and it is equal to the measured refractive index of DI water. The k value is 0.001282, it means that the increase of the signal is low. Despite that, the probe is able to capture differences of solute concentration, but these changes are in the same order of magnitude of the maximum resolution of the probe.

The same procedure is performed with the conductivity probe. Conductivity of DI water is measured and its value is 1±0.5. For this reason the y-intercept is imposed to be equal to 1. The results are reported in the Figure below.

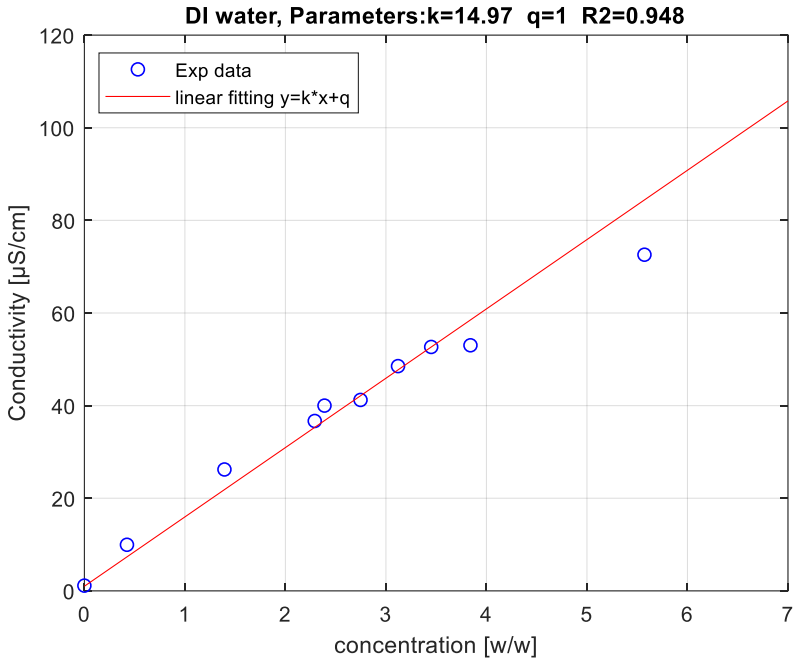

Figure 4.6: Calibration of the conductivity probe.

Also in this case the linear fitting gives good result (R-square=0.948). Moreover, the k value is 14.97. It is higher than the refractive index one, thus also small changes in concentration can be properly captured. For this reason it has be decided to analyse the results based on the conductivity probe.

4.2.2. Results analysis, category A.

Cubes that are considered inside the category A are reported in Table 2.4 and Figure 2.13. They have in common dimension *b*, *c* and *d* (width of material between 2 holes, holes width, holes height). Hence, they are designed to verify if dimension *a* (total length of the cube), porosity and weight affects the dissolution behaviour. Three tests repetition are performed on geometries square9, square25 and square36, while on geometry square49 and square64 was possible to perform only one repetition due to printing difficulties described previously (§4.1). The first 45 minutes of each test are recorded with a frame every 3 seconds. The record is used

to perform a qualitative analysis. Afterwards, the quantitative analysis is performed, data obtained from the conductivity probe are normalized as described in equation 2.8 and time to reach the 10% and the 90% of the final value is evaluated (t10 and t90).

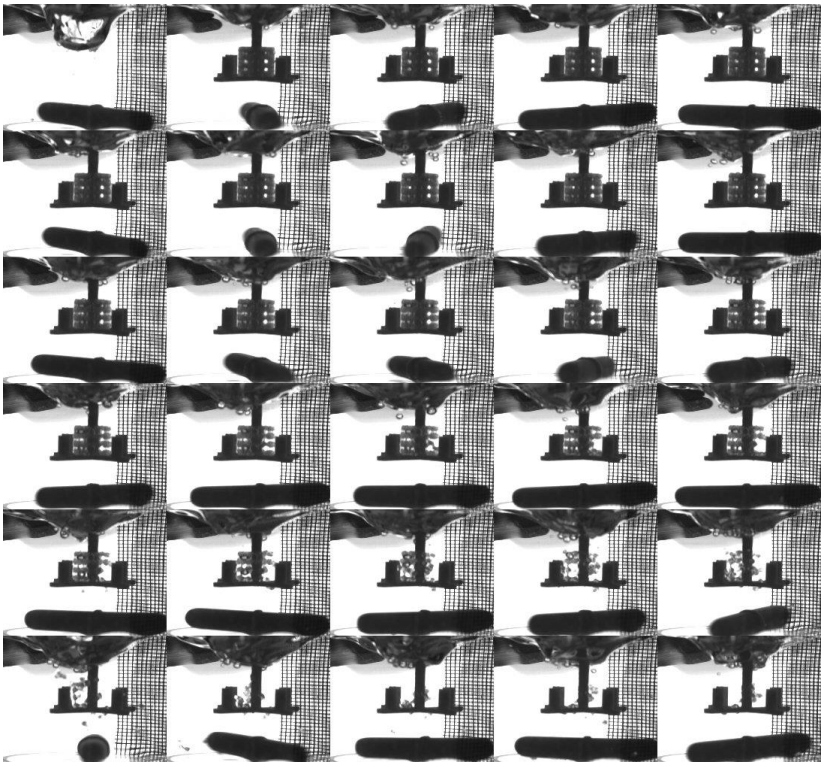

Figure 4.7: Montage of the dissolution test of geometry square9. Time between 2 consecutive frames= 1.5 min.

Figure 4.8 shows the first 45 minutes of the dissolution test performed on geometry square9. The time between 2 consecutive frames is 90 seconds (1.5 minutes). The cube is gradually immersed in the first 20 seconds to reduce the amount of trapped air between the holes. Despite that, during the test some bubbles arises from the object, meaning that some air remains trapped when the cube is immersed. The cube seems to completely dissolved in around 45 minutes.

Figure 4.9: Montage of the dissolution test of geometry square25. Time between 2 consecutive frames= 1.5 min.

Figure 4.9 illustrates the montage of the geometry square25. All the montage are made with the same time between two consecutive frames. The mesh that is visible in the picture is installed in order to avoid accumulation of material near the probe. In fact, an accumulation of material could affect the local concentration and the measurement. After 30 minutes (frames in the 5th row) the cube starts to collapse. The total dissolution happens in around 45 minutes.

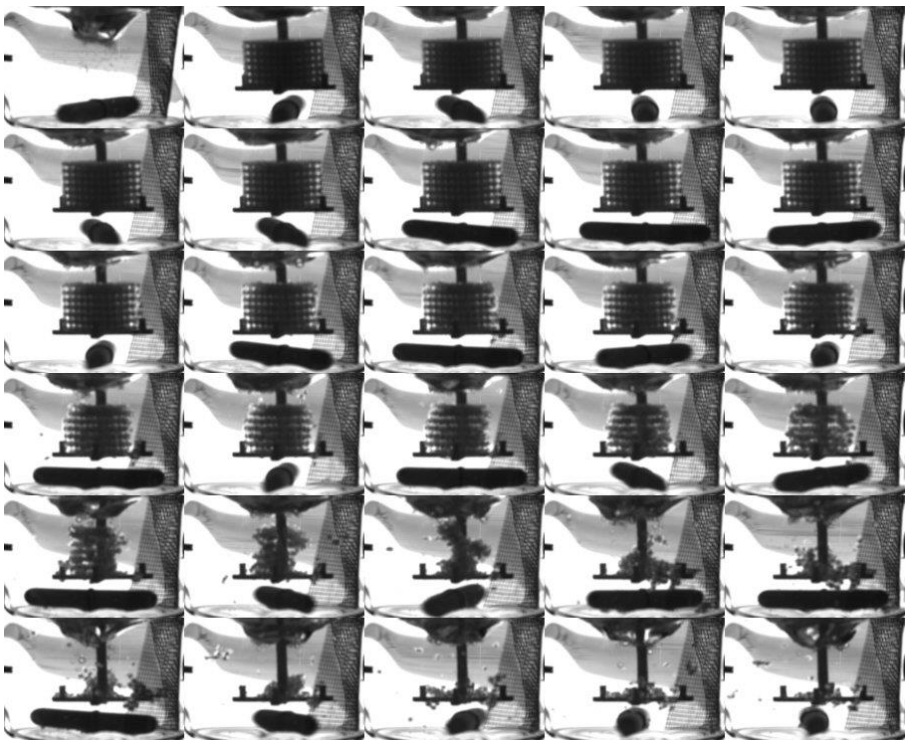

Figure 4.10: Montage of the dissolution test of geometry square36. Time between 2 frames= 1.5 min.

The dissolution behaviour of the geometry square36 is reported in the picture 4.10. It is similar to the behaviour of the square25. Thus, it seems that a difference in the number of holes and in weight does not influence the dissolution.

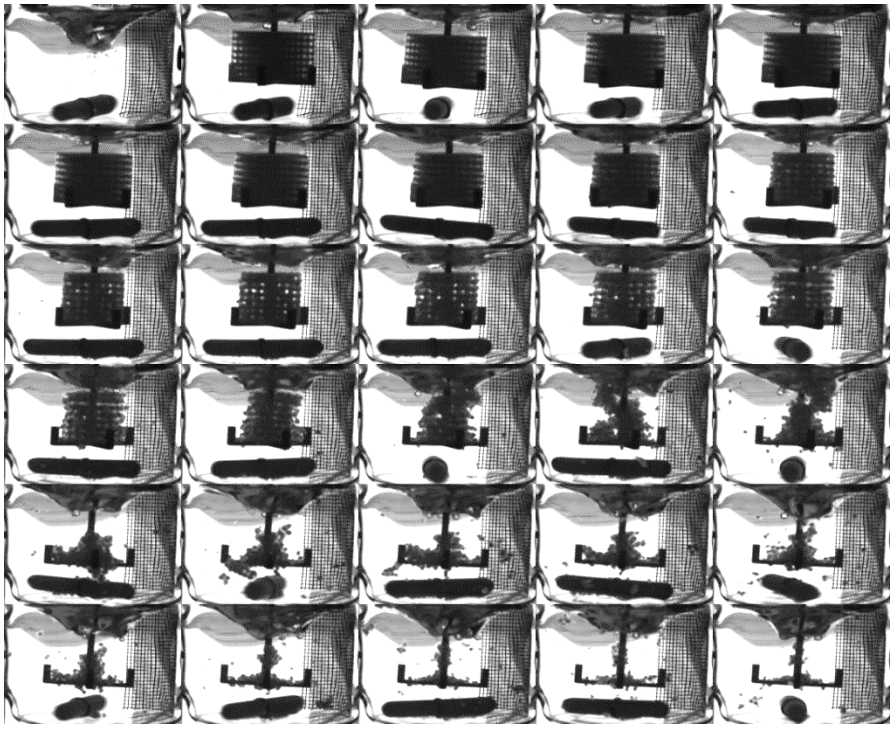

Figure 4.11: Montage of the dissolution test of geometry Square49. Time between 2 frames= 1.5 min.

In this case the collapse of the cube starts around 25 minutes after the test started. The cube breaks in pieces that are dragged by the water flow. Also in this case after 45 minutes are present only few residues.

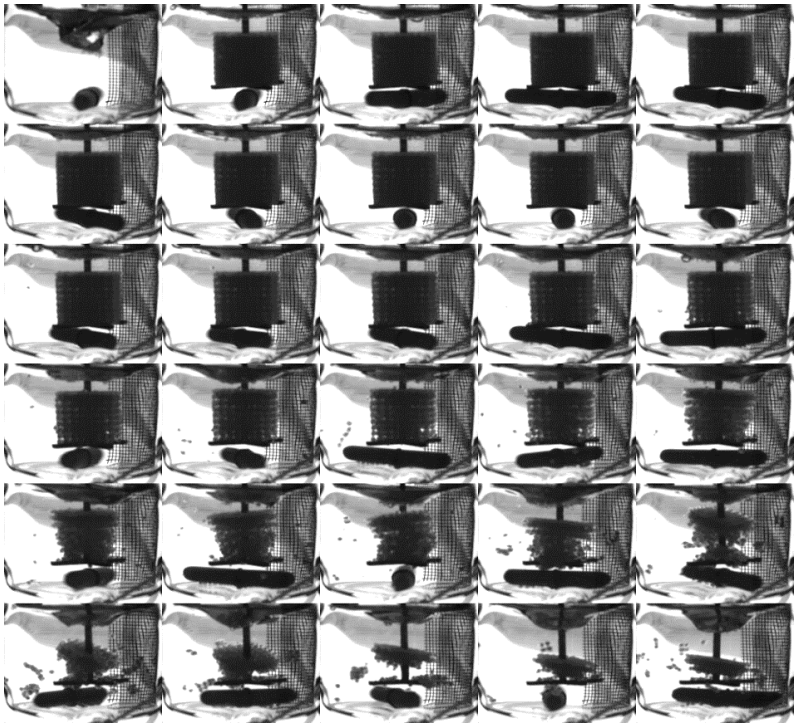

Figure 4.12: Montage of the dissolution test of geometry Square64. Time between 2 frames= 1.5 min.

The geometry square64 is the one with the highest weight and total dimension. Despite that, also in this case the response is similar. A breakage occurs after 33 minutes and the cube almost dissolved after 45 minutes. From the visual analysis it seems that the dimension *a* and *e* (total length and number of holes), as well as the weight does not affects the dissolution. In order to verify it, t10 and t90 are evaluated as a function of the dimension *a*. Afterwards, also porosity is evaluated as describe in chapter 2 (§2.2.10) and t10 and t90 are plotted as a function of it.

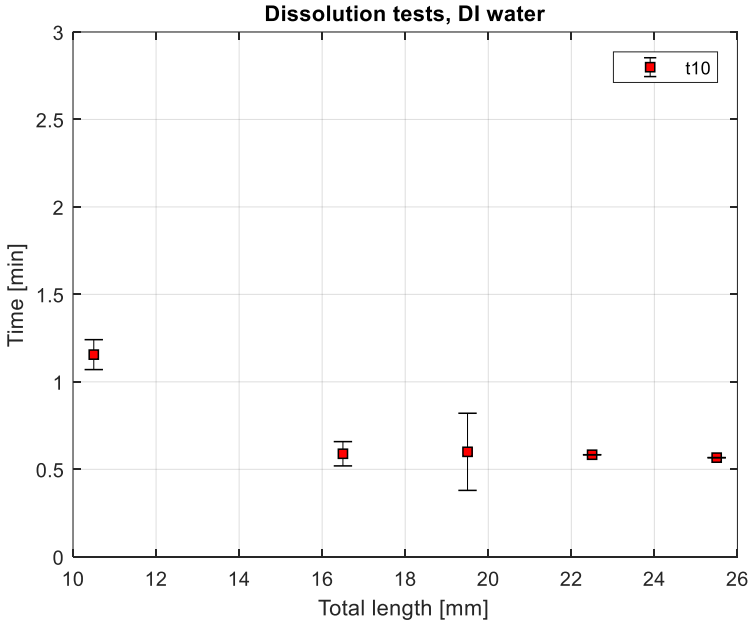

Figure 4.13: time to reach the 10% of the final conductivity value t10 versus the total length of the cube evaluated for the different 5 geometries of category A.

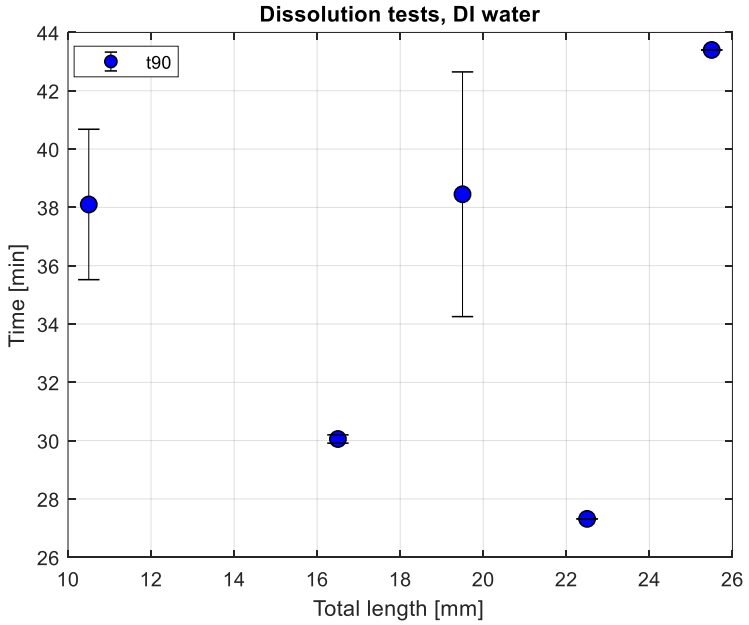

Figure 4.14: time to reach the 90% of the final conductivity value t90 versus the total length of the cube evaluated for the different 5 geometries of category A.

As described qualitatively, there are not significant differences in the dissolution behaviour between the different geometries. t10 is almost constant, whereas t90 fluctuates around 35 minutes. The lowest value of t90 is 27 minutes for a total length of 22.5mm (geometry square49). Whereas, the highest value is 43 minutes for a total length of 25.5mm (geometry square64). The same trend can be obtained plotting t10 and t90 versus the number of holes. In fact, the 2 dimensions are related.

t10 and t90 as a function of the evaluated porosity are reported in Figure 4.15 and 4.16.

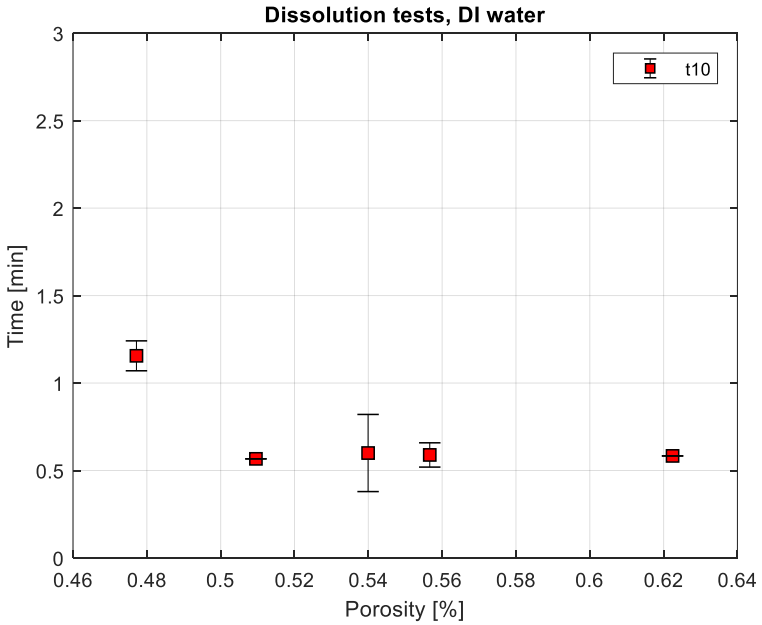

Figure 4.15: time to reach the 10% of the final conductivity value t10 as a function of the porosity.

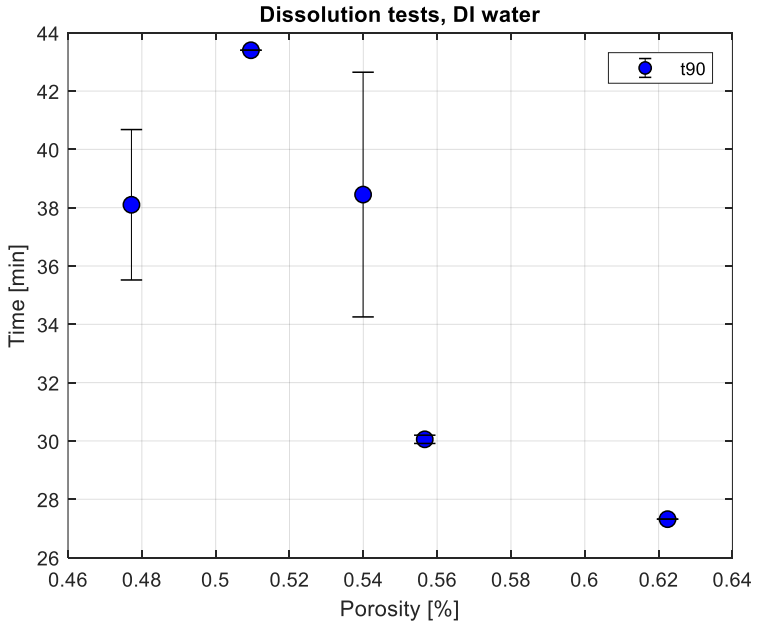

Figure 4.16: time to reach the 90% of the final conductivity value t90 as a function of the porosity.

Dissolution time (expressed as t10 and t90) versus the porosity is illustrated in Figure 4.15 and 4.16. It can be seen that also in this case that t10 is almost constant while t90 has a random

trend. Hence, the characteristic dissolution time, t90, is not affected by the porosity for this geometry.

Lastly, the dissolution path for geometry square9, square25 and square36 is analysed.

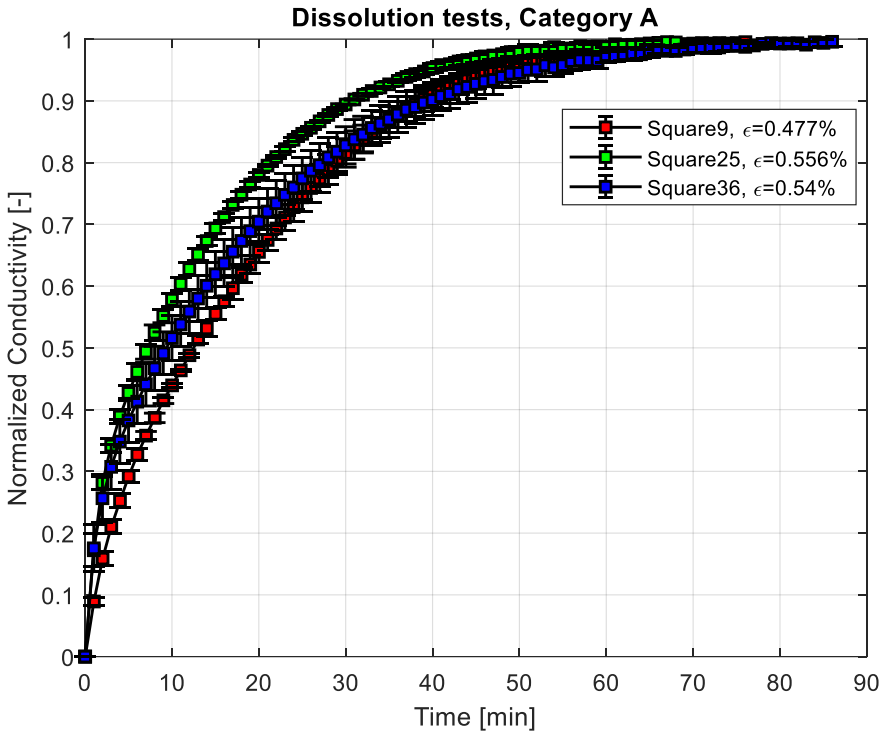

Figure 4.17: Normalized conductivity versus time plot.

Mean and standard deviation of the tests performed with different geometries are plotted in Figure 4.17. Standard deviation is low, thus the tests have good repeatability. The dissolution is initially faster, as described by t10, and then it gradually decreases. Geometry Square25 has the higher porosity and it seems to have a faster dissolution even if t90 is not influenced by the porosity. Moreover, there are not significant differences among the 3 geometries.

In conclusion, for square pores of 1.5 mm (dimension c=1.5mm), the total length of the cube (dimension a), as well as the number of holes per face and the porosity do not significantly influences the result.

Goyanes et al. [14] proposed also another parameter to compare the dissolution of different geometries. This parameter is the Specific surface area (SA/V), evaluated as Surface area divided by the total volume. These two values are assessed from the CAD file. The surface area is evaluated as the theoretical contact area between the cube and the water considering both the external area of the cube and the internal area of the pores. The total volume is estimated as reported in Eq. 2.6

The results are reported in figures B.9 and B.10 (appendix B). Unfortunately, also in this case the trend of the characteristic dissolution time, t90, is random. These results suggest that the controlling parameter can be the width of material between two holes (dimension b).

4.2.3. Results analysis, category B

The analysis performed on geometries of category A, has been expanded to understand the influence of the dimensions *b*, *c* and *d* on the dissolution of porous structures. Geometries of category B, shown in figure 2.14, can be described as multiple cuboids of different dimensions, placed together to form a cube. The dimension *b* can be seen as the length of the cuboid, while *c* and *d* are the distances between 2 cuboids. The results, both qualitatively and quantitatively are reported in this section.

Figure 4.18: Montage of the dissolution test of geometry G1. Time between 2 consecutive frames= 1.5 min.

The record of the first 45 minutes performed on geometry G1 does not allow to view the complete dissolution. In 45 minutes only a gradual dissolution of the external layers is visible. Compare this result with the one reported in Figure 4.10, concerning geometry square36, a significant difference is visible. Therefore, the dimensions b and c affects the dissolution.

In order to better understand how *b* and *c* affects the dissolution the dissolution records of the other geometries are reported.

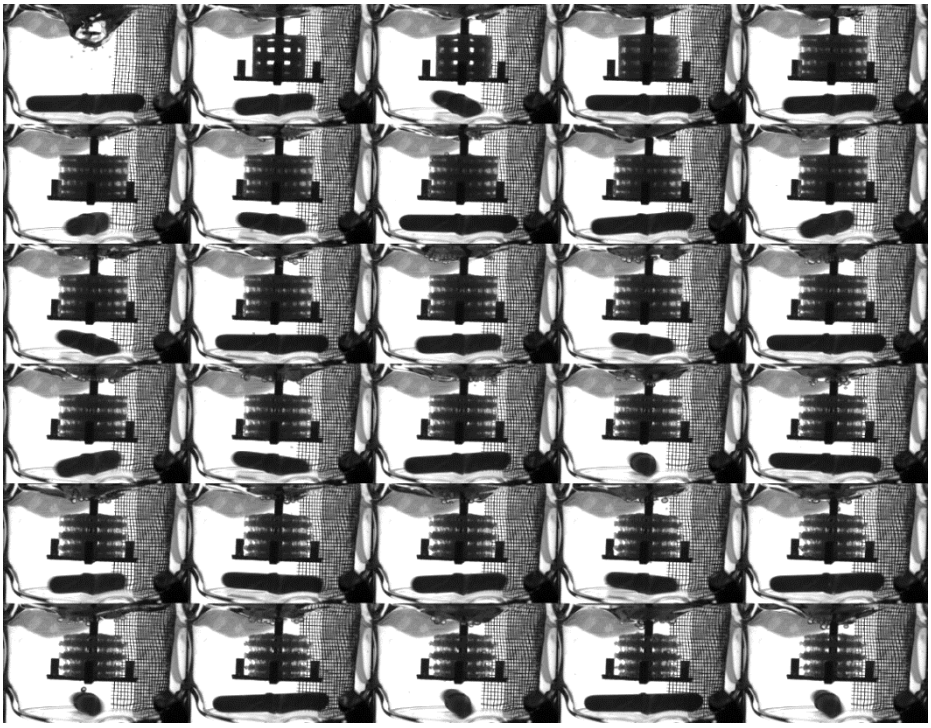

Figure 4.19: Montage of the dissolution test of geometry G2. Time between 2 consecutive frames= 1.5 min.

Geometry G2 is characterized by the smallest holes in the external area and biggest holes in the central area of the cube. The dissolution is similar to the previous one, with a faster dissolution of the external layers, characterized by a smaller width, and lower dissolution of the central ticker layer.

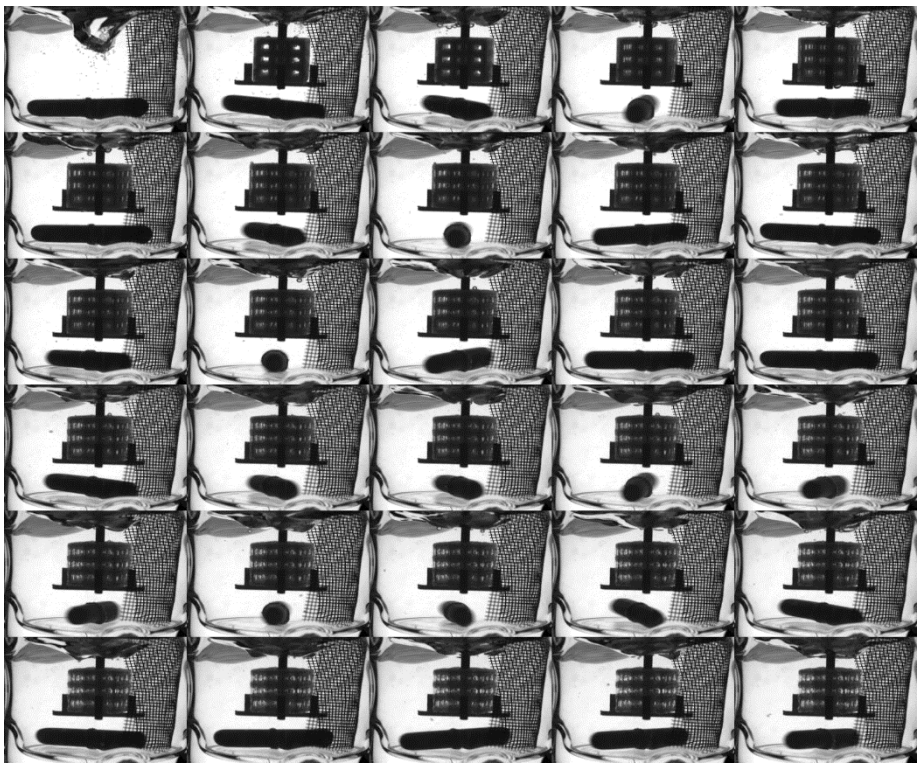

Figure 4.20: Montage of the dissolution test of geometry G3. Time between 2 consecutive frames= 1.5 min.

The last geometry of the category B is the geometry G3. It is a symmetrical structure; it has 9 square pores of 3 mm and the width between pores is of 3mm. Figure 4.20 illustrates the dissolution of geometry 3. As in the previous cases dissolution does not occurred completely in 45 minutes. In conclusion G1, G2 and G3 dissolve slowly compared with square36, despite all of them have similar mass and the same volume. In order to have a quantitative result porosity and t90 are evaluated. Afterwards, mean and standard deviation of the tests performed are plotted in order to analyse all the dissolution behaviour.

Table 4.1: Porosity and t90 evaluation.

Geometry	Porosity [%]	t90 [min]
Square36	0.53994 ± 0.0103	38.449 ± 4.196
G1	0.4487 ± 0.0139	66.077 ± 3.442
G2	0.4945 ± 0.0065	67.092 ± 2.156
G3	0.4929 ± 0.0189	69.5 ± 3.894

Table 4.1 shows the porosity and the time to reach the 90% of the final value. Also in this case porosity does not affect the dissolution characteristic time t90. In fact, t90 of geometry G1, G2 and G3 does not have significant differences. It means that porosity is not the key parameter for dissolution of structures with macroscopic pores. Moreover, G1, G2 and G3 have different pores dimensions, while they have in common the maximum width between 2 pores (dimension b), for at least one cuboid (3mm). It can explain the differences between dissolution time of geometries G1, G2 and G3 and geometry Square36. To further investigate it all the data obtained are reported in Figure 4.21

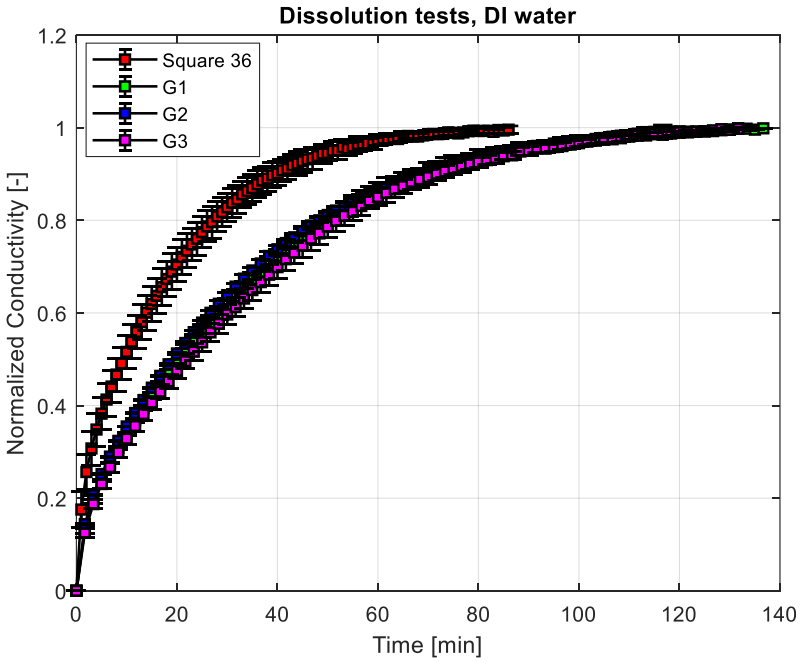

Figure 4.21: Normalized conductivity versus time plot.

The pattern shows in Figure 4.21 confirm the previous hypothesis. Geometry square36 has a faster dissolution, while there are not significant differences between the other 3 geometries. It means that the dissolution is controlled by the width of material between 2 pores (dimension *b*). Similar results are found by Maroni et al. [25] on the study of the dissolution behaviour of capsules with different wall width. To further prove this result geometry G4 and G5 are developed and results are reported in the next section.

4.2.4. Results analysis, category C

Geometry G4 and G5 are designed to study the dissolution behaviour of geometries with same dimensions *c*, *d* and *e* but different dimension *b* (width between holes). Moreover, to confirm the previous results and to verify if holes size can affect the dissolution, pores size is decreased and selected as 1mm.

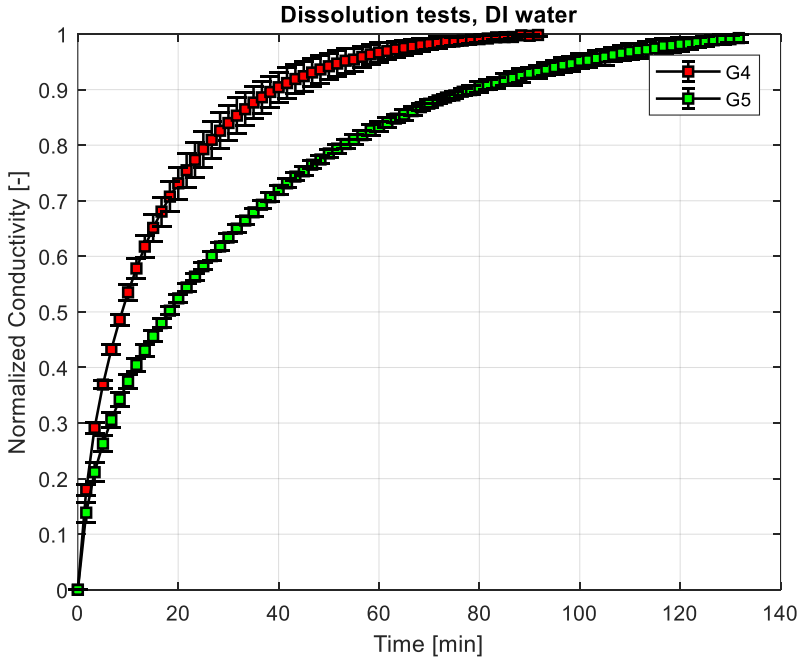

Figure 4.22: Normalized conductivity versus time plot.

Figure 4.22 illustrates the mean and the standard deviation of the normalized conductivity as a function of the time. As it could be expected, the geometry G4, that has a smaller *b*, has a faster dissolution. It confirms the result previously reported, (§4.2.3). Hence, the width of printed material influences the dissolution. Moreover, it can be seen that the dissolution is generally slower than the one of the previous geometries.

To compare the results, t90 of all the significant geometries is reported in Table 4.2.

Table 4.2: Dissolution characteristic time t90 evaluation.

Geometry	t90 [min]
Square9	38.100 ± 2.579
Square25	30.055 ± 0.141
Square36	38.449 ± 4.196
G1	66.077 ± 3.442
G2	67.092 ± 2.156
G3	69.5 ± 3.894
G4	38.506 ± 5.562
G5	76.067 ± 2.223

Considering t90 of geometry G5, it is the highest one, despite the dimension *b* is 1.5mm, thus lower than the one of geometries G1, G2 and G3. Considering G4, it has a dissolution characteristic time comparable with the one of geometries square9 and square36 even if the dimension *b* is lower. It means that for pores smaller than 1.5mm also the pores dimension affects the dissolution. To prove it the dissolution of geometry square25 and G5 are compared in the Figure 4.23.

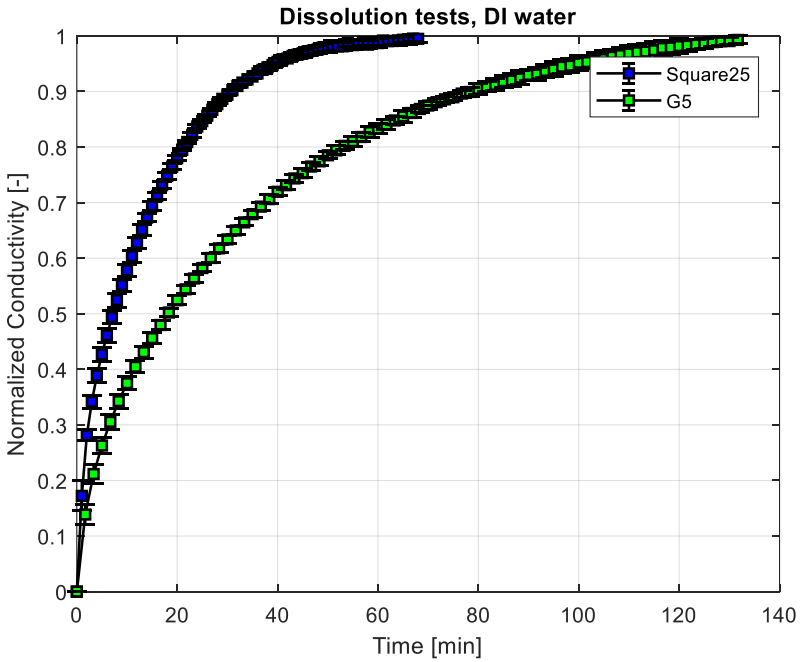

Figure 4.23: Normalized conductivity versus time plot.

Geometry square25 and square G5 has same dimension *b* and *e*, but they have different pores size, named *c*. It means that the dissolution time, for pores smaller than 1.5 mm is strongly affected by the pores size.

Mean and standard deviation of all the geometries are reported in appendix B.

4.3. Chocolate printing and G-code generation

In this section of the thesis, the research performed on G-codes is described.

The aim of this study is to develop a tool to control the sequence of movements that a 3D printer is performing when prints simple shapes. As described in chapter 2 (§2.2.14), the 3D printer movements are controlled throughout a programming language, named G-code. Hence, in order to better understand how to generate a G-code, study of software-sliced G-codes, was first performed. In particular, analysis on the most used commands was done. Then, new G-codes were generated using Matlab.

The most used commands are reported in Table 4.3

Table 4.3: Main G-code commands.

Command	Meaning
G1	Linear movement to the specified location
Xnnn	A X coordinate, usually to move to.
Ynnn	A Y coordinate, usually to move to.
Znnn	A Z coordinate, usually to move to.
Ennn	Length of extrudate. It represents the amount of material that has to be extruded.
Fnnn	Feedrate in mm per minute. (Speed of print head movement)
G90	Set to Absolute positioning
G91	Set to relative positioning, the coordinate is relative to the last position
G92	Set position, usually used to set extrusion to zero

As mentioned above (§2.2.14), each printer has its own G-code. In particular, the first lines of the algorithm are specific for each machine and usually set the initialisation of the printer (e.g. calibration, home position movements, set of default temperature). After that, it is necessary to decide whether it is more convenient to work in absolute or relative positioning. In this project absolute positioning was selected, because the default absolute origin is placed in the centre of the build plate.

4.3.1. Star geometry

The first geometry to be analysed was the Star. From a visual analysis it was possible to see that the printing was performed in an unusual way. The Star is printed in almost 7 minutes and for each layer the nozzle stops and starts extruding 8 times. This consequently reduces the quality of printing due to dripping problems, while the printer stops extruding.

In order to improve the quality of printing a G-code was implemented using Matlab to control the sequence of operation.

First of all the movements were decided and the coordinates designed in a square paper to obtain the same dimensions of the CAD file.

Then, the coordinates were obtained and a matrix with all the coordinates was built.

The following plot shows the 2D coordinates on an X-Y Cartesian coordinate system. The planned movements are represented by the black arrows.

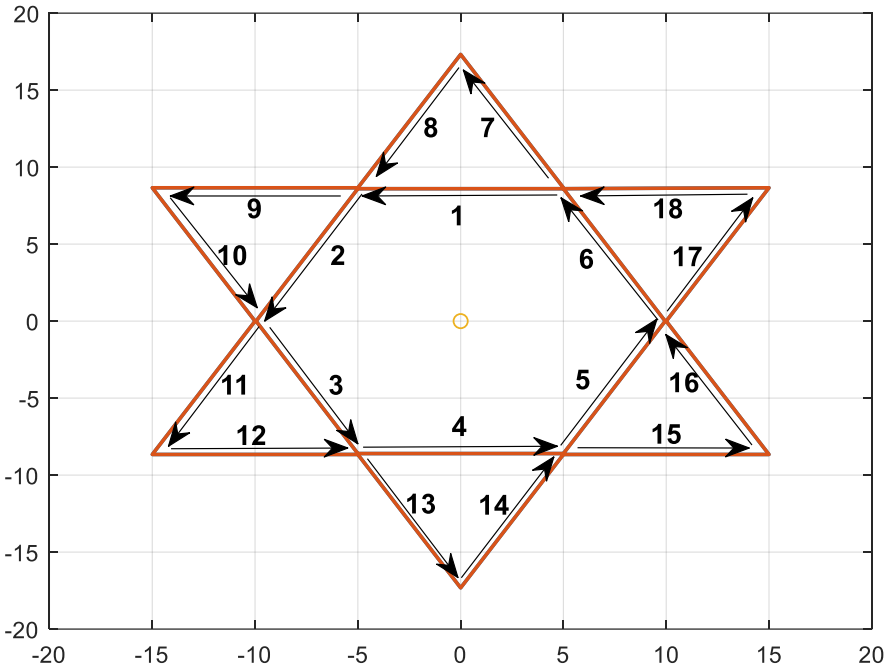

Figure 4.24: 2D coordinates designed for the star geometry

The movements are studied in order to print continuously without stops and the coordinates are developed in order to avoid roads overlap in the corners.

From the 2D coordinates and knowledge of the most important G-code commands, the script is developed in order to generate a file txt that can be used as G-code. In particular, the 2D coordinates are repeated for n layers on Z direction. Each layer is overlapped to the previous one. The number of layers is directly related to the height of the printed object. Moreover, it can influence the quality of the printing and the mechanical properties of the printed object. The number of layers is selected in order to obtain a height of 10mm. Its value is 16 (0.6mm per each layer).

The possibility, for the users, to modify the height without changing the printing conditions/movements allows to further study mechanical properties of the bottom layer and the maximum weight supported. An example of G-code is shown below.

```
%% initialisation
G90
G21 %%homing positioning
G92 E0
M108 S0.02129 %%set default temperature
M108 S0.02129

G1 X5 Y8.66 Z0.3 F1800 %% initial coordinates

G1 F720
G1 E1.7
G1 F1800
G92 E0 %relative extrude position
G90 %absolute coordinates

```

Figure 4.25: G-code generated using Matlab

The picture shows the first part of the G-code. This part of the G-code is specific for each printer. Furthermore, only the initial coordinates and the printing speed are set.

```
%% printing of first layer
G1 X0 Y17.321 Z0.3 F480 E0.030
G1 X-5 Y8.66 Z0.3 F480 E0.060
G1 X-15 Y8.66 Z0.3 F480 E0.090
G1 X-10 Y0 Z0.3 F480 E0.120
G1 X-15 Y-8.66 Z0.3 F480 E0.150
G1 X-5 Y-8.66 Z0.3 F480 E0.180
G1 X0 Y-17.321 Z0.3 F480 E0.210
G1 X5 Y-8.66 Z0.3 F480 E0.240
G1 X15 Y-8.66 Z0.3 F480 E0.270
G1 X10 Y0 Z0.3 F480 E0.300
G1 X15 Y8.66 Z0.3 F480 E0.330
G1 X5 Y8.6 Z0.3 F480 E0.360
G1 X-5 Y8.6 Z0.3 F480 E0.390
G1 X-9.95 Y0 Z0.3 F480 E0.420
G1 X-5 Y-8.6 Z0.3 F480 E0.450
G1 X5 Y-8.6 Z0.3 F480 E0.480
G1 X9.95 Y0 Z0.3 F480 E0.509
G1 X5 Y8.6 Z0.3 F480 E0.539

```

Figure 4.26: G-code generated using Matlab

The picture illustrates the algorithm that is developed to print the 2D coordinates shown in picture 4.26 In particular, in each row the X,Y,Z coordinates are set. Moreover, the printing velocity is set. Finally, the quantity of material that has to be extrude is set. In this case the coordinates are set in absolute value (as shown in the 2D plot), while the extrude value is cumulative. The speed is set constant at and it is 8 mm/s.

The part of the G-code shown in Figure 4.26 gives the command to print the roads in order to obtain the 2D structures. The same commands are repeated n times with an increase of Z direction.

In conclusion, the selected movements, defined by the G-code developed with Matlab, enable to print in a continuous way the object with a reduction of the printing time of 50% and an increase of the precision.

Some pictures are presented below and shows the improvement in the printing quality:

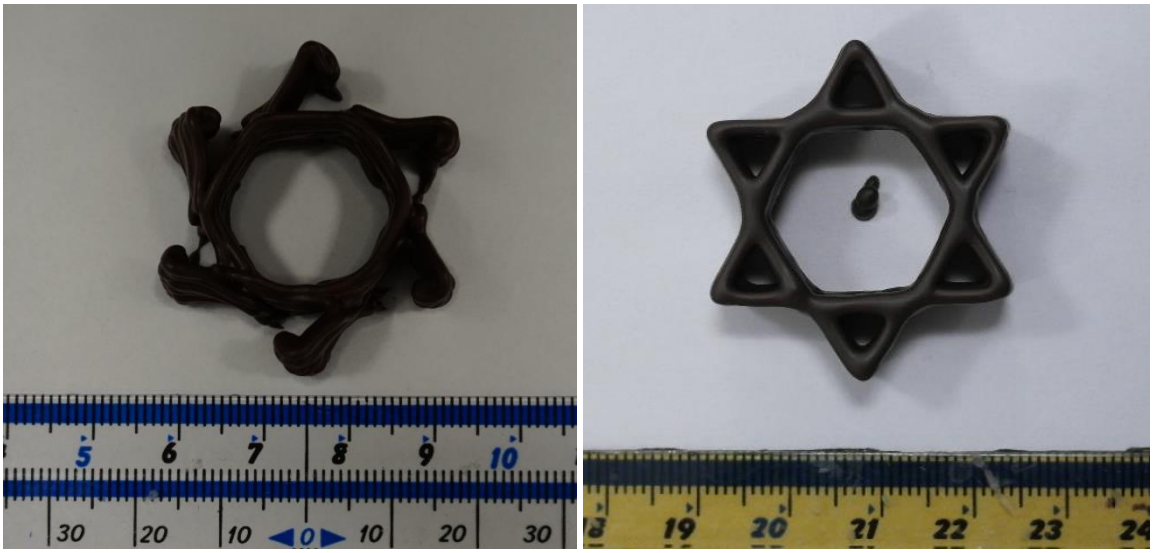

Figure 4.27: Star printing, comparison between 2 printing stars. On the left the Choc-Edge G-code is used. On the right the customize G-code is used.

Despite an initial dripping, continuous movements allowed to obtain a visible improvement in the quality of the printed object.

4.3.2. Dashed line geometry

The second geometry analysed was the dash line. The dash line is a very important geometry because it allows to study some of the most interesting printing questions, including:

- Quality of non-continuous extrusion printings
- Quality of welding between layers in Z direction
- Quality of welding between roads in Y direction
- Analysis of how length and number of lines influences the dash line quality.

For this purpose more files were generated. The main issues reported were that:

- Choc-Edge software was not able to print the dash line in a reasonable way (e.g. the lines were printed in a random way and not from left to right)
- Dripping problems
- Small geometrical changes in the CAD file generate a completely different way of printing.

First of all a script able to solve these problems was generated. It was developed to control 3 parameters:

- Length of lines
- Length of space between lines

- Number of lines

In this case the total length of the dash line is not fixed, but the Matlab script allows to study properly how length of lines and the space between lines influence the quality of printing.

The Matlab tool enables to print dashed lines with different geometrical parameters in the same way, from the left to the right. Hence, the generated G-code solve one of the issues reported.

Moreover, thanks to the new G-code, the travelling time is reduced, so printing time and probability of dripping is reduced. The differences between the G-code sliced by the software and the one developed with Matlab are summarized in the picture below.

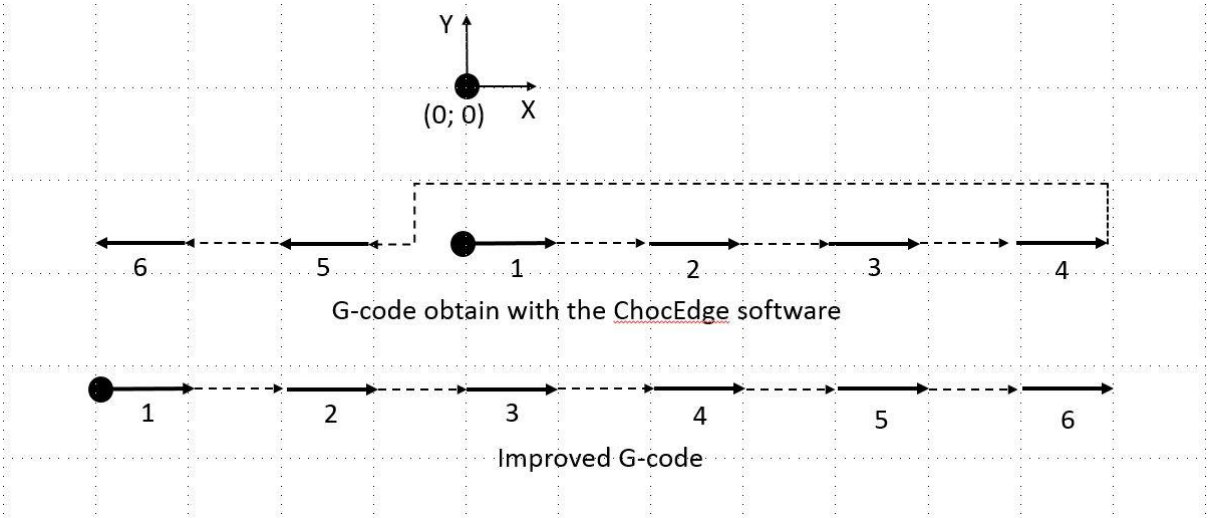

Figure 4.28: 2D coordinates of the Dashed line

As it can be seen from the previous picture the new G-code prints in a streamlined way. It is easy to understand that the new G-code improves the quality of the print compared to the first one. In fact, the printing time is reduced by 50% and also the nozzle movement time without printing is reduced. Hence, dripping probability is reduced. The G-code implementation was not trivial. In particular, in this case it is necessary to develop coordinates that change every time, considering the users' needs. Furthermore, it is necessary to also generate all the commands to control movements without printing. An example of G-code is shown below.

```
%% printing of first dash line
G1 X-39 Y0 Z0.3 F420 E0.0297

% stop extrusion commands
G1 F720
G1 E-1.672
G1 F480

% movements without extrusion
G1 X-31 Y0 Z0.9 F840
G1 X-30.5 Y0 Z0.7 F840
G1 X-30 Y0 Z0.3 F840

% start extrusion commands
G1 F720
G1 E0.0297
G1 F600
G92 E0
G90
%second dash lines
G1 X-19 Y0 Z0.3 F420 E0.0297

% stop extrusion commands
G1 F720
G1 E-1.672
G1 F480
```

Figure 4.29: G-code generated using Matlab

The picture shows all the command sequences that are necessary to be generated to print a dash line. In this case, the length of the line is 11mm, while the space between 2 lines is 10mm. This 2 parameters are set as input and can be modified. It would be easier to fix that 2 parameters but the Matlab script is developed to be also useful for further studies on how geometry affects the printing behaviour.

In order to gain a more complete understanding of how geometry influences the quality of the object a more complex Matlab Script is generated. Three new adjustable parameters are included. The new parameters are:

- height of the dash line (e.g. number of layers)
- thickness of the dash line
- printing velocity

The thickness is the most difficult parameter to be modified. In order to modify it, it is necessary to repeat n times, with a shift of Y axes, the same sequence of movements developed on X axes.

The Script enables to generate a dashed line, modifying all the geometrical parameters. This allows to further study sintering problems. In particular, the welding between two adjacent extruded roads can be observed. Moreover, the interaction between two consecutive layers can be investigated, so that surface tension and extensional properties can be studied.

This tool can be easily employed for other simple geometries that have a constant 2D shape.

Conclusions

The present work of thesis deals with the applicability of Fused Deposition Modeling as additive manufacturing technique to produce 3D food porous structures. An initial literature review was performed to outline the research aim. A knowledge gap about the use of FDM in the food industry was found, and the research work was addressed to the investigation of this technique. For this purpose, maltodextrin amorphous powder, provided by Roquette, was selected as main compound.

An initial characterization of maltodextrin (consisting of thermo-gravimetric, differential vapor sorption and differential scanning calorimetry measures) provided an indication of the degradation behaviour, the humidification and the glass transition temperature T_g of the powder. This procedure helped to better understand the main ingredient properties. Specifically, moisture content after storage at different relative humidity was determined, using 3 different techniques, providing similar results. Moreover, dry maltodextrin T_g was determined by DSC and was found to be equal to 111.72 ± 4.82 °C and fitting of the experimental data, using the the Gordon-Taylor equation, was performed to estimate the T_g of maltodextrin with different moisture content. Results are comparable to the literature ones [1],[4].

From this information, a first guess of the temperature required in the extrusion process was evaluated. Despite the process complexity, maltodextrin DE19 and DE21 were successfully extruded in filaments. Two extruders, Noztek and FilaFab PRO, equipped with different configurations (screws, motor power, speed velocity) were used. The first extruder led to poor quality filaments and had continuous mechanical failures, while the second one performed better yielding straight and transparent filaments with no expansion. With this apparatus, extrusion was performed at temperatures in the range 165-185°C. The extruder design (screw, heating zones and also motor power) is critical for a successful extrusion. Specifically, maltodextrin easily degrade and it is necessary to provide the proper amount of energy (in form of heat and mechanical energy) to obtain a viscous fluid without burn the powder.

Afterwards, these filaments were optically and mechanically characterized. From the optical analysis, filaments with non-suitable diameter and degradation/contamination evidences were discarded. Filaments extruded at lower temperature exhibit better homogeneity then those obtained at the higher temperatures (bubbling). Mechanical tensile tests were performed on microstructurally homogeneous samples obtained at 165°C and results were compared with

ABS filaments. The breakage of maltodextrin filaments occurred under a load 25 times lower than that of ABS. On this basis, mechanical properties of maltodextrin filaments are not satisfying, and this compound appears unsuitable for 3D printing.
Furthermore, filaments maintained at different storage conditions (different humidity) were mechanically tested. It is observed that mechanical properties of maltodextrin filaments are enhanced as the water content increases (plasticizer effect).

Lastly, 3D porous structures were designed and printed with PVA, which was selected for its high solubility in water. Three-dimensional PVA structures with macroscopic pores were successfully printed. These experiments were performed to simulate the maltodextrin printing and to develop a dissolution method useful to have a general information of the object dissolution and its behaviour inside the human mouth. Dissolution tests reveals a relative slow dissolution of the printed structures. Characteristic time of dissolution, t_{90}, has been found between 30 and 70 minutes. It has been proved that dissolution is affected by two geometrical parameters: pores size and material width *b* between pores. Similar values has been found by Maroni et al. [25]. Specifically, for pores bigger than 1.5 mm only the material width *b* affects the dissolution, while for pores smaller than 1.5 mm also the pores size affects the results.

Finally, the tool to control the sequence of operation during the 3D printing of simple shapes is developed. The work presented in chapter 4 (§4.3) allowed the users to generate customized structures managing all the movements. The Matlab tool was firstly developed for the star geometry and the dashed line geometries. Printing time was reduced selecting more streamlined movements that allowed also to improve the printing quality. Moreover, this tool can be also used for other simple geometries printed with a constant 2D shape.

In conclusion, the present work represents a first step in the study of FDM as food production technique. This study highlights the importance of the extrusion technique to produce filaments and the difficulties that can arises during the extrusion of food materials. Maltodextrin appears unsuitable for 3D printing, but the experimental work can be extended changing the powder composition. For instance, plasticisers with higher boiling point, such as glycerol and D-sorbitol, can be used to enhance extrusion and increase mechanical properties of the produced filaments.

Appendix A

DSC results

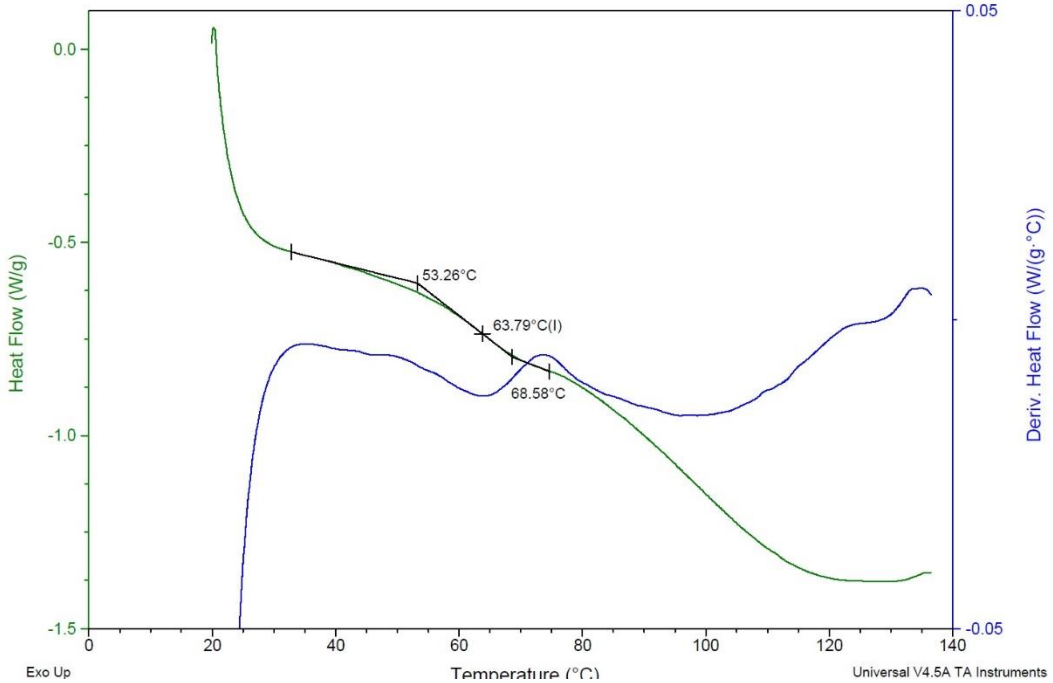

Figure A.1: DSC analysis of humidified maltodextrin at 32% RH and T = 21°C. Sample 1

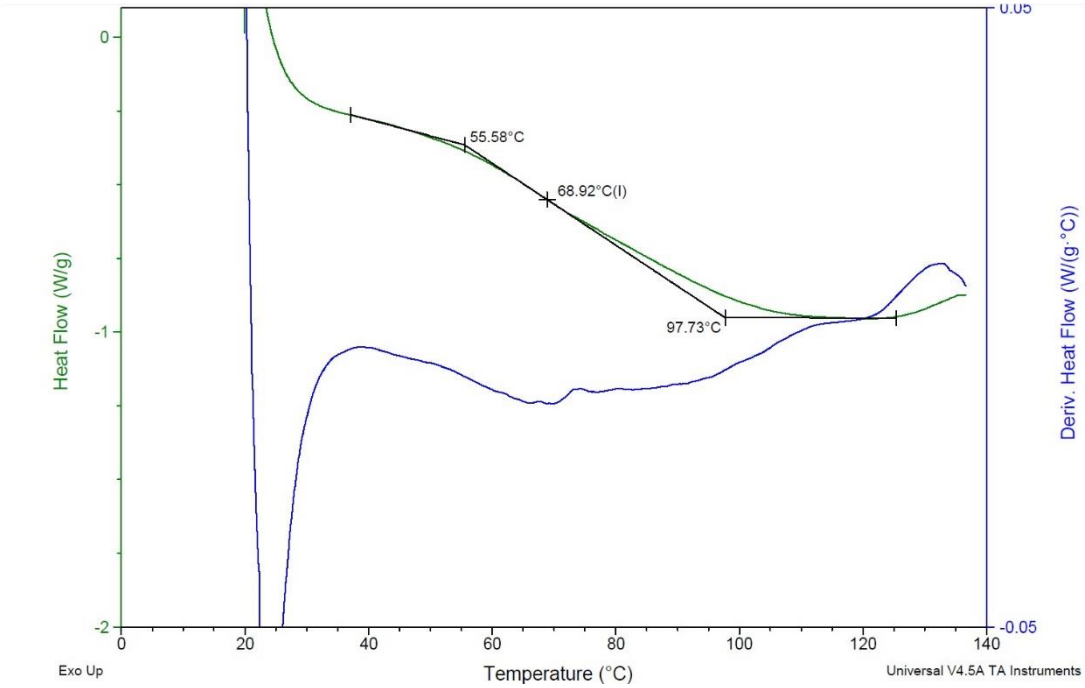

Figure A.2: DSC analysis of humidified maltodextrin at 32% RH and T = 21°C. Sample 1

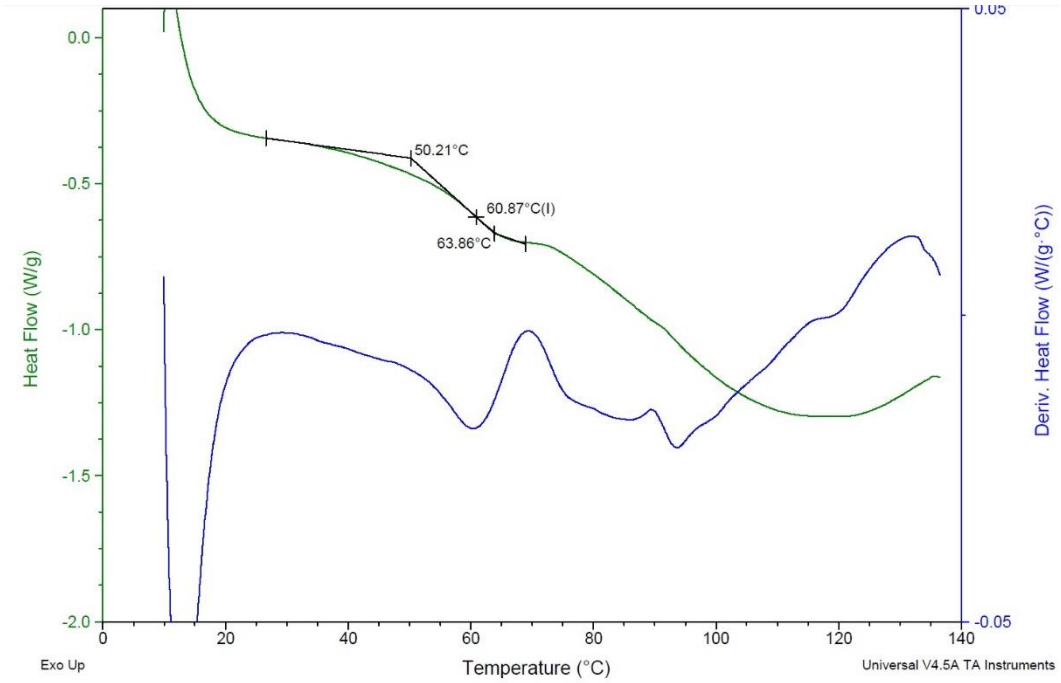

Figure A.3: DSC analysis of humidified maltodextrin at 43% RH and T = 21°C. Sample 1

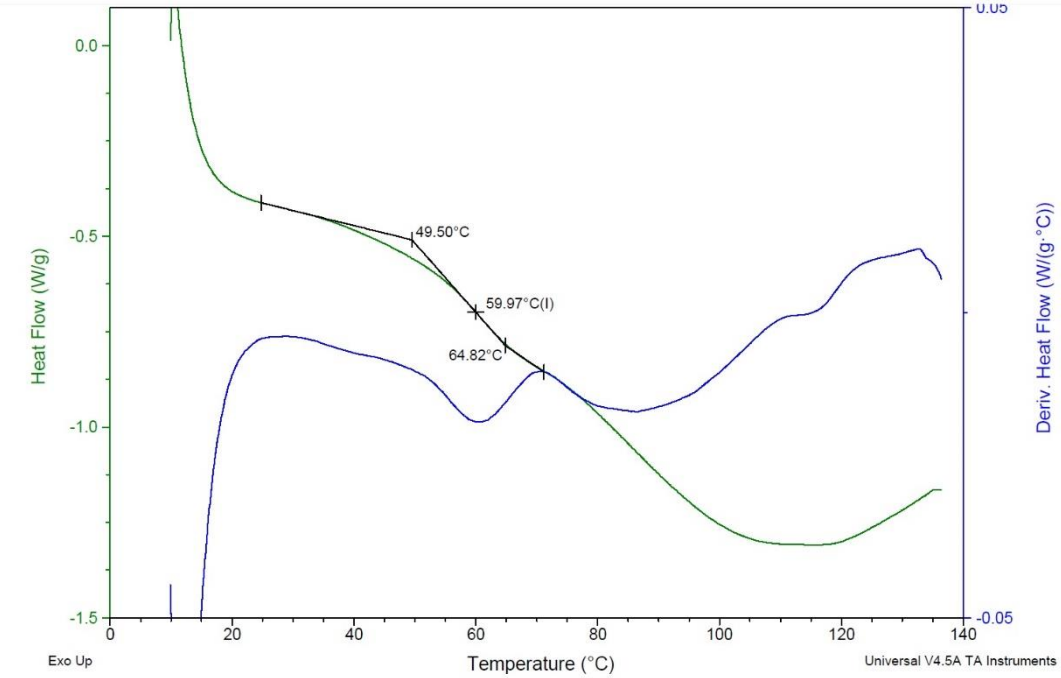

Figure A.4: DSC analysis of humidified maltodextrin at 43% RH and T = 21°C. Sample 2

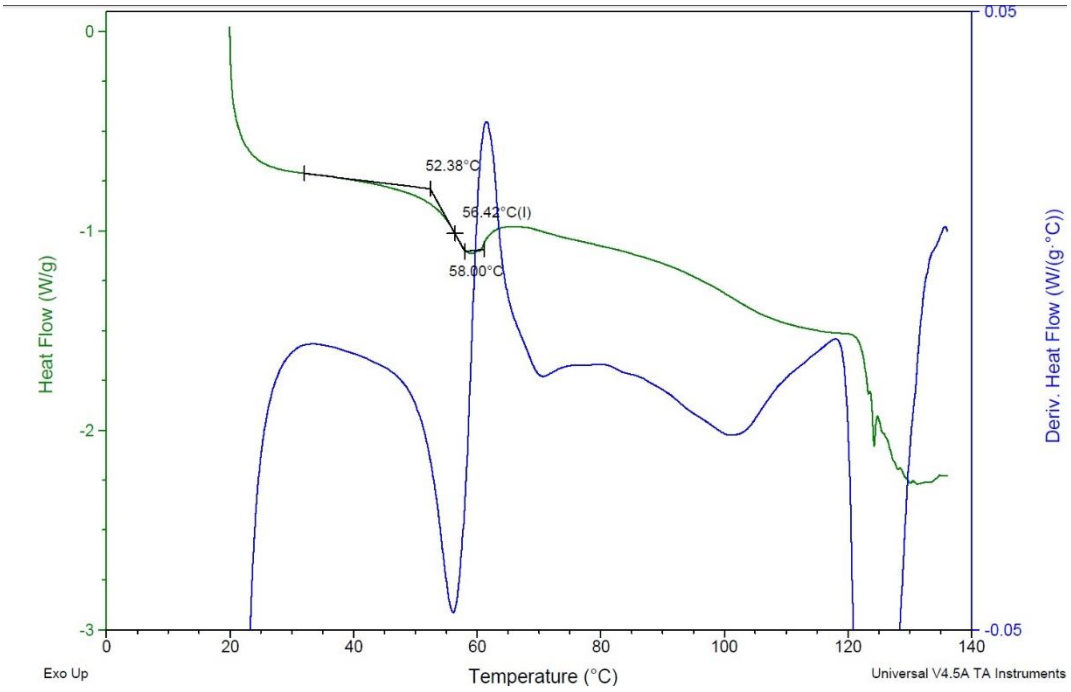

Figure A.5: DSC analysis of humidified maltodextrin at 50% RH and T = 21°C. Sample 1

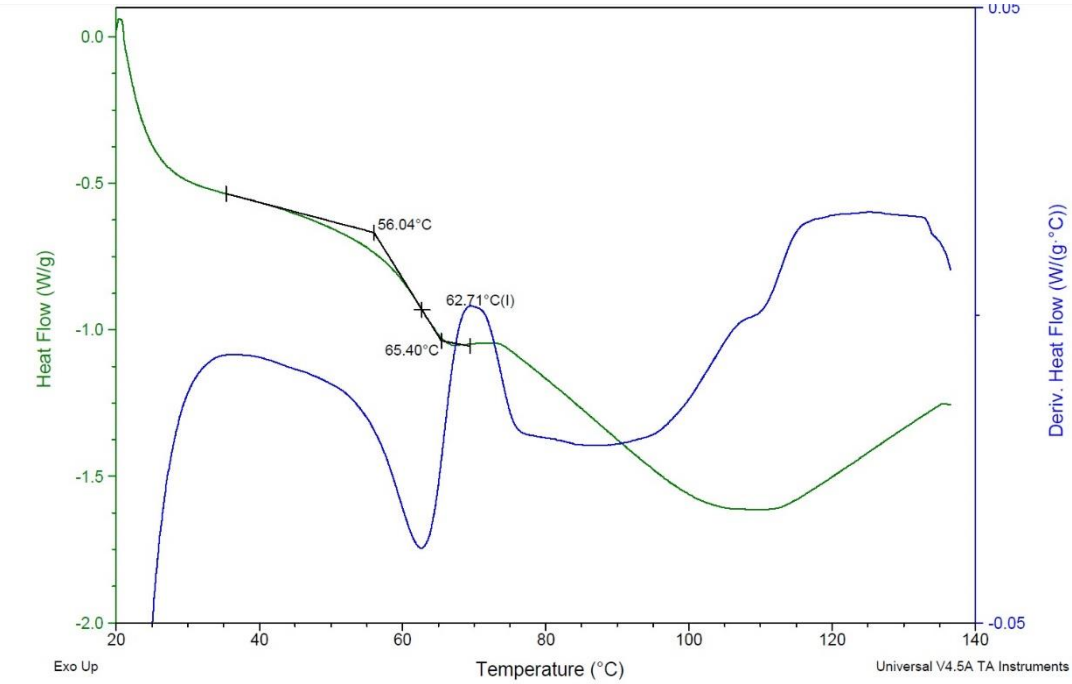

Figure A.6: DSC analysis of humidified maltodextrin at 50% RH and T = 21°C. Sample 2

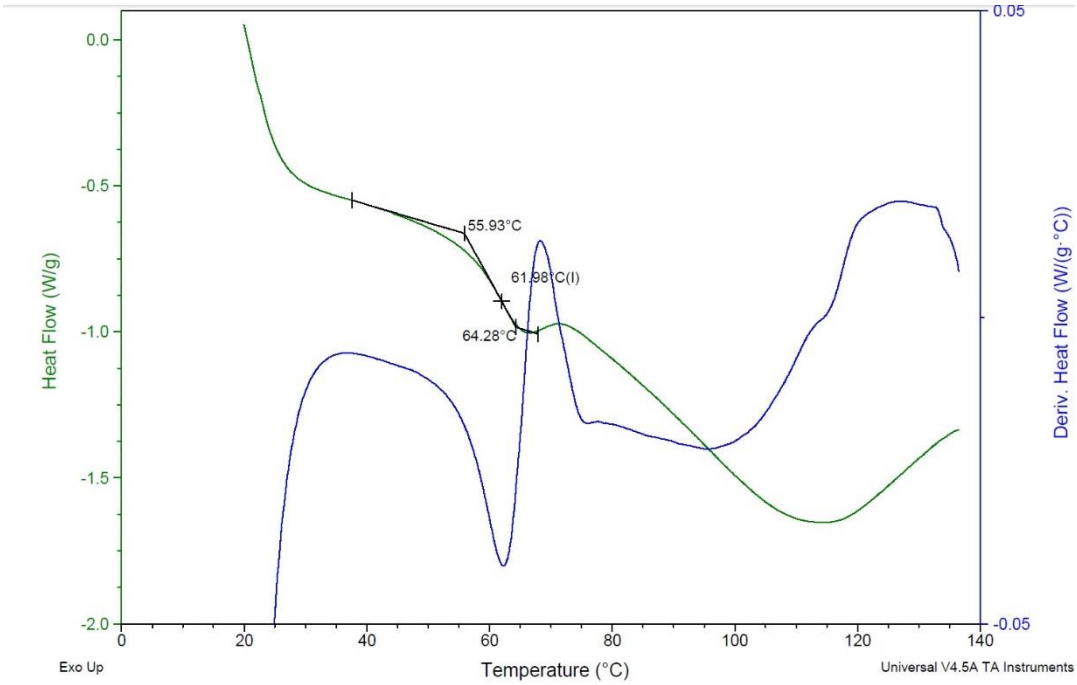

Figure A.7: DSC analysis of humidified maltodextrin at 50% RH and T = 21°C. Sample 3

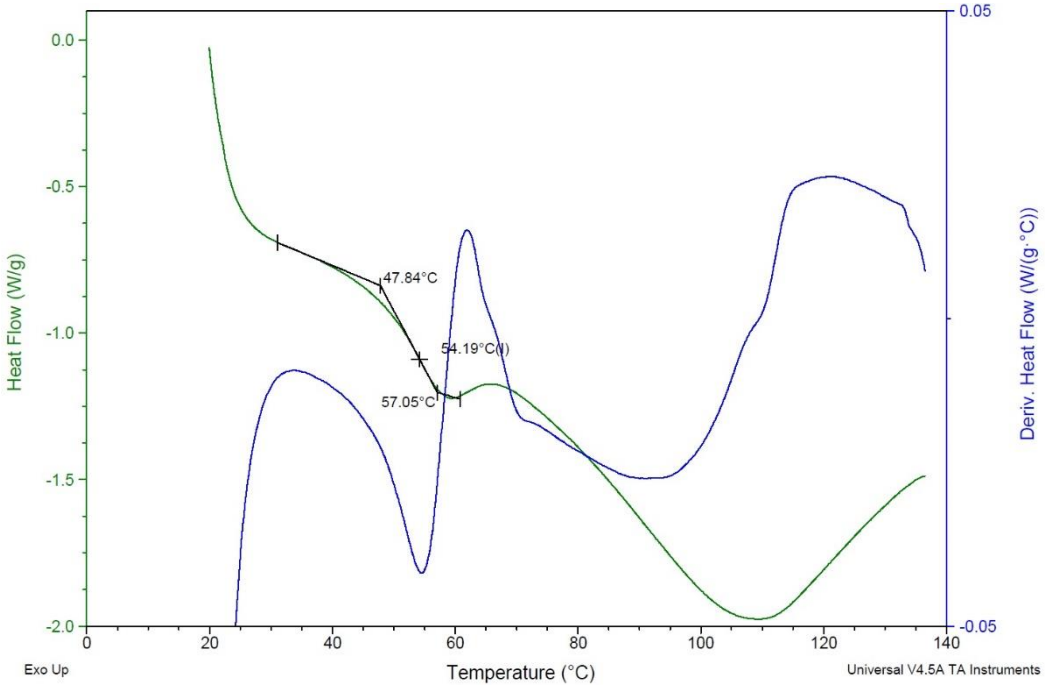

Figure A.8: DSC analysis of humidified maltodextrin at 65% RH and T = 21°C. Sample 1

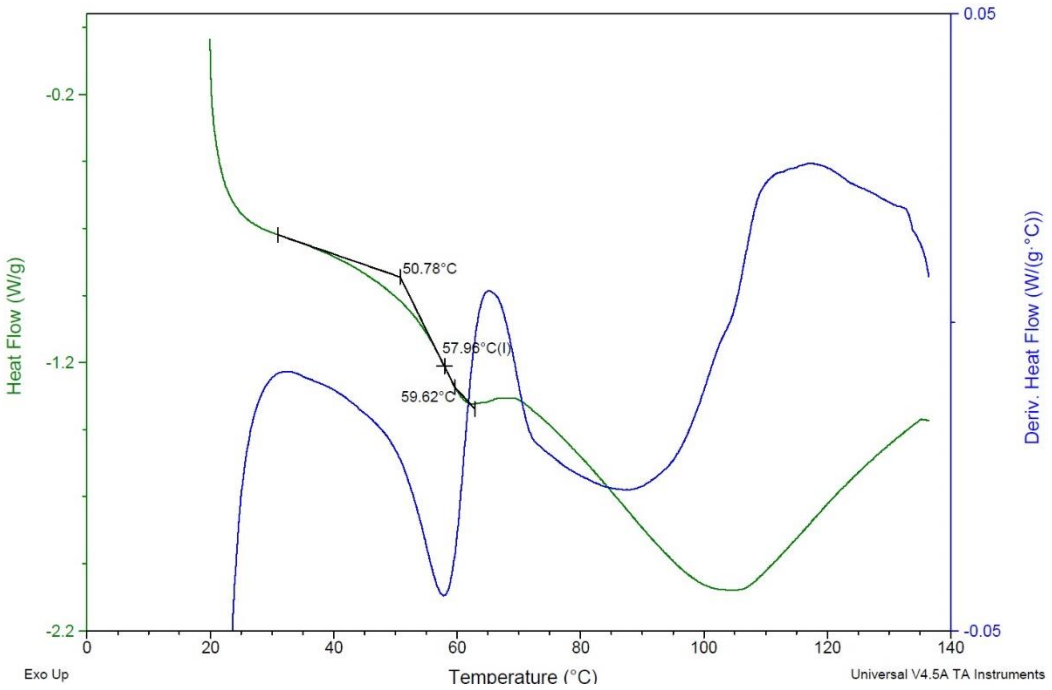

Figure A.9: DSC analysis of humidified maltodextrin at 65% RH and T = 21°C. Sample 2

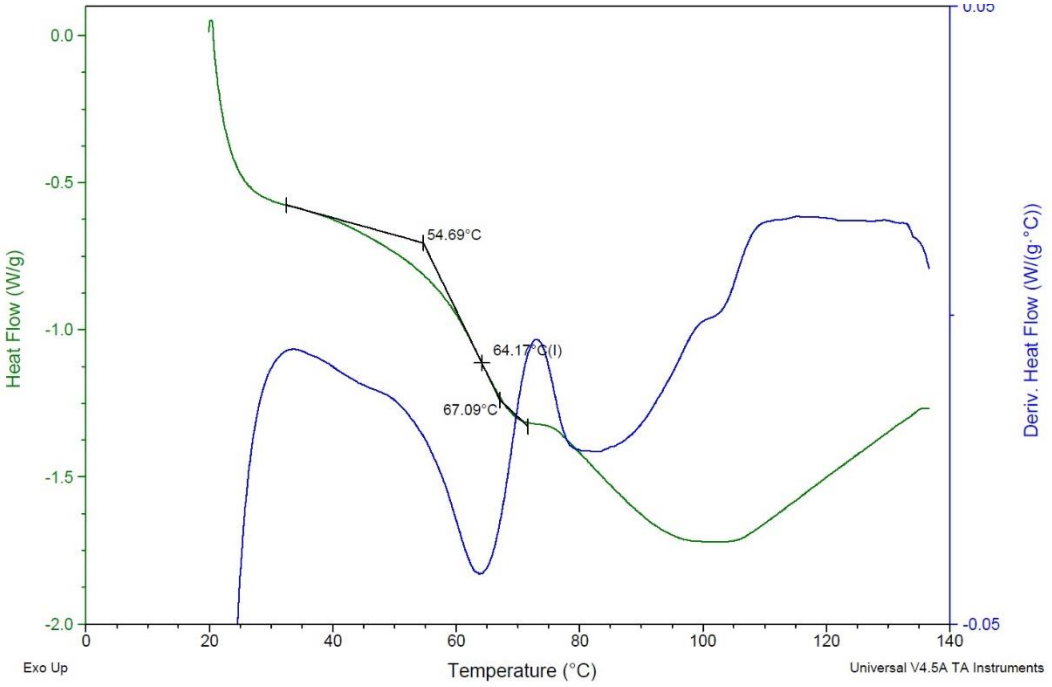

Figure A.10: DSC analysis of humidified maltodextrin at 65% RH and T = 21°C. Sample 3

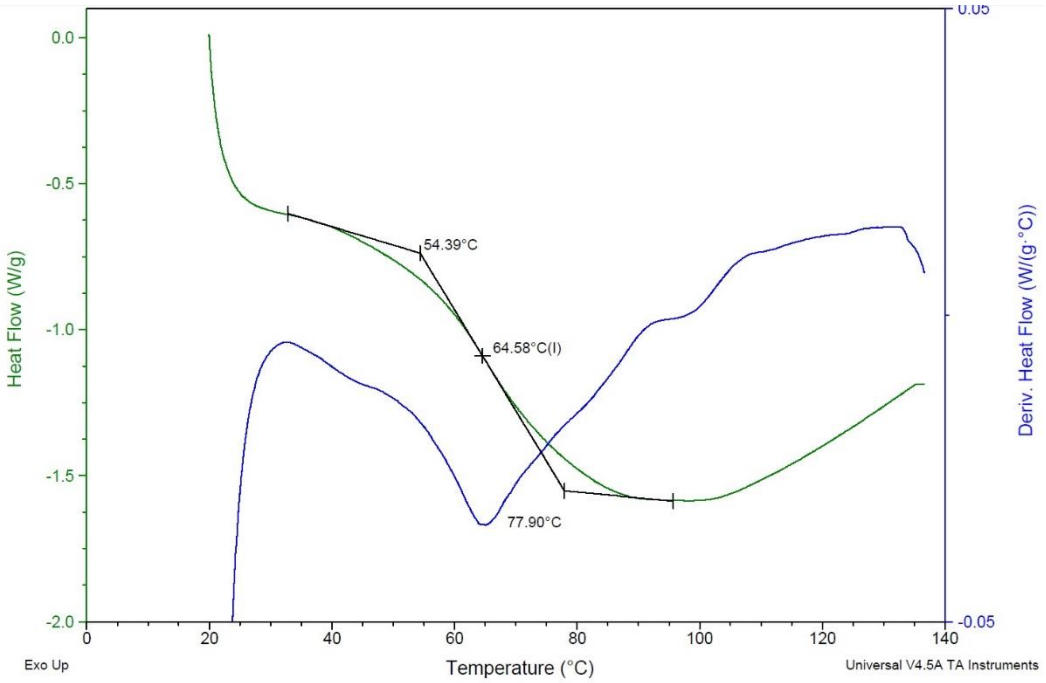

Figure A.11: DSC analysis of humidified maltodextrin at 65% RH and T = 21°C. Sample 4

Appendix B

Dissolution tests results.

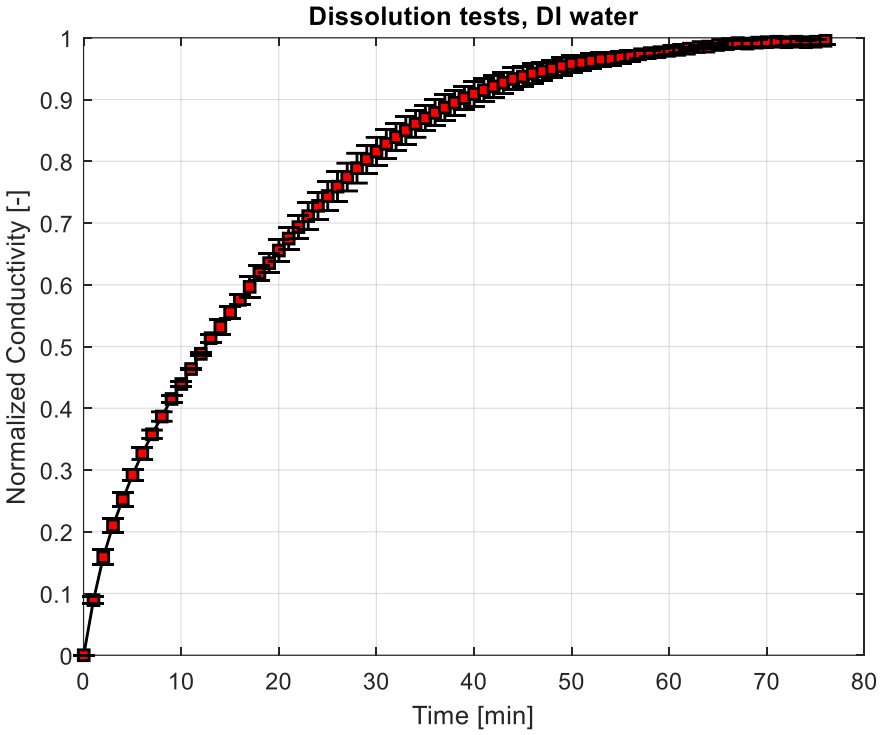

Figure B.1: Normalized conductivity versus time plot for geometry square9.

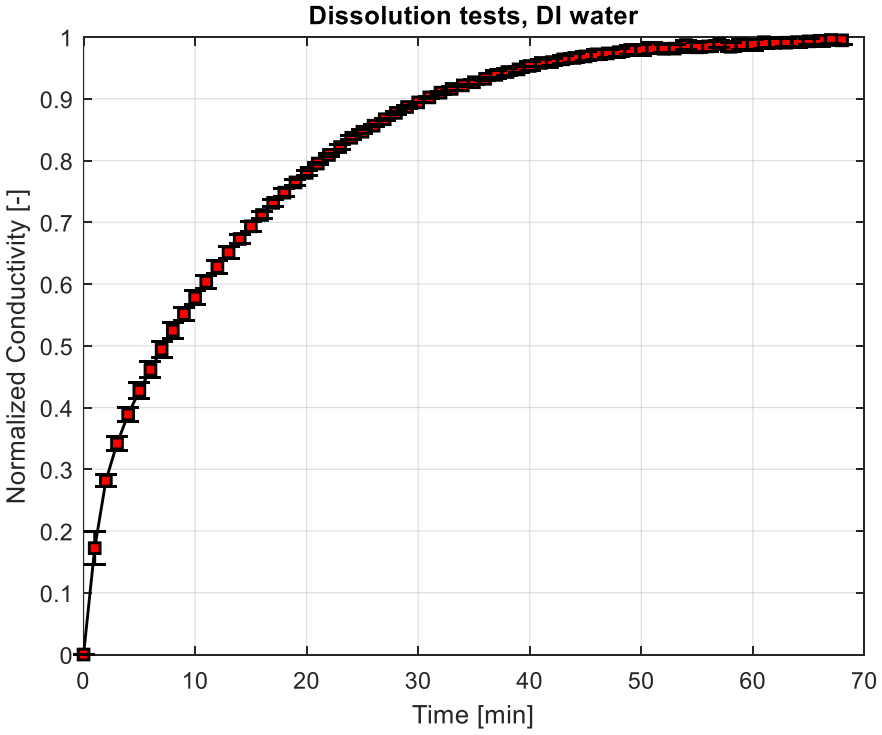

Figure B.2: Normalized conductivity versus time plot for geometry square25.

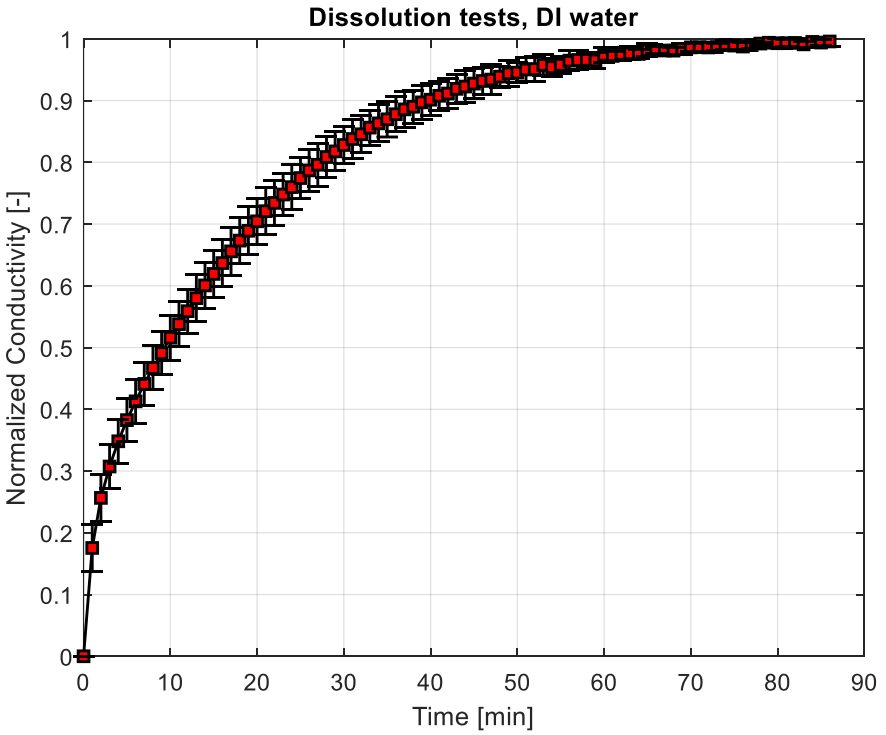

Figure B.3: Normalized conductivity versus time plot for geometry square36.

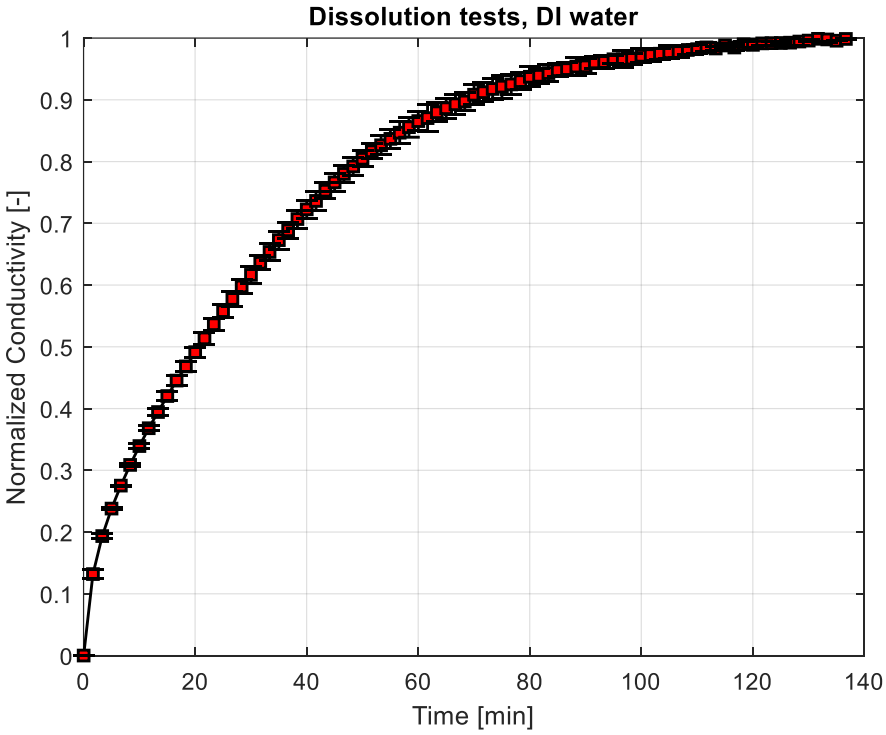

Figure B.4: Normalized conductivity versus time plot for geometry G1.

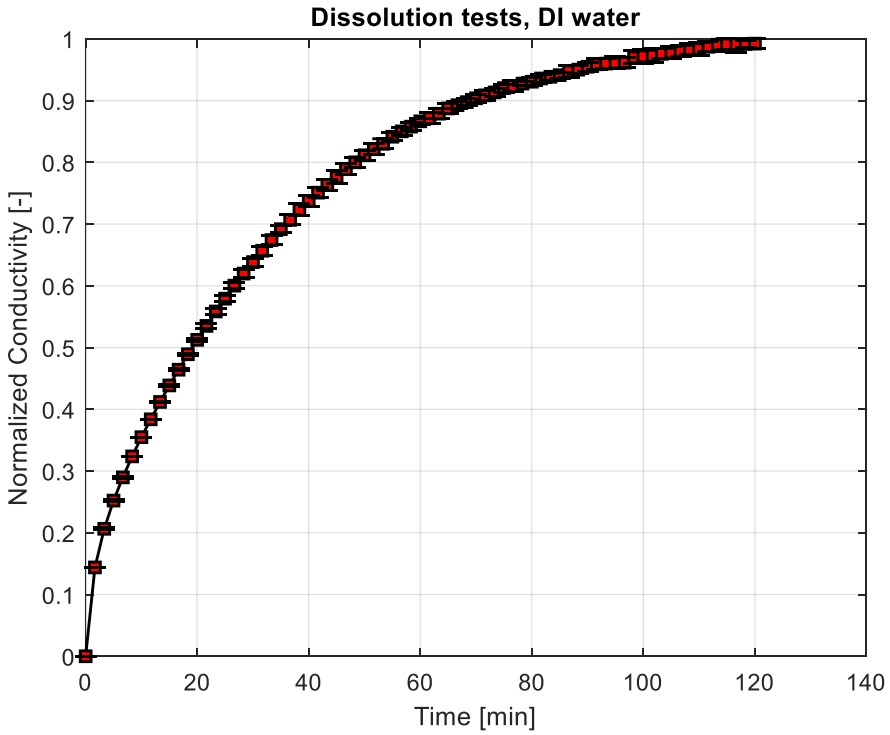

Figure B.5: Normalized conductivity versus time plot for geometry G2.

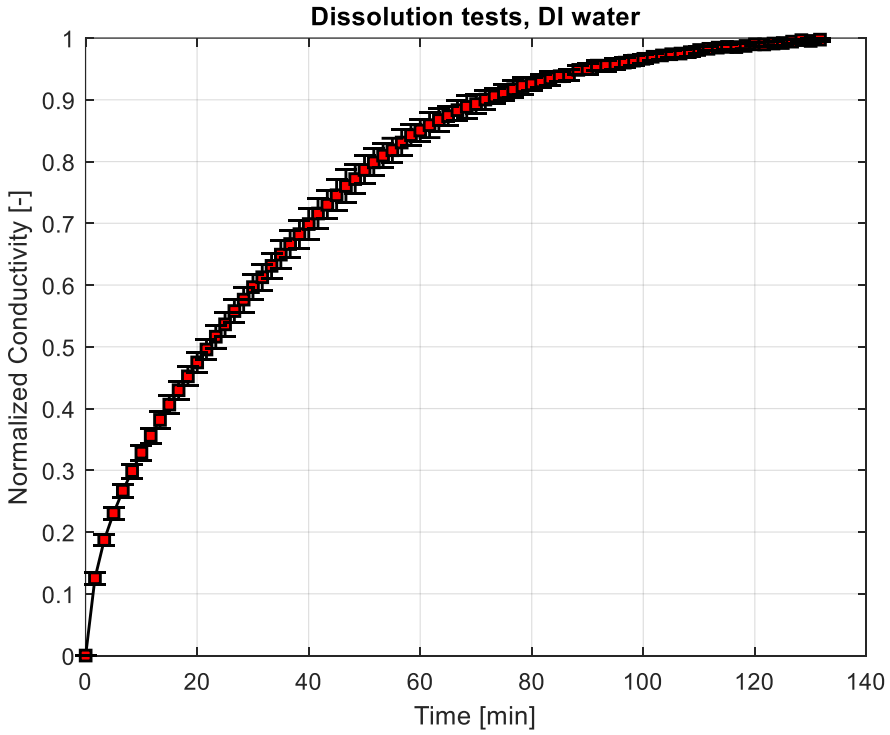

Figure B.6: Normalized conductivity versus time plot for geometry G3.

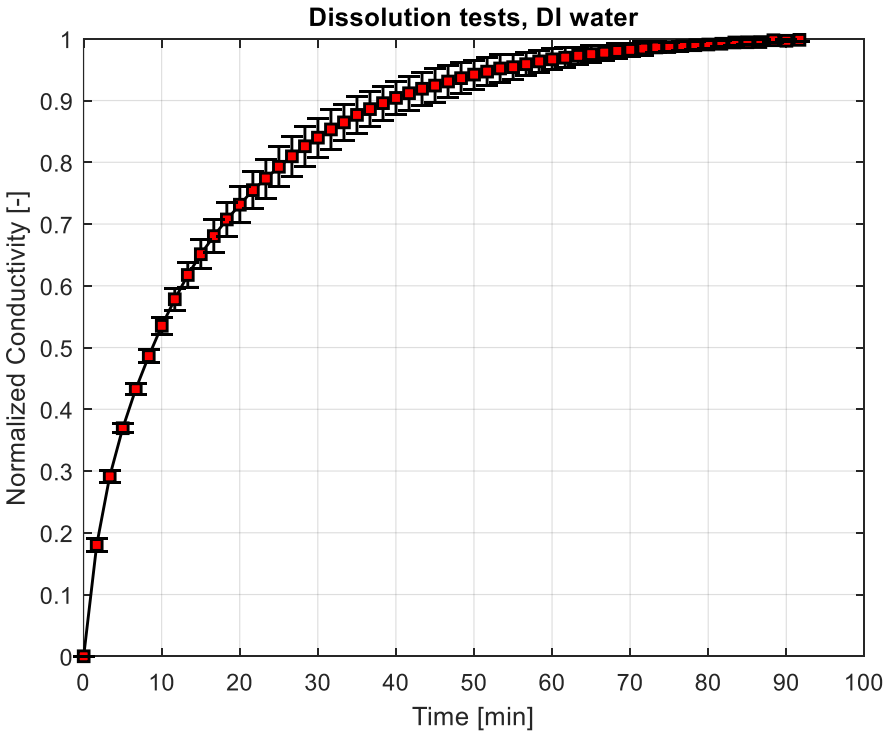

Figure B.7: Normalized conductivity versus time plot for geometry G4.

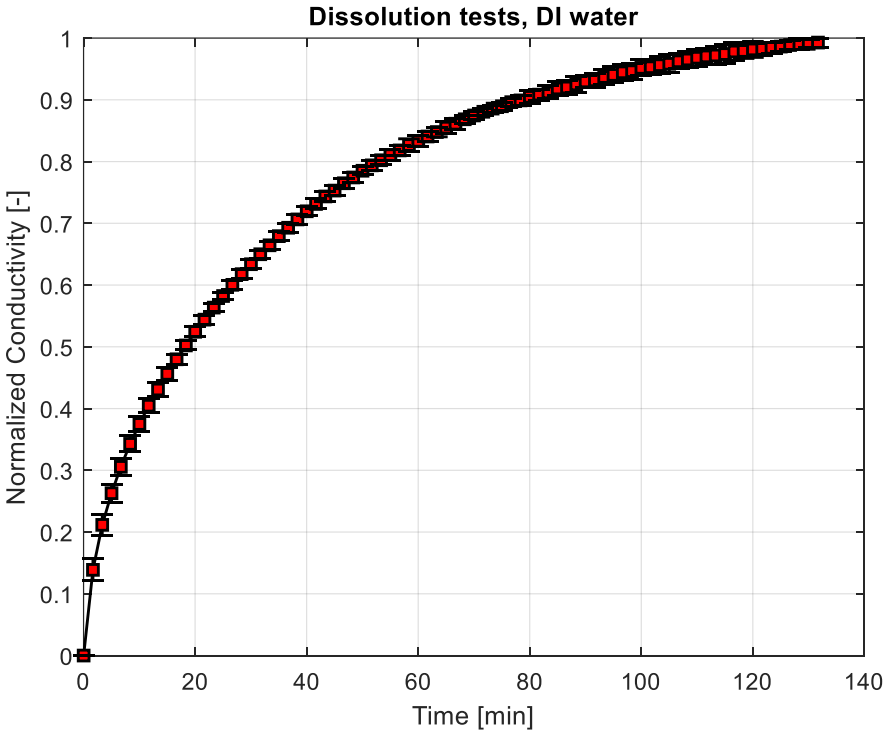

Figure B.8: Normalized conductivity versus time plot for geometry G5.

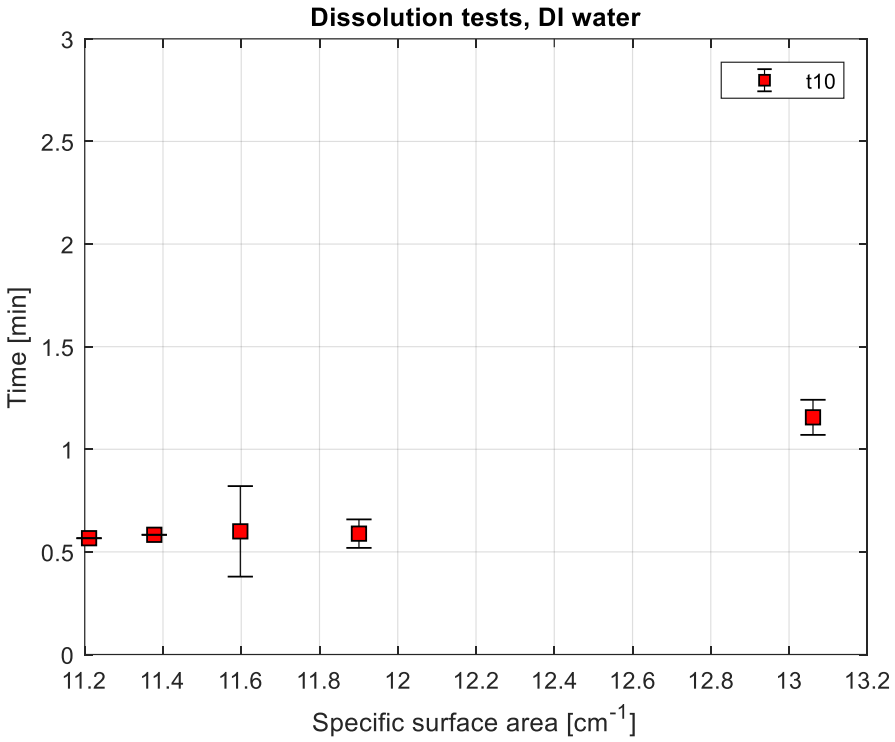

Figure B.9: t10 versus Specific surface area for geometries of category A

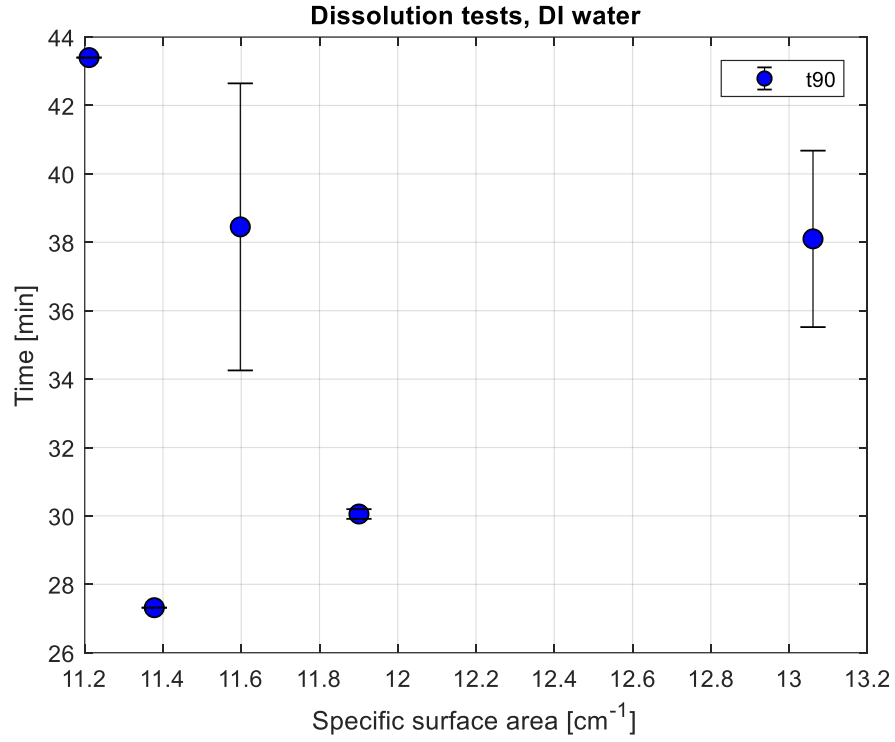

Figure B.10: t90 versus Specific surface area for geometries of category A

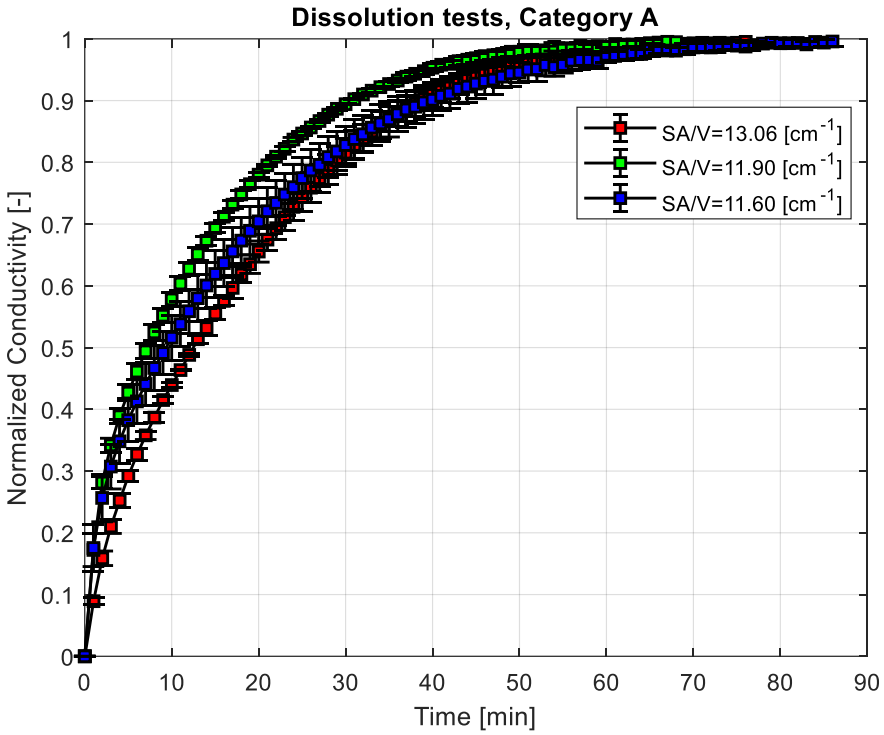

Figure B.11: Normalized conductivity versus time plot for geometries of category A.

References

[1] F. Avaltroni, P.E. Bouquerand, V. Normand.

Maltodextrin molecular weight distribution influence on the glass transition temperature and viscosity in aqueous solutions. Carbohydrate Polymers 58 (2004) 323-334.

[2] P. Burey, B.R. Bhandari, R.P.G. Rutgers, P.J. Halley, P.J. Torley.

Confectionery gels: a review on formulation, rheological and structural aspects. International Journal of Food Properties. Volume 12, 2009.

[3] O.S. Carneiro, A.F. Silva, R. Gomes.

Fused deposition modeling with polypropylene, Materials and Design Vol.83 (2015) 768-776.

[4] N. Castro, V. Durrieu, C. Raynaud, A. Rouilly.

Influence of De-value on the physicochemical properties of maltodextrin for melt extrusion processes. Carbohydrate Polymers 144 (2016) 464-473.

[5] Nicholas Cheremisinoff.

Guidebook to extrusion technology. Prentice Hall (June 1, 1993).

[6] A. Derossi, R. Caporizzi, D. Azzollini, C. Severini.

Application of 3D printing for customized food. A case on the development of a fruit-based snack for children. Journal of Food Engineering xxx (2017) 1-11.

[7] N. Descamps, S. Palzer, Y. H. Roos, J. J. Fitzpatrick.

Glass transition and flowability/caking behaviour of maltodextrin DE2. Journal of Food Engineering 119 (2013) 809–813.

[8] P. Dokic, J. Jakovljevic, Lj. Dokic-Baucal.

Molecular characteristics of maltodextrins and rheological behaviour of diluted and concentrated solutions. Colloids and Surfaces, A: Physicochemical and Engineering Aspects 141 (1998) 435–440.

[9] J. Dupas, V. Girard, L. Forny.

Reconstitution properties of Sucrose and Maltodextrin. Langmuir.

[10] F.W. Fifield, D. Kealey.

Principles and Practice of Analytical Chemistry, Wiley-Blackwell.

[11] I. Gibson, D. W. Rosen, B. Stucker.

Additive manufacturing technologies, 3D Printing, Rapid Prototyping, and Direct Digital Manufacturing. (Springer, 2010).

[12] F. C. Godoi, S.Prakash, B. R. Bhandari.

3D printing technologies applied for food design: Status and prospects. Journal of Food Engineering 179 (2016) 44-54.

[13] A. Goyanes a, A. Buanz A. W. Basit, S. Gaisfor.

Fused-filament 3D printing (3DP) for fabrication of tablets, International Journal of Pharmaceutics. 476 (2014) 88-92.

[14] A. Goyanes, M. Kobayashi, R. Martínez-Pacheco, S. Gaisford, A. W. Basit.

Fused-filament 3D printing of drug products: Microstructure analysis and drug release characteristics of PVA-based caplets. International Journal of Pharmaceutics 514 pp. 290-295.

[15] A. Goyanes , G. B. Hatton, H. A. Merchant, A. W. Basit.

G*astrointestinal release behaviour of modified-release drug products: Dynamic dissolution testing of mesalazine formulations.* International Journal of Pharmaceutics 484 (2015) 103–108.

[16] L. Greenspan.

Humidity Fixed Points of Binary Saturated Aqueous Solutions. Journal of Research of the National Bureau of Standards - A. Physics and Chemistry, 1977.

[17] L. Hao, S. Mellor, O. Seaman, J. Henderson, N. Sewell, M. Sloan.

Material characterisation and process development for chocolate additive layer manufacturing. Taylor & Francis.

[18] Hyun Woo Kim, Hojae Bae, Hyun Jin Park.

Classification of the printability of selected food for 3D printing: Development of an assessment method using hydrocolloids as reference material. Journal of Food Engineering 215 (2017) 23-32.

[19] M. Lanaro, D. P. Forrestal, S. Scheurer, D. J. Slinger, S. Liao, S. K. Powell, M. A. Woodruff.

3D printing complex chocolate objects: platform design, optimization and evaluation. Journal of Food Engineering 215 (2017) 13-22.

[20] C. Le Tohic, J. J. O'Sullivan, K. P. Drapala, V. Chartrin, T. Chan, A. P. Morrison, J. P. Kerry, A. L. Kelly.

Effect of 3D printing on the structure and textural properties of processed cheese. Journal of Food Engineering xxx (2017) 1-9.

[21] Jian-Yuan Lee, Jia An, Chee Kai Chua

Fundamentals and applications of 3D printing for novel materials, Applied Materials Today 7 (2017) 120–133.

[22] Z. Liu, M. Zhang, B. Bhandari, Y. Wang.

3D printing: Printing precision and application in food sector. Trends in Food Science & Technology 69 (2017) 83-94.

[23] Z. Liu, M. Zhang, B. Bhandari, Y. Wang.

Impact of rheological properties of mashed potatoes on 3D printing. Journal of Food Engineering xxx (2017) 1-7.

[24] S. Mantihal, S. Prakash, F. Condi Godoi, B. Bhandari.

Optimization of chocolate 3D printing by correlating thermal and flow properties with 3D structure modelling. Innovative Food Science and Emerging Technologies 44 (2017) 21–29.

[25] A. Maroni, A. Melocchi, F. Parietti, A. Foppoli, A. Gazzaniga, L. Zema.

3D printed multi-compartment capsular devices for two-pulse oral drug delivery. Journal of Controlled Release 268 (2017), 10-18

[26] A. Melocchi, F. Parietti, G. Loreti, A. Maroni, A. Gazzaniga, L. Zema.

3D printing by fused deposition modeling (FDM) of a swellable/erodible capsular device for oral pulsatile release of drugs. Journal of Drug Delivery Science and Technology. (2015). 360-367.

[27] A. Melocchi, F. Parietti, A. Maroni, A. Foppoli, A. Gazzaniga, L. Zema.

Hot-melt extruded filaments based on pharmaceutical grade polymers for 3D printing by fused deposition modeling. International Journal of Pharmaceutics 509 (2016), 255-263.

[28] Jehad M. Nasereddin, N. Wellner, M. Alhijjaj, P. Belton. S. Qi.

Development of a Simple Mechanical Screening Method for Predicting the Feedability of a pharmaceutical FDM 3D Printing Filament. CrossMark.

[29] B. Nurhadi, Y. H. Ross, V. Maidannyk.

Physical properties of maltodextrin DE10: Water sorption, water plasticization and enthalpy relaxation. Journal of Food Engineering 174 (2016), 68-74.

[30] K. F. Pitts, J. Favaro, P. Austin, Li Day.

Co-effect of salt and sugar on extrusion processing, rheology, structure and fracture mechanical properties of wheat–corn blend. Journal of Food Engineering, Volume 127, (2014) 58-66.

[31] C. Rauwendaal.

Polymer extrusion, Chris Author, 2013.

[32] M.A.I. Schutys r, S. Houlder, M . de Wit, C. A.P. Buijsse , A .C. Alting.

Fused deposition modelling of sodium caseinate dispersions. Journal of Food Engineering 220 (2018) 49-55.

[33] P. Seville and C.-Y. Wu.

Particle Technology and Engineering: An Engineer's Guide to Particles and Powders: Fundamentals and Computational Approaches. Butterworth-Heinemann, 2016.

[34] D. Skoog, F. Holler, S. Crouch.

Principles of instrumental analysis. Cengage Learning; 7 edition (January 1, 2017).

[35] J. Sun, W. Zhou, L. Yan D. Huang, Lien-ya Lin.

Extrusion-based food printing for digitalized food design and nutrition control. Journal of Food Engineering 220 (2018) 1-11.

[36] Q. D. Tran, W. H. Hendriks, A. FB van der Poel.

Effects of extrusion processing on nutrients in dry pet food. Journal of the Science of Food and Agriculture. Volume 88, 2009.

[37] Brian N. Turner, Robert Strong and Scott A. Gold.

A review of melt extrusion additive manufacturing processes: I. Process design and modeling. Rapid Prototyping Journal.

[38] L. Wang, M. Zhang, B. Bhandari, C. Yang

Investigation on fish surimi gel as promising food material for 3D printing. Journal of Food Engineering xxx (2017) 1-8.

[39] Z. Weng, J. Wang, T. Senthil, L. Wu.

Mechanical and thermal properties of ABS/montmorillonite nanocomposites for fused deposition modeling 3D printing. Materials and Design 102 (2016) 276–283

[40] Chi-Wah Yeung, Hubert Rein.

Hot-melt extrusion of sugar-starch-pellets. International Journal of Pharmaceutics 493 (2015) 390-403

Web sites:

https://en.wikipedia.org/wiki/Maltodextrin (Last access: October 2018)

http://www.tainstruments.com/ (Last access: October 2018)

https://www.surfacemeasurementsystems.com/ (Last access: October 2018)

https://us.ohaus.com/en-US/products-13 (Last access: August 2018)

http://www.noztek.com/ (Last access: October 2018)

http://d3dinnovations.com/filafab/ (Last access: October 2018)

http://chocedge.com/ (Last access: October 2018)

Acknowledgments

I would like to thank all the people who supported me throughout the realisation of this thesis.

A very special gratitude goes out to Dr. Marco Ramaioli for giving me this amazing opportunity at the University of Surrey. I wish to thank also my Supervisor Andrea Santomaso for the useful advice.

I am also grateful to all the research group: Amelie Nasser Addin, Gareth Coffin, Marco Marconati, Pietro Rando, Sadie Fleetwood, Solomon Melides and Xin Yin Ong. I wish to thank also all the colleagues of the department: Anna, Filippo, Mary, Monica and Panos.

In particular, I have to thanks my tutor Pietro and my colleague (and friend) Solomon, without you this experience would have been very difficult and boring. I want also to thank Anna, for the afternoon spent at the university lake speaking about our projects, for the support and for our trips in Southampton, Bath and Bristol with also Mary and Amelie.

Hearfelt thanks goes to Filippo for sharing everything (but not the girlfriend) in these six months. Your presence made everything easier and you became a great chef.

A special mention to all the people I have meet during this incredible Erasmus experience: Andrew, Chiara&Gio, Francesca, Giorgia, Katie, Laura, Mariangela, Michele, Norina, Samantha, Silvia, Taher and all the others. Every one of you teached me something and help me to grow up.

A special thanks to my beloved Samy for all the moments that we shared in these amazing months. I wish you the best for your future and for your life in Spain. I will keep this love in a photograph. May we meet again.

Ed infine grazie a tutte le persone che mi hanno sostenuto in questi due anni, a partire dagli amici di una vita: Alessandro, Barbara, Francesca, Daniel, Elisabetta, Emiliano, GB, Matteo, Roberta e ai nuovi amici conosciuti in Erasmus: Mariangela, Michele e Silvia. In particolare, voglio ringraziare Mariangela per i consigli medici e per il nostro incredibile rapporto e Michele per i pochi ma indimenticabili momenti passati insieme e per la tua incredibile stupidità. Inoltre, non posso astenermi dal ringraziare Barbara e Roberta per l'ospitalità in Newcastle e Bruxelles e per gli incredibili momenti vissuti in quelle due città.

Grazie ai compagni universitari che hanno avuto il coraggio di sopportarmi per due anni: Andrea, Arianna, Chiara, Damiano, Filippo, Eugenio, Gaia, Monica, Patrick e tutti gli altri. In particolare, grazie a Gaia ed Eugenio per il percorso fatto insieme durante il progetto di Process Design.

Infine voglio ringraziare tutti i compagni di basket e a tutte le persone che non ho nominato ma che mi sono vicine.

Ultimo ma non meno importante, grazie alla mia famiglia, per avermi permesso di studiare e di aver finito questo lungo ed estenuante percorso. Senza di voi nulla sarebbe stato possibile.